الجمهورية الجزائريةالديمقراطية الشعبية
وزارة التعليم العالي و البحث العلمي
People's Democratic Republic of Algeria
The Minister of Higher Education and Scientific Research
ⵜⴰⴳⵍⴷⵉⵜ ⵜⴰⵎⴰⵡⴰⵙⵜ ⵏ ⵜⵣⵣⵓⵖⵜ ⴷ ⵜⵙⵙⵏⵜⵉⵔⵜ ⵜⴰⵙⵙⵉⵏⵜⵉⵜ

ABOU BEKR BELKAID UNIVERSITY
TLEMCEN
FACULTY OF MEDICINE- Dr. B. BENZERDJEB
PHARMACY DEPARTMENT

جامعة أبو بكر بلقا يد - تلمسان
كلية الطب- د. ب. بن زرجب
قسم الصيدلة

MEMOIRE DE FIN D'ETUDES POUR
L'OBTENTION DU DIPLOME DE DOCTEUR EN PHARMACIE

THÈME :

Formulation of sustained drug release nanocomposite hydrogel beads of curcuminoids : In silico prediction of anticolorectal cancer

Présenté par :
GUENIFID Wassim
BOUKLI HACENE Anas

Soutenu le
03/07/2022

Jury

Président :	
Pr HIMEUR Zouleykha	Maitre de Conférences A en Dermatologie
Membres :	
Pr SELKA Adil	Maitre de Conférences A en Pharmacognosie
Dr BENATTA Dalila	Maitre assistante en Pharmacie Galénique
Dr LOUZIM Habiba	Maitre assistante en Chimie Thérapeutique
Dr KRID Meryem	Assistante en Toxicologie
Encadrant :	
Dr GUENDOUZ Souheyla	Maitre assistante en Pharmacie Galénique
Co-Encadrant	
Pr CHOUKCHOU BRAHAM Esma	Professeur en Chimie

Année universitaire : 2021-2022

Acknowledgements

First and foremost, we must acknowledge our limitless thanks to Allah, the Ever-Magnificent, the Ever-Thankful, for His help and bless. We are totally sure that this work would have never become truth, without His guidance.

We consider it as a great honor to express the heartfelt appreciation to our admirable supervisor **Dr. GUENDOUZ Souheyla**, and Thank for her willingness to offer continuous guidance, support and encouragement, which are driving forces for the completion of this thesis, her supervision, patience and warm support have made the research journey easier.

We would like to express our sincere thanks and gratitude to our co-supervisor **Pr. CHOUKCHOU-BRAHAM Esma** and **Pr. BENKHALED Amel** for their enormous contribution to this work, encouragement, and enthusiastic involvement in this project and for sharing their research experiences and making supportive suggestions and comments.

We take this opportunity to tell our special thanks to **Mr. TALEB Zoheir**, Engineer of Toxicomed Research Laboratory, for his assistance in experiments and for providing a nice environment of research. We are also thankful to **Dr. BELKHODJA Majid** Ph.D in Organic Chemistry and Macromolecules, for his continuous support and encouragement throughout our research studies.

We express our profound sense of gratitude to **Mr. BENAISSA Zakarya** engineer of the Galenic Pharmacy Laboratory for providing all the necessary laboratory products and for his immense friendly support in all the aspects of the study.

We owe our sincere thanks to the Laboratory of Catalysis and Synthesis in Organic Chemistry, Macromolecules Research Laboratory, Pharmacognosy Laboratory, for the sample analysis and characterizations of our research work.

We would like to sincerely thank our colleagues **Ms. MERZOUGUI Besma** and **Ms. MIDOUN Sarah** pharmacy interns for their help in laboratory experiments related to Curcuma *longa.* extraction and activation of Bentonite.

We extend our sincere gratitude to the president of the committee **Pr HIMEUR Zoleykha** and all the committee members **Pr. SELKA Adil, Dr. BENATTA Dalila, Dr LOUZIM Habiba, Dr KRID Meryem** for reviewing our thesis and for providing constructive comments and suggestions for its improvement.

We feel delighted to express our whole hearted gratitude to all those who gave their helping hands in completing our project successfully, We are also thankful to the Department of Pharmacy a Abou Bekr Belkaid University of Tlemcen for providing us such a great opportunity of higher studies.

Dedications

I would like to express my deepest grateful thank to my family especially my father, my mother, my brothers for supporting me throughout my studies and my life in general, without them I would not have reached up to this position. I owe a deep debt of gratitude to them for their hard work, sacrifice, and blessings led me on this path,

I wish to appreciate my sincere thanks to all my friends for their help, support, understanding and encouragement.

My appreciation goes to my cousin Dr. BERRAZEG Nezha Pharm.D for helping and supporting me throughout this thesis.

I owe my gratitude to all the persons who directly or indirectly have inspired, encouraged and helped me to pursue the path of success in my life.

Wassim

Dedications

To my dearest parents to whom I owe my success, without their sacrifices and encouragement, I could never have succeeded in my studies. No expression can express my gratitude and appreciation to them. May God the Almighty grant them long life and good health.

To my brother,

To my sister,

to all my family,

to all my friends,

Your constant encouragement has always been the most precious to me.

This thesis is dedicated to the memory of our dear friend SEDDIKI Adil, who passed away last year during the Covid-19 pandemic, we are very happy to have shared with you a part of your life, you had the art of cultivating friendship and good humor and you were always helpful. You were one of the most enlightened, noble and generous men. O Allah! Forgive him, have mercy upon him. Indeed we belong to Allah, and indeed to Him we will return.

Anas

Table of Contents

Acknowledgements i

Dedications iii

Table of Contents v

List of Figures viii

List of Tables xiii

List of abbreviations xiv

Introduction 1

Chapter I: Literature Review 4

Subchapter I: Curcuma longa 5

I.1 Curcuma longa 6

I.1.1 Turmeric 6

I.1.2 Curcumin 8

Subchapter II: Ionic Gelation 13

I.2 Ionic Gelation 14

I.2.1 Sodium Alginate 14

I.2.2 Bentonite 21

I.2.3 Hydroxypropyl methylcellulose 25

I.2.4 Characterizations 27

Subchapter III: Nanosuspension 29

I.3 Nanosuspension 30

I.3.1 Definition 30

I.3.2 Methods of Preparation of Nanosuspensions 30

I.3.3 Nanosuspension excipients 33

I.3.4 Evaluation of Nanosuspensions 34

I.3.5 Advantages of Nanosuspension 35

I.3.6 Disadvantages of Nanosuspension 35

Subchapter IV: In Silico Anticolorectal Cancer Prediction 36
I.4 In Silico Anticolorectal Cancer Prediction 37
I.4.1 Molecular Docking 37
I.4.2 Colorectal Cancer 43
Chapter II: Materials and Methods 49
II.1 Description of the study: 50
II.2 Aim and Objectives 50
II.3 Materials 51
II.3.1 Equipments 51
II.3.2 Chemicals 51
II.3.3 Laboratory glassware 51
II.3.4 Computational softwares 51
II.4 Methods 53
II.4.1 Preformulation 53
II.4.2 Formulation 60
II.4.3 Preparation 67
II.4.4 Controls and Characterizations 71
II.4.5 In Silico Molecular Docking 77
Chapter III: Results and Discussion 79
III.1 Powder identification 80
III.2 Curcuminoids Yield 81
III.3 Thin Layer Chromatography 82
III.4 Particule Size Distribution of Nanosuspension 83
III.5 Morphology and Size of Beads 85
III.6 Fourier transform infra red analysis 87
III.7 X-ray diffraction study 90
III.8 Drug entrapment efficiency 94
III.9 Drug loading 95
III.10 Swelling Test 96
III.10.1 Swelling Test in HCl (pH = 1.2) 96
III.10.2 Swelling Test in PBS (pH = 6.8) 97

III.11 Cumulative Drug Release 99
III.11.1 Calibration Curve 99
III.11.2 Cumulative Drug Release in HCl (pH = 1.2) 100
III.11.3 Cumulative Drug Release in PBS (pH = 6.8) 101
III.12 Study of Drug Release Kinetics 104
III.13 In Silico prediction 107
Conclusion 113
References 115

List of Figures

Figure 1 Hermann's drawing of *C. longa (18)*.....7
Figure 2 Turmeric powder (19).....7
Figure 3 Chemical structures of curcuminoids (23).....9
Figure 4 Keto enol tautomerization of curcumin (25).....9
Figure 5 Conventional extraction methods of curcuminoids (36).....11
Figure 6 Novel extraction methods of curcuminoids (36).....12
Figure 7 (Top) Chemical structures of α-L-guluronic acid and β-D-mannuronic acid residue monomer, (Bottom) (1-4) linkages of M blocks and G blocks: MM, MG, GG, and GM (46).....14
Figure 8 Schematic illustration of (top) egg box formation process and (bottom) egg box model of calcium alginate (49).....15
Figure 9 A schematic illustration showing the ionic gelation method (59).....17
Figure 10 Schematic illustration of the interaction between the calcium cross linking ions and the carboxyl groups of Alginate (62).....18
Figure 11 Chemical structure of Montmorillonite (88).....22
Figure 12 Interaction between Alginate and Montmorillonite (88).....24
Figure 13 Chemical structure of HPMC. The substituent R represents either a $–CH_3$, or a $–CH_2CH(CH_3)OH$ group, or a hydrogen atom (120).....26
Figure 14 Bragg's law for parallel planes (134).....28
Figure 15 Two models of molecular docking. (A) A lock-and-key model. (B) Induced fit model(158).....38
Figure 16 Molecular docking process (158).....40
Figure 17 TGF-β Signaling Pathway(189).....45
Figure 18 Analytical balance Ohaus.....52
Figure 19 Drying oven LabTech.....52
Figure 20 Ultrasonic cleaner Branson 200.....52
Figure 21 Centrifuge Sigma 3-18k.....52
Figure 22 Rotary evaporator Isolab Gmbh.....52
Figure 23 pH meter Starter 3000 Ohau.....52

Figure 24 UV-visible spectrophotometer Mecasys Optizen 2120 UV 52
Figure 25 Digital Vernier Caliper ADA mechanic 150 52
Figure 26 Degradation products of curcumin: (A) vanillin, (B) ferulic acid, (C)feruloylmethane, (D) vanillic acid, (E) ferulic aldehyde, (F) 4-vinylguaiacol, (G) p-hydroxybenzaldehyde, (H) p-hydroxybenzoic acid (216) 56
Figure 27 X-ray powder diffraction pattern of the crystal structure of commercially curcumin obtained from *Curcuma longa* (turmeric) containing at least 70% of curcumin (Sigma-Aldrich Chemie GmbH, Germany) (216) 58
Figure 28 Chemical structure of HPMC(57) 63
Figure 29 *Curcuma longa* rhizomes 67
Figure 30 Ultrasound assisted extraction of curcuminoids by acetone 67
Figure 31 Supernatant of the acetone extract centrifugation 67
Figure 32 Solvent separation by rotary evaporator 67
Figure 33 Sieving of Raw Bentonite 68
Figure 34 Bentonite suspension in aqueous sodium carbonate solution 68
Figure 35 Steps of preparation of nanosuspension by acid-base CO_2 assisted effervescence method (243) 69
Figure 36 Dripping of drug-polymers-clay mixtures of the F1 formulation on the cross linking solution by ionic gelation method 70
Figure 37 Dripping of drug-polymers-clay mixtures of the F2 formulation on the cross linking solution by ionic gelation method 70
Figure 38 Malvern Zetasizer ver. 6.30 instrument 72
Figure 39 ATR-FTIR instrument Cary 640 Agilent Technologies 73
Figure 40 Rigaku Miniflex 600X-Ray Diffractometer 73
Figure 41 3D structure of TGF-beta receptor I kinase (1rw8) in Discovery Studio 2021 77
Figure 42 3D structure of curcumin in Discovery Studio 2021 77
Figure 43 3D structure of demethoxycurcumin in Discovery Studio 2021 77
Figure 44 3D structure of bisdemethoxycurcumin in Discovery Studio 2021 77
Figure 45 Bright yellow coloring parenchymatous cells filled with gelatinized starch seen as rounded to oval cells with irregular walls 80
Figure 46 Large reticulately thickened vessel with regularly arranged rectangular pits. 80

Figure 47 Starch granule 80
Figure 48 Unicellular, elongated and bluntly pointed trichome attached to fragments of epidermis 80
Figure 49 *Curcuma longa* powder 81
Figure 50 Amount of curcuminoids extracted 81
Figure 51 TLC of separated curcuminoids 82
Figure 52 Particle size distribution by Intensity of Curcuminoids Nanosuspension 83
Figure 53 Yellow colored curcuminoids nanosuspension at pH of 4.8 83
Figure 54 Orange-red colored curcuminoids nanosuspension at neutral pH 83
Figure 55 Morphology of F1 Beads before Drying 85
Figure 56 Morphology of F1 Beads after Drying 85
Figure 57 Morphology of F2 Beads before Drying 85
Figure 58 Morphology of F2 Beads after Drying 85
Figure 59 Size of F1 Beads 86
Figure 60 Size of F2 Beads 86
Figure 61 Comparison of FTIR spectra of raw and sodium activated bentonite 87
Figure 62 FTIR Spectra of Curcuminoids Hydrogel Beads, F1 without HPMC, F2 with HPMC 88
Figure 63 XRD patterns of raw bentonite and sodium bentonite 90
Figure 64 XRD patterns of curcuminoids, sodium bentonite and F2 hydrogel beads 92
Figure 65 $CaCl_2$ 2% (w/v) cross-linking solution containing the free drug remained and curcuminoids beads 94
Figure 66 Calibration curve of curcuminoids in methanol 95
Figure 67 Swelling Test of F1 in HCl (pH = 1.2) 96
Figure 68 Swelling Test of F2 in HCl (pH = 1.2) 96
Figure 69 Swelling behavior curves of curcuminoids loaded hydrogel beads in simulated gastric fluid HCl (pH = 1.2) 96
Figure 70 Swelling Test of F1 in PBS (pH = 6.8) 97
Figure 71 Swelling Test of F2 in PBS (pH = 6.8) 97
Figure 72 Swelling behavior curves of curcuminoids loaded hydrogel beads in simulated intestinal fluid PBS (pH = 6.8) 97

Figure 73 Calibration curve of curcuminoids nanosuspension in PBS (pH=6.8) for the drug release 99
Figure 74 Cumulative Drug Release of F1 in HCl (pH = 1.2) 100
Figure 75 Cumulative Drug Release of F2 in HCL (pH = 1.2) 100
Figure 76 Cumulative drug release curves of curcuminoids loaded hydrogel beads in simulated gastric fluid HCl (pH = 1.2) 100
Figure 77 Cumulative Drug Release of F1 in PBS (pH = 6.8) 101
Figure 78 Cumulative Drug Release of F2 in PBS (pH = 6.8) 101
Figure 79 Cumulative drug release curves of curcuminoids from nanocomposite hydrogel beads in simulated intestinal fluid PBS (pH = 6.8) 101
Figure 80 Schematic mechanism of curcumin release and degradation of microspheres. (a) Egg-box model in calcium alginate microspheres loaded curcumin, (b) Na^{+} ions replace Ca^{2+} ions, microspheres swells up, curcumin diffuses out; and (c) disruption of 'egg-box' model, alginate matrix is disintegrated and dissolves (287) 102
Figure 81 Adsorption of drugs on the negatively charged bentonite layers (288) 103
Figure 82 Release behavior of curcuminoids from nanocomposite hydrogel beads at pH=1.2 and pH=6.8 (259) 103
Figure 83 Zero order drug release plot of F1 beads 104
Figure 84 First order drug release plot of F1 beads 104
Figure 85 Higuchi drug release model plot of F1 beads 104
Figure 86 Korsmeyer-Peppas drug release model plot of F1 beads 104
Figure 87 Zero order drug release plot of F2 beads 105
Figure 88 First order drug release plot of F2 beads 105
Figure 89 Higuchi drug release model plot of F2 beads 105
Figure 90 Korsmeyer-Peppas drug release model plot of F2 beads 105
Figure 91 3d graphical visualization of the binding mode of curcumin against TGF- β receptor I kinase 107
Figure 92 3d graphical visualization of the binding mode of demethoxycurcumin against TGF- β receptor I kinase 107
Figure 93 3d graphical visualization of the binding mode of bisdemethoxycurcumin against TGF-β receptor I kinase 107

Figure 94 Hydrogen bond binding pocket of curcumin againstTGF- β receptor I kinase..... 108
Figure 95 Hydrogen bond binding pocket of demethoxycurcumin against TGF- β receptor I kinase 108
Figure 96 Hydrogen bond binding pocket of demethoxycurcumin against TGF- β receptor I kinase 108
Figure 97 3d graphical illustration of the interaction between curcumin and TGF- β receptor I kinase 109
Figure 98 3d graphical illustration of the interaction between demethoxycurcumin and TGF- β receptor I kinase 109
Figure 99 3d graphical illustration of the interaction between bisdemethoxycurcumin and TGF- β receptor I kinase 109
Figure 100 Schematic interaction between curcumin and TGF- β receptor I kinase, green dashed lines indicate hydrogen bonds 110
Figure 101 Schematic interaction between demethoxycurcumin and TGF- β receptor I kinase, green dashed lines indicate hydrogen bonds 110
Figure 102 Schematic interaction between bisdemethoxycurcumin and TGF- β receptor I kinase, green dashed lines indicate hydrogen bonds 110

List of Tables

Table I Characteristics of AutoDock software(159) 39
Table II IR spectroscopy peaks of curcumin (216) 57
Table III Chemical composition of Maghnia Raw Bentonite obtained X-ray Fluorescence analyses (228)..... 64
Table IV Mineral content of Maghnia Raw Bentonite determined by XRD (228) 64
Table V Final product formulas of F1 and F2 hydrogel beads 70
Table VI Retention factors of the different components of curcuminoids separated on silica TLC plate (246) 82
Table VII Z-average and Polydispersity index of Curuminoids Nanosuspension 83
Table VIII qualitative analysis of the main components of raw bentonite 90
Table IX Entrapment efficiency of the 2 formulations: F1 and F2 94
Table X Drug Loading of the formulations F1 and F2 95
Table XI Summary of the various kinetic models followed by F1 and F2 formulations 106
Table XII Molecular docking results of curcumin, demethoxycurcumin and bisdemethoxycurcumin against TGF β I..... 111

List of abbreviations

% (w/v) : weight per volume

°C : Celsius

2D : two-dimensional

3D : three-dimensional

A : Alite

Å : angström

Akt : serine/threonine kinase 1

Al_2O_3 : Aluminum Oxide

AMPK : Adenosine monophosphate-activated protein kinase (AMPK)

AP-1 : Activator protein 1

ARG : Arginine

ASP : Aspartic acid

ATR: Attenuated Total Reflection

Ba^{2+} : Barium (II) ion

Bad : BCL2 Antagonist of Cell Death

Bak : Bcl-2 homologous antagonist/killer

Bax : BCL2-Associated X Protein

Bcl 2 : B-cell lymphoma 2

Bcl-xl : B-cell lymphoma-extra large

BDMC: Didemethoxycurcumin

Ca^{2+} : Calcium ion

$CaCl_2$: Calcium chloride

CaO : Calcium oxide

CDKs : Casein-Dependant Kinase

CEC : Cation exchange capacity

CO_2 : carbon dioxide

COO^- : Carboxylate

COX : cyclo-oxygenase

cP : centipoise – viscosity unit

CRC: Colorectal cancer

CRM : Chromosome region maintenance

Cu : Copper

Cur: Curcumin

D : Diaspore

Dab-2 : disabled 2

DL: Drug loading

DLS: Dynamic light scattering

DMC:Monodemethoxycurcumin

DNA : Deoxyribonucleic Acid

EC : ethyl cellulose,

EE: Entrapment efficiency

EGF : Epidermal growth factor

EGFR : Epithelial Growth Factor Receptor

ERK1/2 : extracellular signal-regulated kinase 1/2

F1 : Formulation 1

F2 : Formulation 2

FA : Ferulic aldehyde,

Fe_2O_3 : Iron Oxide

FTIR: Fourier transformed infrared

G: α-L-guluronic acid

G1 phase : growth 1 phase

GA : genetic algorithm

GLU : Glutamic acid

GS domain : glycine- and serine-rich domain

GTP : guanosine triphosphate.

H_3O^+ : Hydronium ion

HCl: Hydrochloric acid

HCT-116 : human colorectal carcinoma cell line

HDCs : histone deacetylase

HIS : Histidine

HPLC: high performance liquid chromatography

HPMC: Hydroxypropylmethylcellulose

HPTLC : High performance thin-layer chromatography

IL-1 : interleukin-1

IL-6 : Interleukin 6

IL-8 : Interleukin 8

ILE : Isoleucine

iNOS : induced nitric oxide synthase

IR: Infrared

K_2O : Potassium oxide

KH_2PO_4 : Potassium Dihydrogenphosphate

kV : Kilovolt

LGA : lamarckian genetic algorithm

LYS : Lysine

M : Montmorillonite

mA : Milliampere

MAPK : Mitogen-activated protein kinase

MC : Methyl cellulose

MCP : Monocyte chemotactic protein-1

MDAMB-231: M.D. Anderson - Metastatic Breast 231

Mg^{+2} : Magnesium ion

MgO : Magnesium Oxide

MH 1 domain : MAD homology 1 domain

MH 2 : Mad-homology 2 domain

MMP -9 : Matrixmetalloproteinase-9

MMPs : Matrix metalloproteinases

MMT: Montmorillonite

Na^{+} : Sodium ion

Na_2CO_3 : Sodium Carbonate

Na_2HPO_4 : Disodium hydrogenphosphate

Na_2O : Sodium oxide

NaB: Sodium Bentonite

Na-CMC : sodium carboxymethylcellulose

$NaHCO_3$: Sodium Bicarbonate

NaOH : Sodium hydroxide

NF-κB : Nuclear factor kappa B

$-OCH_3$: methoxy group

P : Portlandite

p27 : universal cyclin-dependent kinase inhibitor

p38 : mitogen-activated protein kinases

PBS: Phosphate buffer solution

PCS: Photon Correlation Spectroscopy

PDB : Protein data bank

PDGF : Platelet-derived growth factor

PDI: Particles dispersion index

PEG: Polyethylene glycol

pH: Hydrogen potential

PI3K : Phosphatidylinositol 3-kinase

pK_a : log of Ka acid dissociation constant

PKC : Protein kinase C

PS : Particle size

PVP: polyvinyl pyrrolidone

R^2 : correlation coefficient

Rab 5 : Ras-associated binding 5

RCSB : Research Collaboratory for Structural Bioinformatics

Rf: Retention factor

Rpm: Rounds per minute

R-Smads : receptor-regulated Smads

SA: Sodium alginate

SARA : phospholipid-pound carrier

SBE : Smad-binding element

SDF : structural data file

SDS: Sodium dodecylsulfate

SER : Serine

Si : Silicon

SI: Swelling index

Si^{4+} : Silicon(4+)

SiO_2 : Silicon dioxide

Smad : SMA "small" worm phenotype" MAD family ("Mothers Against Decapentaplegic"

SNX6 : sortin nexin 6

SO_3 : Sulfur trioxide

Sr^{2+} : Strontium ion

STAT 3 : Signal transducer and activator of transcription 3

SW480 : human colorectal carcinoma cells

TGF-β : Transforming growth factor beta

TiO_2 : Titanium dioxide

TLC: Thin layer chromatography

TRAP-1 : Tumor necrosis factor receptor-associated protein 1

UV: Ultra violet

VA : Vanillic acid

VEGF : vascular endothelial growth factor.

Wnt : Wingless/Integrated

XRD: X-Ray Diffraction

β2SP/Smad4 : β2-spectrin adaptor protein / smad4

Θ : Theta angle between incident beam of R-ray and crystallographic reflecting plane

Λ : Lambda wavelength of the incident X-Ray beam

Introduction

Cancer is one of the most severe diseases with increasing morbidity and mortality every year around the world. According to statistics in the United States, colorectal cancer is the world most common cancer and the third leading cause of cancer death in both male and female (1, 2).

In spite of the development of novel powerful treatment, chemotherapy still plays an important role in the management of colon carcinoma. However, drug toxicity and undesirable side effects are the major impediments to a successful chemotherapeutic regimen, such as nausea and vomiting, diarrhea, white blood cell decreased, anemia, fatigue, nerve damage, pain, and skin reactions etc (3).

Curcumin is a nature yellow colored and low molecular weight polyphenol compound purified from the rhizome of the plant *Curcuma longa*. (4). Curcumin has been found as a component of many traditional medicines for a long time in Southeast Asia countries (India and China). Curcumin has various pharmacological activities, such as anti-inflammatory, anti-oxidant, and anti-tumor effects etc (5). In addition, Cur has been under investigation in human clinical trials for many years and has indicated clinical benefits for patients with colorectal cancer (6-8).

Despite of the safety and the broad pharmacological effects of Cur, the application in clinic has been hampered due to its extremely poor oral bioavailability resulted of low aqueous solubility, instability, and rapid metabolism (9, 10). Therefore, drug delivery systems, are needed to improve the solubility of curcumin to facilitate the targeted release of curcumin within the intestinal environment.

Different techniques were used to overcome the drawbacks of curcumin, with recent attention focusing on approaches based on encapsulation and nanotechnology. Clay-polymer nanocomposites are getting to play a role in formulations for drug delivery. This is due to their improved pharmaceutical properties, and sustained drug release characteristics compared to their individual components, clays and polymers.

Alginate/Na-Bentonite nanocomposite are used as drug delivery system for a wide variety of drugs due to numerous advantages of both components such as the high loading capacity of MMT and the ability of alginate release encapsulated drugs in a controlled manner.

The present work focuses on the nanocomposite hydrogel beads using sustained drug delivery materials. As well as the study of anti-colorectal cancer effect by in silico computational tools. The first chapter (**Chapter I**) is divided to four subchapters:

The first subchapter provides an overview on the Curcuma *longa* plant, curcuminoids, and biological properties of curcumin and methods of extraction. **The second subchapter** focuses on the polymers such as sodium alginate and HPMC, and the clay material like bentonite, these excipients have the swelling and the sustained release properties for the oral drug delivery of curcuminoids, additionally methods of characterizations are briefly described in this part.

The third subchapter covers the definition of a nanosuspension, methods of preparation and characterization to produce an enhanced solubility formulation that can be used as an intermediate for the incorporation of the drug inside nanocomposite hydrogel beads. **The fourth subchapter** is a review on colorectal cancer previous studies, TGF beta 1 receptor signaling pathway and the molecular docking computational approach that helps the understanding of the binding lignad into its receptor.

The second chapter (**Chapter II**) provides the materials used for the study and steps from preformulation to formulation of curcuminoids nanosuspension and polymers-clay nanocomposite hydrogel beads of curcuminoids to achieve the sustained release of curcuminoids.

Next, **Chapter III** focuses on the results and discussion of different swelling, entrapment, drug release controls of the nanocomposite beads and characterizations of the raw materials, intermediate and final formulations, besides that, the in silico prediction results of the binding of curcuminoids to TGF beta 1 receptor are also shown.

Finally a conclusion of the overall present study where future outcomes can be expected to raise for the possibility of using the drug delivery systems to poorly soluble bioactive compounds and in silico applications for the potential effect against diseases after its delivery to the receptor .

Chapter I: Literature Review

Subchapter I: Curcuma longa

I.1 Curcuma longa

I.1.1 Turmeric

Curcuma longa is a perennial herb commonly known as turmeric belonging to the family Zingiberaceae. It is distributed in tropical and subtropical regions throughout the world and widely cultivated in Asian countries, mostly in India and China (11, 12). It is known for its coloring, flavoring, and medicinal properties for thousands of years. It is believed that it has reached Europe via Silk Road from India and was initially used as a dye. Later, it has been used in coloring foods (13).

I.1.1.1 Turmeric Rhizomes

The rhizome of C. longa plant is oblong, ovate, pyriform, and short branched. The rhizomes are 5 to 8 cm long and 2 to 3 cm wide. A nature plant has 10 to 15 such rhizomes which are connected to a bulb. Rhizomes have a brownish yellow skin with few scales, bright orange-yellow flesh and a spicy aroma. The plant has a leafy body which can grow more than a meter (rarely) and has eight to twelve leaves (13).

Fresh rhizome contains 11 to 13% water, 6 to 8% protein, 5 to 10% fat, 60 to 70 % carbohydrates, 2 to 7% fiber (14). Curcuminoids content depends on many factors such as place of cultivation, irrigation cycle, seed quality etc., and typically ranges from 3 to 9% with an average content of around 5%.

Turmeric is mostly imported as a whole rhizome, which is then processed into powder or oleoresin by flavor houses and the industrial sector (15, 16). Rhizomes come as fingers, ulbs and splits. Fingers are the secondary branches from the mother rhizome, the bulb, and splits are the bulbs cut into halves or quarters before curing (16, 17). The fingers are 2 to 8 cm long and 1 to 2 cm wide, and are easier to grind than the more fibrous bulbs and splits, and therefore command a higher price (15).

Figure 1 Hermann's drawing of *C. longa (18)*

Figure 2 Turmeric powder (19)

I.1.1.3 Turmeric Powder

Ground turmeric is mostly used on the retail market, and by the food processors. Rhizomes are ground to approximately 60-80 mesh particle size (20). Since curcuminoids, the color constituents of turmeric, deteriorate with light and to a lesser extent, under heat and oxidative conditions (20), it is important that ground turmeric be packed in a UV protective packaging and appropriately stored.

Turmeric powder is a major ingredient in curry powders and pastes. In the food industry, it is mostly used to color and flavor mustard (15), It is also used in chicken bouillon and soups, sauces, gravies, and dry seasonings (17). Recently the powder has also been used as a colorant in cereals (20).

I.1.1.4 Oleoresin

An oleoresin is a mixture of compounds such as volatile oils, fixed oils and other solvents which provide a distinct flavor. Any combination of such compounds which distracts the mixture from original flavor or quality (depending on end use) cannot be an oleoresin (16).

Turmeric extractives, or oleoresins, are obtained by solvent extraction of the powdered rhizome. This process yields about 12 % of an orange/red viscous liquid depending on the solvent used for extraction and on the turmeric type and cultivar. The compounds of interest in turmeric oleoresin are the curcuminoids (40 to 55%), and the volatile oils (15 to 20%) (21).

I.1.2 Curcumin

Curcumin, also known as diferuloylmethane, is the most active curcuminoid found in the rhizome of *Curcuma longa*. Basically, curcuminoids are polyphenolic compounds, which are responsible for the yellow coloration of turmeric. Demethoxycurcumin (DMC) and bis-demethoxycurcumin (BDMC) are two different types of curcuminoids present in turmeric (22).

The chemical structure of curcuminoids is shown in Figure 3. Curcumin is a major secondary metabolite of the perennial Asian plant turmeric (*Curcuma longa*).

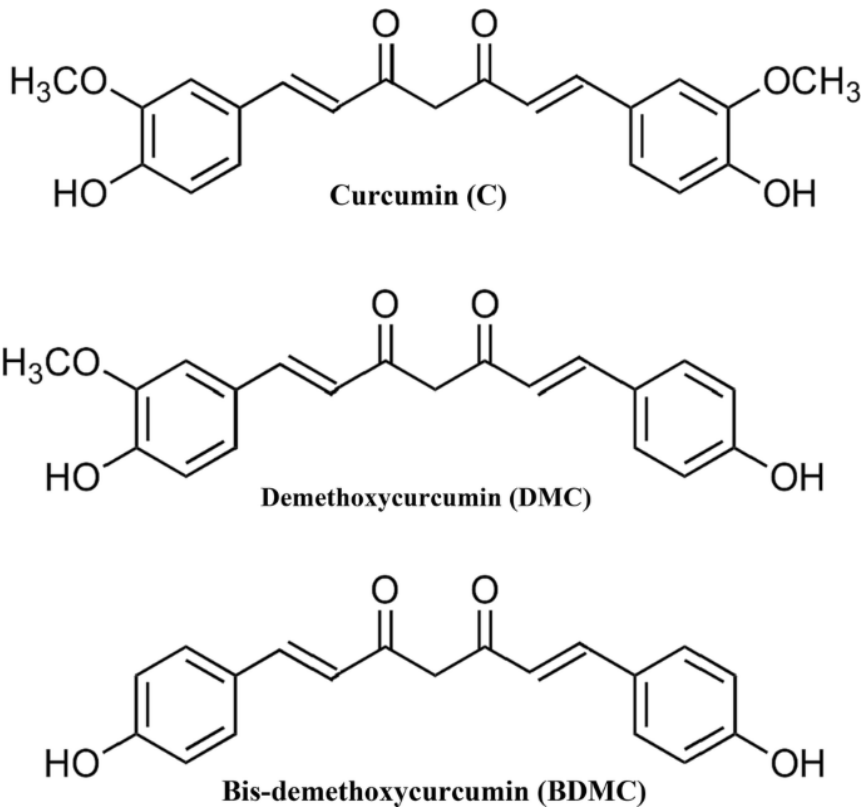

Figure 3 Chemical structures of curcuminoids (23)

Curcumin is a natural compound, which is hydrophobic in nature. It's a symmetric molecule that consists of two polyphenolic rings, which are substituted by methoxy ether at the ortho position, the phenolic groups are connected by a seven carbon link consisting of an α,β-unsaturated β-diketone. The diketo group exhibits a keto-enol tautomerization of curcumin arises in a pH-dependent condition (24). Keto-enol tautomers are indicated in Figure 4.

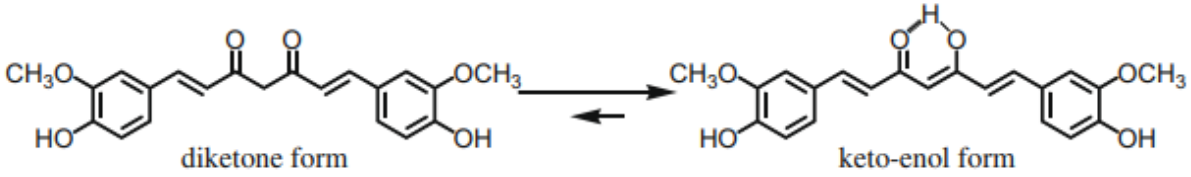

Figure 4 Keto enol tautomerization of curcumin (25)

I.1.2.1 Properties of Curcumin

I.1.2.1.1 Anti-inflammatory property of curcumin

The presence of keto form and double bonds in the structure of curcumin are mainly responsible for its anti-inflammatory action (26). Curcumin has been known to control various enzymes, proteins, protein kinase, cytokines and transcription factors, which are related to the process of inflammation (27). From previous work of researchers, it was found that curcumin is an anti-inflammatory agent whose activity can be compared with that of steroidal and nonsteroidal drugs indomethacin and phenylbutazone (28). Studies of curcumin have focused mainly on the cyclo-oxygenase (COX) enzyme, which is used for the conversion of arachidonic acid to prostaglandin and decreases the synthesis of prostaglandin (28, 29).

I.1.2.1.2 Antioxidant property of curcumin

Researchers have studied the antioxidant property of curcumin and its derivatives demethoxycurcumin and bisdemethoxycurcumin (28). Curcumin exhibits a higher superoxide-scavenging activity compared to demethoxycurcumin and bisdemethoxycurcumin (26). Research revealed that curcumin prevents the oxidation of hemoglobin at a concentration of 0.08 mm. The lower level of oxidation induced by nitrate can be inhibited by diacetyl curcumin (27).

Moreover, curcumin is active against the oxidative damage of DNA, proteins, and is protective against chronic diseases such as cancer, atherosclerosis, neurodegenerative diseases, and aging (30).

I.1.2.1.3 Anticancer property of curcumin

The in vitro activity of curcumin is tested on animal models like rats. The studies demonstrated that curcumin has the potential to inhibit carcinogenesis at three stages: tumor promotion, angiogenesis, and tumor growth (31). Curcumin has been nominated as an anticancerous agent by the National Institute of Cancer (30, 32). It has been reported that curcumin has been recognized as an agent that can induce apoptosis, suppresses cell cycle progression, and finally prevents cancerous cell growth progression (33, 34).

I.1.2.2 Extraction of Curcuminoids

Several extraction and purification processes of curcumin from turmeric are in practice at the laboratory and industrial scales. Laboratory extraction methods include Soxhlet, microwave, ultra-sonic, and supercritical extraction.

Conventional extraction methods, such as Soxhlet extraction, maceration or solvent extraction, are widely used to extract curcumin from plants. These methods are simple, but are generally non-selective, are time consuming and in some cases cause degradation of heat-sensitive substances (35).

To surmount such obstacles, novel extraction methods such as, ultrasound-assisted extraction, microwave-assisted extraction, enzyme-assisted extraction, and supercritical liquid extraction have been developed as more efficient alternatives to conventional extraction. These advanced techniques, which are regarded as eco-friendly green technologies (36).

Ultra-sonic assisted extraction is similar to the microwave assisted extraction except for that ultra-sonic waves are employed instead of microwaves. Here the power of sonication is kept constant. Also, when acetone is used as a solvent, yields of curcumin are high. Ultra-sonic assisted extraction yields less amount of curcumin when compared to microwave assisted extraction (37).

Power and time of irradiation, choice of solvent are the major factors which affect the amount of curcumin extracted. It is found that high amount of curcumin is extracted when acetone is used as a solvent (38).

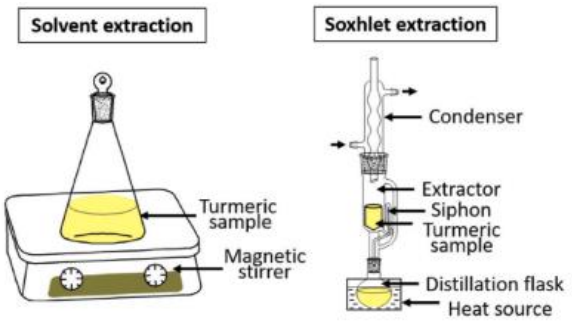

Figure 5 Conventional extraction methods of curcuminoids (36)

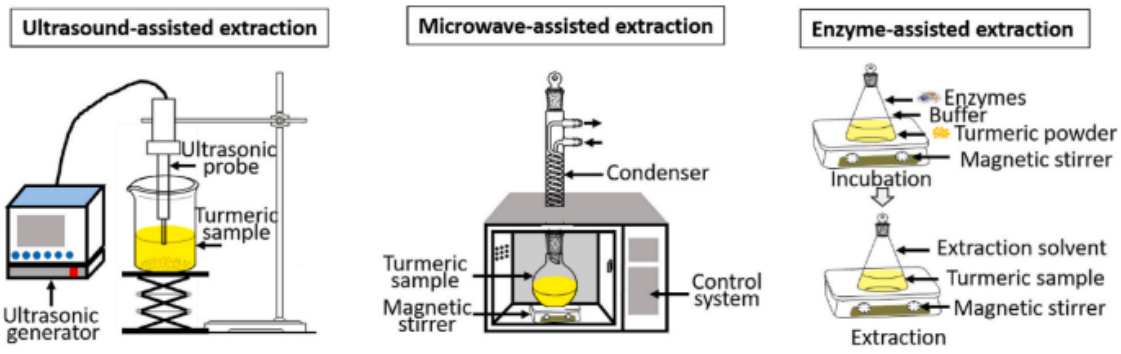

Figure 6 Novel extraction methods of curcuminoids (36)

I.1.2.3 New Curcumin Delivery Systems

The water insolubility and low bioavailability of curcumin in cells have prompted researchers to develop new formulations based on biocompatible organic substances like liposomes, polyethylene glycols, biopolymers, cellulose, corn oil, hydrogels etc. (39-41).

All these systems have not only shown improved water solubility but also increased curcumin bioavailability. Due to their biocompatibility all these systems could be successfully investigated for anti-cancer activity in cancer cells, and in vivo systems, where significant increase in the anticancer activity due to improved bioavailability of curcumin was reported (42).

Subchapter II: Ionic Gelation

I.2 Ionic Gelation

Ionic gelation is a chemical reaction between sodium alginate and calcium chloride, where the sodium ions are replaced by the calcium ions to form a gel-like structure. This unique property of the alginate makes it a suitable material for encapsulation of bioactive compounds (43).

I.2.1 Sodium Alginate

I.2.1.1 Definition

Alginate is a naturally occurring anionic polysaccharide obtained from brown seaweed algae, from three different species: Ascophyllum nodosum, Laminaria hyperborean, and Macrocystis pyrifera and occurs as a mixture along with various types of cations: Na^{+} , Mg^{+2}, Sr^{2+} and Ba^{2+}, in nature (44) Alginate is commercially available in a powder form of sodium alginate, which is also called alginic acid sodium salt.

I.2.1.2 Molecular structure

Sodium alginate is a water soluble biopolymer compound that has linear polysaccharide fibers. The linear fibers consists of (1-4) linkages of α-L-guluronic acid (G) and β-D-mannuronic acid (M) residues, meaning that α-L-guluronic acid and β-D-mannuronic acid residues bind each other and form alginate fibers (45).

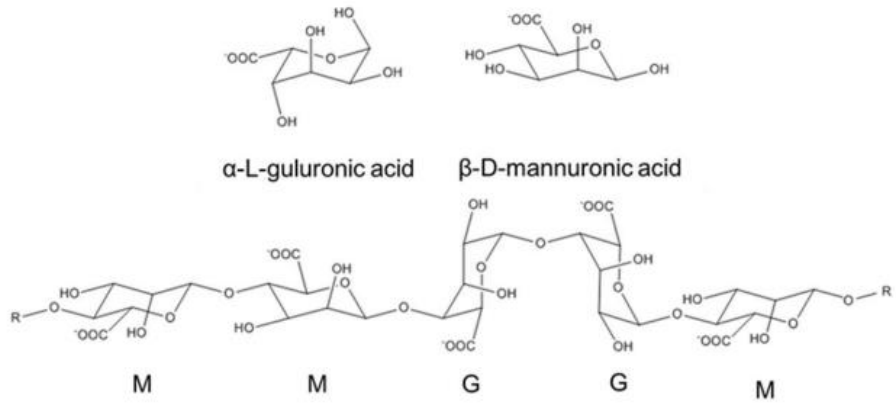

Figure 7 (Top) Chemical structures of α-L-guluronic acid and β-D-mannuronic acid residue monomer, (Bottom) (1-4) linkages of M blocks and G blocks: MM, MG, GG, and GM (46)

.

The unique conformations of residues: α-L-guluronic acid (G) and β-D-mannuronic acid (M), provide homogenous blocks of MM and GG, and it can also be alternating blocks of MG and GM. G block is aligned vertically, while M block is arranged horizontally. Hence, the configuration of two GG blocks that face against each other provides a little space for a divalent cation to be entrapped inside of the cavity of two GG blocks.

This special structural result is called an egg box model, which will further form alginate gels. The flat configuration of MM or alternating sequence of MG or GM, is not suitable for confining divalent cations. After forming egg box structures, each egg box structure is stacked with other structures to produce a gel network. This process undergoes aqueous sol-gel transformation under mild conditions which provides an ideal environment for drug encapsulation because no external forces are applied to damage the carrier (47, 48).

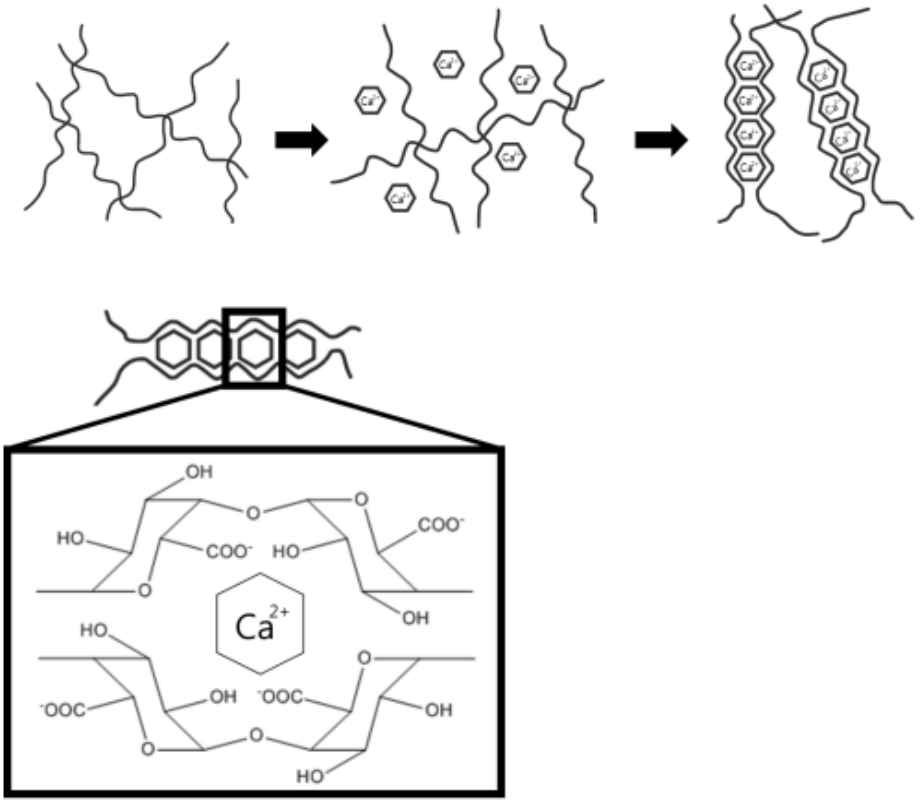

Figure 8 Schematic illustration of (top) egg box formation process and (bottom) egg box model of calcium alginate (49)

I.2.1.3 Molecular weight

The molecular weight of alginate generally falls in the range of 32- 400 kDa depending on their sources, species, or extraction process (50-52). Molecular weight of alginate can significantly influence its gelling properties, including swelling, shrinking, mechanical rigidity, and ability to resist monovalent cations interference. Alginate may lose part of its biological activity if the molecular weight is reduced, which accordingly affects the performance of its functional characteristics (45, 53, 54).

I.2.1.4 Immunogenicity and Biocompatibility

Biocompatibility and immunogenicity of materials are important factors for successful application in carriers for drug delivery. Chemical composition and the mitogenic contaminants found in alginates are the two main contributors to alginate immunogenicity (55). Alginate is known to exhibit minimum cytotoxic effects and reduced hemolysis when in contact with blood. Alginate biocompatibility has been studied by injecting calcium alginate into kidney capsules of rats, and it has been reported that calcium alginate is biocompatible (56).

I.2.1.5 Toxicity

Calcium alginate gels are found to be non-toxic to cells and hence are suitable for drug delivery. Numerous studies have tested the high level of safety of sodium alginate in foods. Allergy tests conducted with sodium alginate have shown that the material is not allergic. Sodium alginate has not been shown to possess any eye or skin irritation properties (57).

I.2.1.6 Preparation of Alginate-based Beads by Ionic Gelation

The ionotropic gelation is a very simple method and inexpensive by using polysaccharides (alginate, gellan and pectin) dissolved in water or in weak acidic medium. These solutions are then added drop wise via a needle, a pipette or a burette to a gently agitated cross linking solution containing counter ions (58).

Due to the complexation between charged polysaccharides (Chitosan, sodium alginate, gellan, pectin) and the counter ions (calcium chloride, barium chloride, zinc chloride, copper chloride, cobalt chloride, pyrophosphate) gelation occurs to form spherical particles (microcapsules or beads). The beads are then separated by filtration washed with distilled and dried.

Figure 9 A schematic illustration showing the ionic gelation method (59)

I.2.1.6.1 Size and shape of the beads

In general, beads are greater than 1.0 mm in diameter; the diameter of the beads formed is dependent on the size of the needle used and the viscosity of the alginate solution. A larger diameter needle and higher viscosity solutions will produce larger diameter beads (60). The viscosity of SA can also influence the shape of the beads produced. The beads become more spherical as the concentration of SA increased. However, in general SA solutions of greater than 5% are difficult to prepare.

I.2.1.6.2 Molecular interactions

Formulation of delivery devices for drugs under aqueous conditions are desirable to avoid the undesirable decrease of bioactivities which may occur when using organic solvents and/or heat during formulations. Since relatively stable alginate gels can be formed in aqueous environments through chelation or complexation, which are more promising delivery of matrixes for bioactive compounds. It has been suggested that the cross links were caused either by ionic bridging of two carboxyl groups on adjacent polymer chains via calcium ions or by chelation of single calcium ions by hydroxyl and carboxyl groups on each of a pair of polymer chains (61).

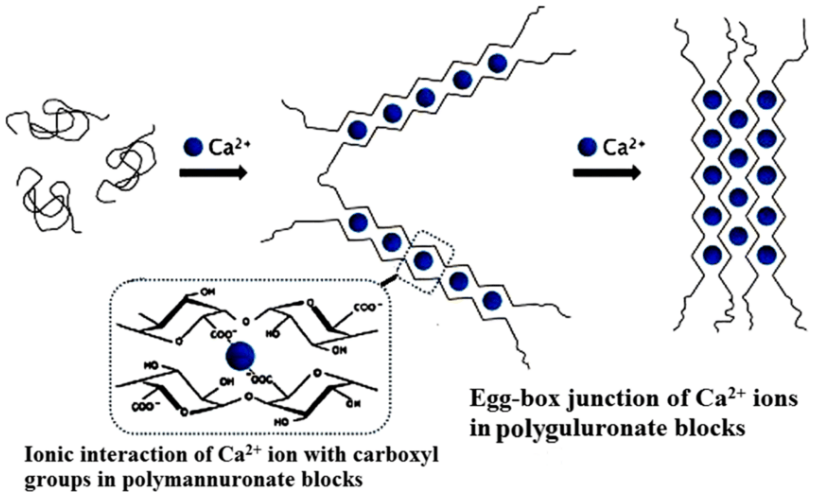

Figure 10 Schematic illustration of the interaction between the calcium cross linking ions and the carboxyl groups of Alginate (62)

Monovalent metal ions form soluble salts with alginate whereas divalent and multivalent cations (except Mg^{2+}) form gels or precipitates. The various cations show different affinity for alginate, and selective ion binding is the basis for the ability of alginate to form ionotropic hydrogels. Alginates with a high content of guluronic acid blocks give gels of considerably higher strength compared to alginates rich in mannuronate, as the G residues exhibit a stronger affinity for divalent ions than the M residues (63).

I.2.1.6.3 pH sensitivity of Calcium Alginate beads

Release of drugs from alginate beads in low pH solutions is significantly reduced which could be advantageous in the development of an oral delivery system (64-66). Theoretically, alginate shrinks at low pH (gastric environment) and the encapsulated drugs are not released (67). In gastric fluid, the hydrated sodium alginate is converted into a porous, insoluble. Once passed into the higher pH of the intestinal tract, the alginic acid skin is converted to a soluble viscous layer. This pH dependent behaviour of alginate can be exploited to customize release profiles. However, the rapid dissolution of alginate matrices in the higher pH ranges may result in burst release of drugs. Therefore many modifications in the physicochemical properties are needed for the prolonged controlled release of drugs (44).

When calcium alginate beads are treated with HCl 0.1M, alginate gets hydrolyzed to lower molecular weight fractions of alginic acid. Due to conversion of COO^- group into unionized carboxylic group, the electrostatic attraction between Ca^{2+} ions and COO^- ions in the egg-box junction almost disappears. Moreover, there may occur ion-exchange between H^+ ions (presence in the external HCl solution) and free Ca^{2+} ions inside the beads. Thus a reduced Ca^{2+} ions concentration within the beads results in a weaker Ca^{2+} cross linked beads when put in phosphate buffer at pH 7.4. Therefore, the acid-treated beads are a loosely cross linked structure containing more soluble alginate as constituent (68).

When such beads are put in the phosphate buffer of pH 7.4, the beads swell at faster rate but do not attain a higher water uptake value due to loosely bound structure of the beads which is unable to retain large amount of water within the matrix. Moreover, there is possibility of ion-exchange between H^+ ions produced due to ionization of carboxylic groups in the buffer of pH (68).

Alginate gel beads seem to be most effective in retarding drugs at higher alginate concentrations (69). The cross-linker type and concentration seem to have a pronounced influence on the drug release (70-72). Calcium alginate beads displayed prolonged release profiles when compared to alginate beads prepared from other cross-link agents like Ba^{2+} and Sr^{2+} (73).

Combinations of liposomes and alginate have been investigated in order to modify the release of drugs from such phospholipid vehicles and to stabilize the products. Alginate either served as a vehicle for the liposomes (74) or formed a gel inside the liposome (75) leading to stabilization and a delayed drug release respectively. Alginates are demonstrated to have antioxidative activity and will thereby further stabilize the liposome preparation (76)

Highly lipophilic drugs can be incorporated into alginate microspheres by use of a multiple-phase emulsion technique (77). The drug is dissolved in oil (e.g., soybean oil) and the resulting alginate microspheres contain immobilized drug containing oil microdroplets. The microspheres can be coated further, allowing a pH-dependent release.

I.2.1.7 Pharmaceutical Applications

Alginates have attracted much attention as a potential device for controlling drug release (hydrophilic and hydrophobic). Alginate has been successfully used as a matrix for entrapment and/or delivery of drugs (78) and bioactive molecules such as proteins or growth factors (79-82).

The encapsulation and release of proteins from alginate gels can increase their efficacy and release (83). The molecules are encapsulated into the polymers, for their protection and controlled release (79).

They have many advantages such as the following: they protect the stomach mucosa from the aggressive drug effect or protect acid-sensitive drugs from gastric fluid, they offer a controlled drug delivery, and they are non-toxic when orally administered (84-86). Drugs with non-favorable solid-state properties (e.g., low solubility) benefit from encapsulation, too.

I.2.2 Bentonite

I.2.2.1 Definition

Bentonite is a natural clay containing clay minerals in the smectite group that was formed by devitrification of volcanic ash that fell into water (87). Bentonite was named after Fort Benton near Rock River, Wyoming, USA where it was originally found, by W.C. Knight in 1898. This clay has excellent swelling, adsorption, and colloidal properties.

Raw bentonite is composed of diverse mineral substances, such as quartz, cristobalite, feldspars, zeolites, and several kinds of clay minerals. Above all, the major component of bentonite is montmorillonite, which is a dioctahedral smectite. The swelling and adsorption properties of bentonite originate from montmorillonite. Pure montmorillonite is necessary for the medical applications, and it can be obtained by purifying raw bentonite (88)

I.2.2.2 Montmorillonite

Montmorillonite is a porous clay mineral composed of a 2:1-layered structure with exchangeable cations between the layers (89). The thickness and breadth of each nanoclay sheet are around 1 and 100–1000 nm, respectively (90). The 2:1 layer consists of two tetrahedral silica sheets sandwiching an octahedral sheet of alumina. In this layer, substituting the Si^{4+} in the silica tetrahedral sheets to Al^{3+} and the Al^{3+} in the alumina octahedral sheets to Mg^{2+} produces a net negative charge, which is usually balanced by adsorption of cations, such as Li^{+}, Na^{+}, and Ca^{2+}, between the layers (89, 91). These cations can be easily replaced by other organic or inorganic cations, which is related to the unique hydrophilicity, swelling, adsorption, and fluidity properties of montmorillonite (92).

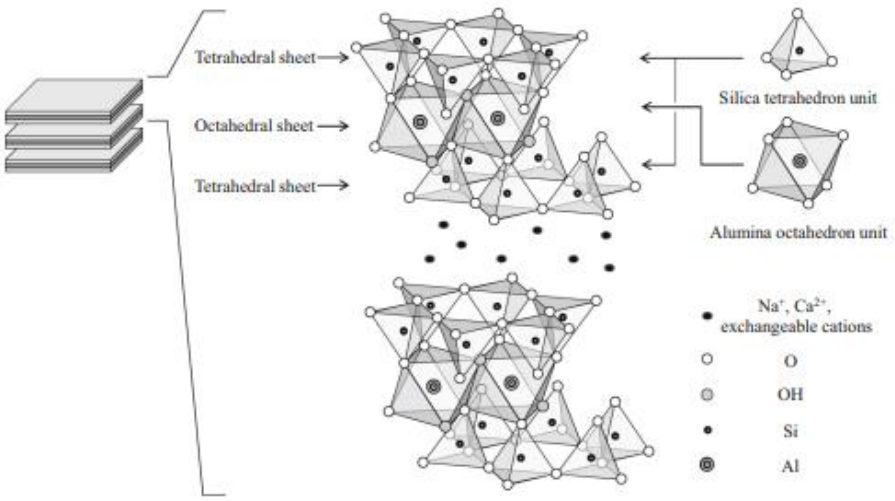

Figure 11 Chemical structure of Montmorillonite (88)

I.2.2.3 Sodium montmorillonite versus calcium montmorillonite

The characteristics of montmorillonite can be altered based on the cations adsorbed in the interlayers, such as sodium and calcium. Industrial bentonite mainly contains either sodium montmorillonite or calcium montmorillonite, which have different physical properties, so each montmorillonite-based bentonite is used in different fields.

Sodium montmorillonite can expand its original volume by absorbing a large volume of water, and its swelling capacity is higher than that of calcium montmorillonite. In addition, sodium montmorillonite has great colloidal and rheological properties, so it has been used in many industrial applications, including drilling mud and sealants (93, 94).

On the other hand, calcium montmorillonite has less swelling capability than that of sodium montmorillonite. However, it has excellent green strength among mineral binders, so it is useful as a bonding agent in foundry molding sands (93). In addition, it has strong adsorption activity against various solutions and oils, so calcium montmorillonite also has medical applications, such as detoxification (95).

I.2.2.4 Swelling property of Montmorillonite

One of the unique physical properties of montmorillonite is that it exhibits a hydrophilic property and swells with water. As the surface of a montmorillonite sheet has a negative charge, H_3O^+ from autoionization of water easily infiltrates into the interlayer (96). This hydrophilicity contributes to the swelling of montmorillonite.

The physical state of montmorillonite changes from an anhydrous solid to a hydrated material, semi-rigid plastic, gel, and suspension with increasing water content (97-100). The change in physical state from an anhydrous solid to a gel is called swelling Sodium montmorillonite has the capability to increase its volume up to 20 times by absorbing water (97). The swelling occurs as ions are hydrated when water enters the 2:1 layers and is followed by osmotic absorption of water. This swelling pattern depends on the mineralogy, size, negative charge, and hydration energy of exchangeable cations (97, 101, 102).

I.2.2.5 Application of montmorillonite in controlled drug delivery systems

Although drugs have specific therapeutic effects, they also have pharmaceutical limitations, such as poor absorption, rapid elimination, and low bioavailability. Insufficient bioavailability can be caused by low solubility and/or poor permeation (103).

It is also possible to prolong duration of action by preparing a sustained-release formulation (104, 105). Moreover, a solubilizing effect can be achieved by applying a carrier system to hydrophobic drugs, which enhances bioavailability. Similar to other polymers, montmorillonite has been investigated in drug delivery systems.

The adsorption property of montmorillonite usually contributes to enhance drug entrapment and sustained-release. In addition, montmorillonite affects the physical and mechanical properties of the formulation, including elasticity and tensile strength of a gel or film.

I.2.2.6 Alginate / Bentonite formulation

Alginate can be used to fabricate drug-loaded gel-based beads using this gelation mechanism. Generally, alginate beads show faster drug release under a higher pH, so alginate is useful to prepare pH sensitive drug carriers. Moreover, the beads disintegrate easily in a high pH environment, which causes rapid drug release, so it cannot be used as a sustained release system.

To overcome these drawbacks, alginate-montmorillonite-based hydrogel formulations have been proposed (106-112). alginate does not intercalate with the montmorillonite interlayer. However, as the edges of the montmorillonite layer are positively charged, they interact with alginate electrostatically to enhance rigidity of the alginate matrix (107, 109).

Montmorillonite enhances drug encapsulation and decreases drug release rate from an alginate matrix because of its adsorption property (106, 110, 112, 113). Even after incorporating montmorillonite, an alginate-based formulation shows more rapid drug release in a neutral condition than that in an acidic condition (106, 110, 111) because the protonated carboxyl group of alginate maintains intermolecular hydrogen bonds under low pH (110). However, the negatively charged carboxyl group loses a hydrogen bond in neutral pH and is affected by the intermolecular repulsive force (114). This phenomenon induces swelling and disintegration of the alginate formulation, which cause rapid drug release.

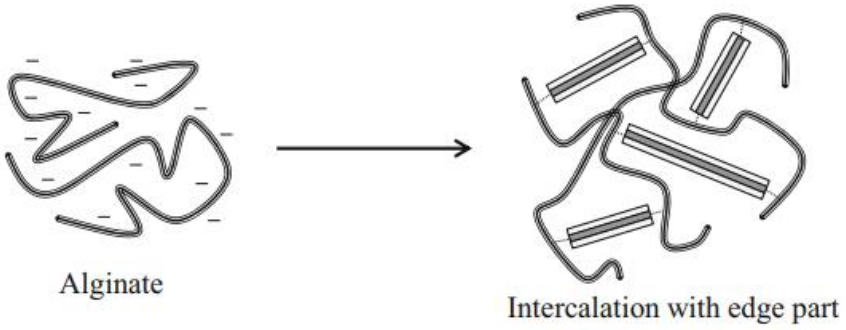

Figure 12 Interaction between Alginate and Montmorillonite (88)

I.2.3 Hydroxypropyl methylcellulose

I.2.3.1 Definition

Hydroxypropyl methylcellulose (HPMC) is a semisynthetic, inert, viscoelastic polymer used as an excipient in pharmaceutical formulations and a controlled-delivery component in oral medicaments (115).

It is a non-ionic, odourless, tasteless, white or creamy white fibrous or granular powder. It is soluble in cold water, forming a viscous colloidal solution; practically insoluble in hot water, chloroform, ethanol (95%), and ether, but soluble in mixtures of ethanol and dichloromethane, mixtures of methanol and dichloromethane, and mixtures of water and alcohol. It is available in several grades that vary in viscosity and extent of substitution (116).

HPMC contains a two-fold helix conformation similar to MC and cellulose but the presence of -OCH_3 and hydroxypropoxy groups (- $CH_2CH(OH)CH_3$) on Anhydroglucose units induce steric hindrance which opens up the cellulose backbone in a similar manner to MC. This modification in chemical structure of HPMC also confers the ability to dissolve in cold water same (117). However, the presence of different levels of -$CH_2CH(OH)CH_3$ groups in various HPMC grades affects their gelation behavior (118).

Many commercial hypromelloses are identified by codes. For instance, for those manufactured by the Dow Chemical Company, the first part of the nomenclature is a letter (E, F or K) that relates to the degree of substitution. The K grades (hypromellose 2208) have a methoxy substitution of 19–24% and a hydroxypropyl substitution of 7–12%. F grades (hypromellose 2906) have a methoxy substitution of 27–30% and a hydroxypropyl substitution of 4.0–7.5%. E grades (hypromellose 2910) have a methoxy substitution of 28–30% and a hydroxypropyl substitution of 7–12% (Dow Commercial Information 2002) (119).

One of its most important properties is its high swelling property, which has a significant impact on the release kinetics of the incorporated drug (120) .

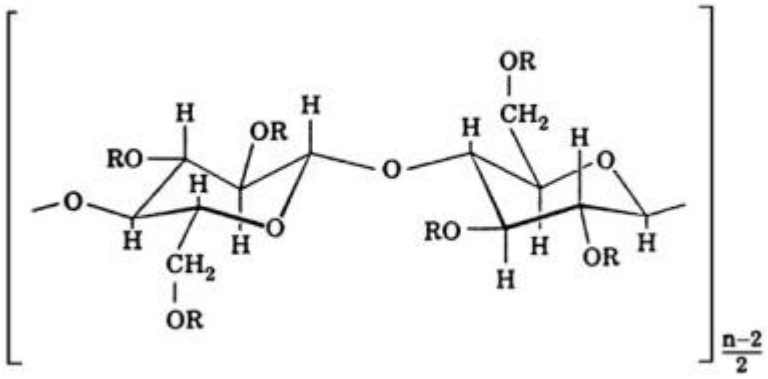

Figure 13 Chemical structure of HPMC. The substituent R represents either a $–CH_3$, or a $–CH_2CH(CH_3)OH$ group, or a hydrogen atom (120).

I.2.3.2 Applications as extended release excipient

Cellulose derivatives are very simple and efficient systems for controlling drug release from dosage forms. Cellulose ethers, in particular MC and HPMC, are widely used to develop extended release hydrophilic matrices (121, 122).

Hydrophilic matrices effectively increase the duration of release of a drug to prolong its therapeutic effect. Following ingestion, it is important for the drug to be released in a controlled manner (123).

Varying concentration of HPMC can be used to delay or control the drug release profiles regardless of their solubility characteristics, however, the relative solubility of the drug can affect the release mechanism; water soluble drugs are released mainly by diffusion but poorly water soluble drugs are released predominantly by erosion (123, 124).

I.2.4 Characterizations

I.2.4.1 Fourier transform infrared (FTIR) analysis

Infrared Spectrometry (IR) is a widely used technique in both research and industry. It is a simple and reliable technique for the identification of unknown materials, determination of the amount of components in a mixture as well as for quality control of materials (125).

Infrared (IR) spectroscopy gives molecular structural information using the frequencies of the vibrational modes for a compound (126). IR is a type of energy absorption spectroscopy that uses the infrared region of the electromagnetic spectrum. Fourier Transform Infra Red (FTIR) spectroscopy is a measurement technique whereby IR spectra are collected by using a time domain measurement. The original IR spectrometers are of the dispersive or filter types. They measure the amount of energy at each frequency of the IR spectra with the aid of a prism or grating. FTIR uses an interferometer which measures the signal and performs a Fourier transform on the data to provide an IR spectrum (125).

There are several advantages for FTIR over dispersive IR methods such as (125): The measurement time is faster, simultaneous measurement can be performed, It is a non-destructive technique, It requires no external calibration, inexpensive, provides improved sensitivity and resolution and it has mechanical simplicity.

Advancements in computing techniques have enabled FTIR to become a popular tool to characterize various types of materials including polymers, Molecular reaction mechanisms of biomolecules have been studied using time resolved FTIR (127).

In Pharmaceutical research, FTIR is used to identify and analyze structure of drugs, excipients, polymorphism (128) and dissolution (129), Drug polymer interaction studies can be performed using this technique in dosage forms containing nanoparticles (130).

I.2.4.2 X-ray diffraction (XRD)

X-ray diffraction (XRD) is a widely used technique to assess the crystallinity and structure of solid samples. In summary, the crystal X-ray diffraction phenomenon results from a scattering process in which X-rays are scattered by the electrons of atoms present in the sample without changing the wavelength. Since X-rays have wavelengths (between 0.2 and 10 nm) comparable to the interatomic spacing of a crystalline solid, the incident X-ray beam diffracts in specific directions predicted by Bragg's law. The resulting diffraction pattern, given by the positions and intensities of the diffraction effects, is a fundamental physical property of the material, providing not only the identification but also the complete elucidation of its structure to demonstrate the crystalline or amorphous nature of a solid or a powder, as well as to determine the different crystalline phases (131).

Bragg's law can be used to relate the X-ray half-scattering angle θ to the aforementioned spacing parameter, d.

$$n\lambda = 2d \sin\theta \qquad (132)$$

The parameter λ is the wavelength of the incident X-ray radiation, with a typical value of approximately 1.54 Å for a Cu X-ray radiation source. n is an integer and can best be understood through the explanation of why Bragg's law holds. Consider a case of many parallel scattering planes each of which is a collection of previously introduced point-scattering centers reflecting incoming X-ray radiation of wavelength λ at the angle θ (133). The two diffracted waves will interfere with each other either constructively (adding together to produce stronger peaks) or destructively (subtracting from each other to some extent) (134, 135).

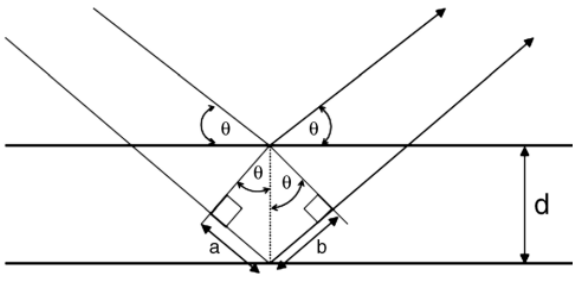

Figure 14 Bragg's law for parallel planes (134)

Subchapter III: Nanosuspension

I.3 Nanosuspension

I.3.1 Definition

Size reduction to nanometer range has been shown to be a very promising approach as it increases specific area and thus leads to enhanced dissolution characteristics and increased system exposure (136). Thus, the poor solubility may be overcome by particle size reduction using nanoscience approaches.

One of the nanoscience approaches that have quickly gained a proven record within the pharmaceutical sciences is the formulation as nanosuspension (137). Nanosuspensions for drug delivery have gained much interest as way to address solubility problems (138).

Nanosuspension of drug is a sub-micron colloidal dispersion of pure particles of the drug, which is stabilized by surfactants (139). Production of drugs in the form of nanosuspension was shown to be more cost effective and technically simpler alternative, particular for poorly soluble compounds (136, 140).

The small particle size and increased surface area which can lead to an enhanced dissolution rate and improved bioavailability is the main advantages of nanosuspension (141). Thus, formulating as drug nanosuspension has significant importance to improve its physicochemical properties, especially its solubility and bioavailability.

I.3.2 Methods of Preparation of Nanosuspensions

I.3.2.1 Bottom Up Technology

The conventional methods of precipitation are called Bottom Up technology. Using a precipitation technique, the drug is dissolved in an organic solvent and this solution is mixed with a miscible anti-solvent. In the water-solvent mixture the solubility is low and the drug precipitates. Precipitation has also been coupled with high shear processing. The Nano-edge process (is a registered trademark of Baxter International Inc. and its subsidiaries) relies on the precipitation of friable materials for subsequent fragmentation under conditions of high shear and/or thermal energy (142). This is accomplished by a combination of rapid precipitation and high-pressure homogenization. Rapid addition of a drug solution to an anti-solvent leads to sudden supersaturation of the mixed solution, and generation of fine crystalline or amorphous

solids. Precipitation of an amorphous material may be favored at high supersaturation when the solubility of the amorphous state is exceeded.

I.3.2.2 Top-Down Technology

The Top-Down technologies mainly include the insertion of a drug fluid dispersion into the equipment where particle size reduction is achieved various ways such as high pressure homogenization or media milling (10). When the ‘‘top-down” technique is used, the drug often exists as crystalline state (143).

I.3.2.2.1 High pressure homogenization

High pressure homogenization has been used to prepare nanosuspension of many poorly water soluble drugs (144). In the high-pressure homogenization method, the suspension of a drug and surfactant is forced under pressure through a nanosized aperture valve of a high-pressure homogenizer. The principle of this method is based on cavitation in the aqueous phase. The particles cavitations forces are sufficiently high to convert the drug microparticles into nanoparticles. The concern with this method is the need for small sample particles before loading and the fact that many cycles of homogenization are required.

I.3.2.2.2 Lipid emulsion template

Lipid emulsions as templates are applicable for drugs that are soluble in either volatile organic solvents or partially water miscible solvents. This technique follows an organic solvent or mixture solvent loaded with the drug dispersed in an aqueous phase containing suitable surfactants to form an emulsion. The organic phase is then evaporated under reduced pressure to make drug particles precipitate instantaneously to form the nanosuspension which is stabilized by surfactants.

I.3.2.2.3 Media milling

Nanocrystal is a patent protected technology developed by Liversidge et al. In this technique, the drug nanoparticles are obtained by subjecting the drug to media milling. High energy and shear forces generated as a result of impaction of the milling media with the drug provide the necessary energy input to disintegrate the microparticulate drug into nanosized particles. In the media milling process, the milling chamber is charged with the milling media,

water or suitable buffer, drug and stabilizer. Then the milling media or pearls are rotated at a very high shear rate. The major concern with this method is the residues of milling media remaining in the finished product could be problematic for administration.

I.3.2.2.4 Dry co-grinding

Recently, nanosuspensions can be obtained by dry milling techniques. Successful work in preparing stable nanosuspensions using dry-grinding of poorly soluble drugs with soluble polymers and co-polymers after dispersing in a liquid media has been reported. Itoh et al reported the colloidal particles formation of many poorly water-soluble drugs; griseofulvin, glibenclamide and nifedipine obtained by grinding with polyvinylpyrrolidone (PVP) and sodium dodecylsulfate (SDS). Many soluble polymers and co-polymers such as PVP, polyethylene glycol (PEG), hydroxypropyl methylcellulose (HPMC) and cyclodextrin derivatives have been used. Physicochemical properties and dissolution of poorly water soluble drugs were improved by co-grinding because of an improvement in the surface polarity and transformation from a crystalline to an amorphous drug.

I.3.2.3 CO_2-assisted in situ nanoamorphization

The process utilizes an organic solvent to dissolve water-insoluble drugs along with organic acids and stabilizers. Then, the organic solvent is evaporated—leaving an organic acid-phase material. Finally, drug nanosuspensions are obtained following the addition of aqueous carbonate, which rapidly generates CO_2 bubbles by acid-base reaction. Alternatively, the solid acid-phase material can be blended with dry carbonate and prepared into final solid dosage forms at a later time. Of importance, the nanosuspensions could not be produced in the absence of the organic acid or carbonate; rather, the drugs gradually aggregated together and precipitated over time. In this new approach, CO_2 bubbles exert a rapid micro-mixing effect to suppress crystal growth while stabilizers simultaneously absorb onto the hydrophobic surface of the drugs and prevent aggregation and agglomeration. Unlike the top-down and bottom-up techniques, it was demonstrated that the drugs of final nanosuspensions existed as amorphous form. Ideally, formulated nanosuspensions occur in the amorphous form to improve solubility and the dissolution rate (145).

I.3.3 Nanosuspension excipients

I.3.3.1 Stabilizer

The main function of a stabilizer is to wet the drug particles thoroughly, and to prevent ostwalds ripening and agglomeration of nanosuspension in order to yield a physically stable formulation by providing steric or ionic barrier. The type and amount of stabilize has a pronounced effect on the physical stability and in vivo behavior of nanosuspension. Stabilizers that have been used so far are poloxomers, polysorbate, cellulosics, povidones, lecithins and Tween 80 (146).

I.3.3.2 Organic Solvent

Organic solvents are used in the formulation of nanosuspension if emulsions or microemulsions are used as a template. The pharmaceutically acceptable less hazardous water miscible solvent, such as methanol, ethanol, chloroform, isopropanol, and partially water miscible solvents ethyl acetate, ethyl formate, butyl lactate, triacetin, propylene carbonate, benzyl alcohol, are preferent in the formulation over the conventional hazardous solvents, such as dichloromethane (146).

I.3.3.3 Other additives

Nanosuspensions may contain additives such as buffers, salts, polyols, osmogent and cryoprotectant, depending on either the route of administration or the properties of the drug moiety (146).

I.3.4 Evaluation of Nanosuspensions

I.3.4.1 Dynamic Light Scattering (DLS)

DLS is also known as Photon Correlation Spectroscopy (PCS), Quasi-elastic Light Scattering, and Diffusing Wave Spectroscopy (147). It is used to determine the particle size, and size distribution. It can also measure the polydispersity index (PDI) of various types of samples including nanoparticles, colloids, gels, emulsions, pigments, liquid crystals, DNA, polymers and proteins (148). It can measure submicron particles in the range of 0.6 nm to 6 µm.

DLS provides a type of diameter of samples called Z-average diameter which means diameter based of laser scattering intensity.

The polydispersity index (PDI) can also be measured from Dynamic light scattering instruments. PDI is an index of width or spread or variation within the particle size distribution. Monodisperse samples have a lower PDI value, whereas higher value of PDI indicates a wider particle size distribution and the polydisperse nature of the sample.

There are several advantages for using the DLS method such as non-destructive, noninvasive technique, no need for calibration, small volume of sample. It also doesn't require extensive sample preparation, has a short analysis time, and modest development costs. Particle size, size distribution (including the polydisperisity index) can be measured for various systems such as proteins, polymers, micelles, carbohydrates, nanoparticles, colloidal dispersions, emulsions and microemulsions (149, 150).

I.3.5 Advantages of Nanosuspension

- Enhance the solubility and bioavailability of drugs.

- Suitable for hydrophilic drugs.

- Higher drug loading can be achieved.

- Dose reduction is possible.

- Enhance the physical and chemical stability of drugs.

- Provides a passive drug targeting [101, 102].

I.3.6 Disadvantages of Nanosuspension

- Sedimentation.

- It is bulky and sufficient care must be taken during handling and transport.

- Improper dose.

- Uniform and accurate dose cannot be achieved [102].

Subchapter IV:

In Silico Anticolorectal Cancer Prediction

I.4 In Silico Anticolorectal Cancer Prediction

I.4.1 Molecular Docking

I.4.1.1 Definition

Molecular docking (151) is a structure-based drug design method that simulates the molecular interaction and predicts the binding mode and affinity between receptors and ligands.

Molecular Docking is a method which anticipates the favored orientation of ligand against receptor (Protein) to make a stable complex (152). Favored orientation possibly utilized to predict the strength of connection or binding affinity among ligand and protein by utilizing scoring functions. Docking is often applied to anticipate the binding orientation of drug candidates against protein targets in order to predict the affinity and activity of the drug. Therefore docking plays a pivotal role in the drug design and discovery process (153).

The main aim of molecular docking is to computationally simulate the molecular identification process and accomplish an optimized conformation so that the free energy of overall system is minimized. The process of discovery of a new drug is a very difficult task. Modern drug discovery is mainly based In-silico–chemico biological approach. Use of computer aided techniques in drug discovery and development process is rapidly gaining popularity, implementation and appreciation (154).

In recent years, this technology has been widely used in drug design research field. Using the compounds database to screen the potential pharmacophores is not only convenient for researchers to purchase, synthesize and complete follow-up pharmacological tests, but also greatly improves the efficiency and reduces the research cost.

I.4.1.2 Types of Molecular Docking

Molecular docking is utilized to simulate the optimal conformation according to the complementarity and pre-organization, which could predict and obtain the binding affinity and interactive mode between ligand and receptor (151).

Figure 15 below shows the first proposed "lock-and-key model" (155), which refers to the rigid docking of receptors and ligands to find the correct orientation for the "key" to open up the "lock". This model emphasizes the importance of geometric complementarity.

However, the real docking process is so flexible that receptors and ligands have to change their conformation to fit each other well. Thus, we develop "induced fit model" (156). Based on geometric complementarity, the energy complementarity and pre-organization guarantee that receptors and ligands would obtain the most stable structure in such a manner that minimizes the free energy (157).

Flexible Docking-In induced fit docking both the ligand and the receptor are conformationally flexible. Every rotation the surface cell occupancy and energy is calculated; later the most optimum pose is selected.

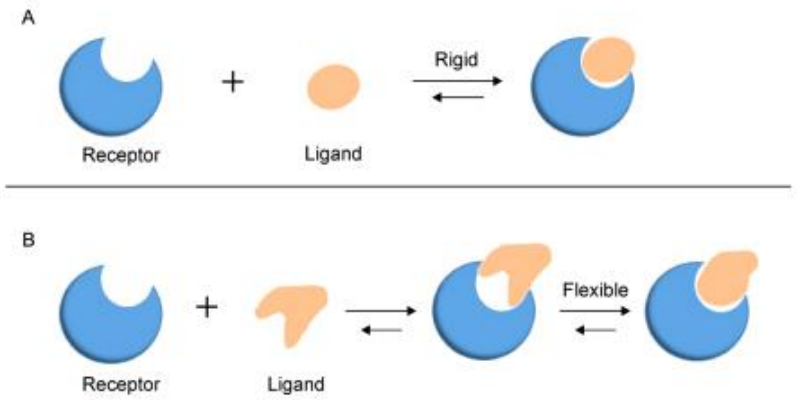

Figure 15 Two models of molecular docking. (A) A lock-and-key model. (B) Induced fit model(158)

I.4.1.3 Molecular Docking Softwares

The molecular docking software can help us to find the optimal conformation and orientation according to complementarity and pre-organization with specific algorithm, followed by applying a scoring function to predict the binding affinity and analyze the interactive mode.

I.4.1.3.1 AutoDock

Table I Characteristics of AutoDock software(159)

Name	Search algorithm	Evaluation method	Speed	Features & Application areas
AutoDock	GA (genetic algorithm) LGA (lamarckian genetic algorithm)	Semi-empirical calculation on free energy	Medium Flexible-rigid docking	This software is always used with Autodock-tools and it is free for academic use

I.4.1.3.2 Autodock Tools

A Graphical interface for setting up and running AutoDock, it's an automated docking software designed to predict how small molecules, such as substrates or drug candidates, bind to a known 3D structure receptor.

I.4.1.3.3 BIOVIA Discovery Studio Visualizer :

A free molecular modeling software for displaying, and analyzing protein and small molecular data.

.

I.4.1.4 Major steps involved in molecular docking

Molecular Docking is the process in which the intermolecular interaction between 2 molecules was studied in In-silico. In this process, the Macromolecule is the protein receptor. The micro molecule is the Ligand molecule which can be acted as an inhibitor. So, the Docking process involves the following steps:

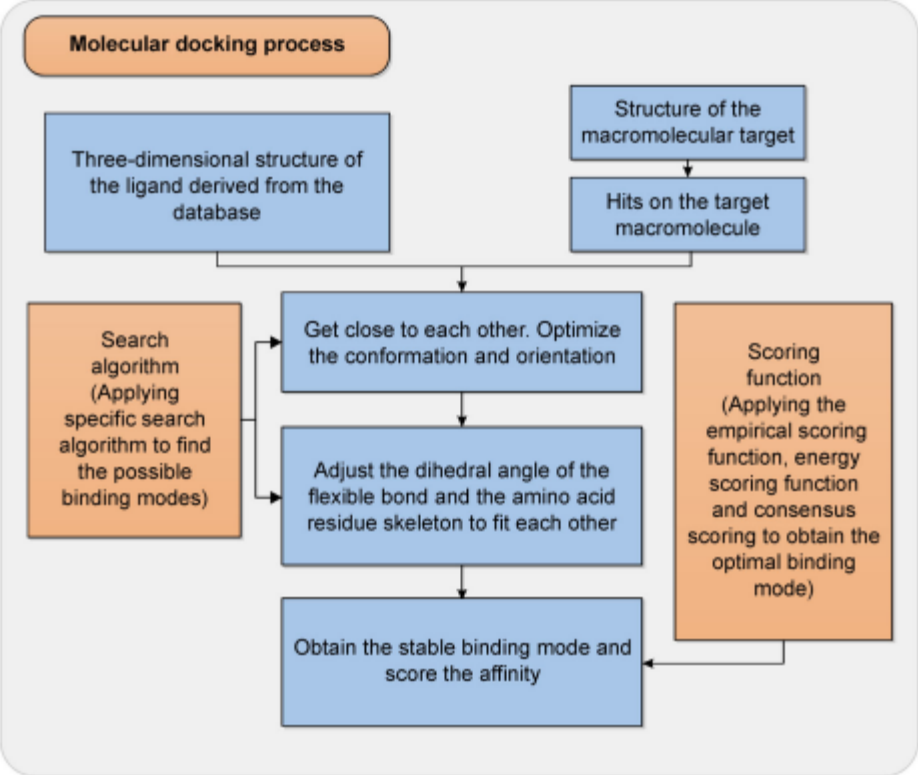

Figure 16 Molecular docking process (158)

Step I – preparation of protein

Three dimensional structure of the Protein should be retrieved from Protein data bank (PDB); afterward the retrieved structure should be pre-processed. This should admit removal of the water molecules from the cavity, stabilizing the charges, filling the missing residues, generation the side chains etc. according to the parameters available.

Step II – active site prediction

After the preparation of protein, the active site of protein should be predicted. The receptor might possess lots of active sites merely the one of the concern should be picked out. Mostly the water molecules and hetero atoms are removed if present (160, 161).

Step III – preparation of ligand

Ligands can be retrieved from several databases such as ZINC, PubChem or can be sketched applying Chemsketch tool. While picking out the ligand, the LIPINSKY'S RULE OF 5 should be utilized. Lipinski rule of 5 assists in discerning amongst non-drug like and drug like candidates. It promises high chance of success or failure due to drug likeness for molecules abiding by with 2 or more than of the complying rules. For choice of a ligand allowing to the LIPINSKY'S RULE:

1. Less than five hydrogen bond donors
2. Less than ten hydrogen bond acceptors
3. Molecular mass less than 500 Da
4. High lipophilicity (expressed as LogP not over 5)
5. Molar refractivity should be between 40-130

Step IV- docking

Ligand is docked against the protein and the interactions are analyzed. The scoring function gives score on the basis of best docked ligand complex is picked out (154).

I.4.1.5 Scoring Function

The scoring function furnishes a mode to rank positioning of ligands proportional to some other. Ideally, the score should correspond directly to the binding affinity of the ligand for the protein, so that the best scoring ligands are the best binders. Scoring functions can be empirical, knowledge based, or molecular mechanics based. Scoring is actually compiled of three different expressions applicable to docking and drug design:

1. Generated configurations ranking by the docking search.

2. Ranking different ligands against protein (virtual screening).

3.One or more ligands ranking against different proteins by their binding affinity (selectivity and specificity) (162-164).

I.4.1.6 Different Types of Molecular Interactions

Interaction forces are generally separated into four classes:

1. Electrostatic forces - dipole-dipole, charge-dipole and charge-charge.

2. Electrodynamics forces- Van der Waals interaction.

3. Steric forces - Caused by entropy.

4. Solvent-related forces - Hydrogen bond and hydrophobic interactions (165, 166).

I.4.2 Colorectal Cancer

I.4.2.1 Definition

Colorectal cancer is the second most common type of malignancy and the fourth leading cause of the cancer related death worldwide (167). In terms of cancer etiology, and CRC as a particular example, the mechanism of cancer development is a complex multistage process, involving sequential mutational events occurring along with progression of the cancer (168).

I.4.2.2 Colon Cancer Signaling Pathways

EGFR/ MAPK, Notch, PI3K, TGF-β and Wnt signaling pathways are implicated in the regulation of several biological processes, including cell proliferation, differentiation, angiogenesis, apoptosis and survival (169).

I.4.2.2.1 TGF-β signaling pathway

TGF-β signaling has the potential to function as a tumor suppressor and regulates various biological processes including cell growth, differentiation, apoptosis, extracellular matrix modeling, and immune response (170).

Three TGF-β isoforms are expressed in mammals (TGF-β1, TGF-β2, and TGF-β3). Each is encoded by a unique gene and expressed in both a tissue-specific and developmentally regulated fashion (171).

Once activated, the TGF-β ligands regulate cellular processes by binding to three high-affinity cell surface receptors—the type 1 TGF-β receptor (TβRI), the type 2 TGF-β receptor (TβRII), and the type 3 TGF-β receptor (TβRIII) serine/ threonine kinases—on the cell surface and induce heterotetrameric receptor complexes (171, 172).

Activated receptors recruit adaptors such as disabled 2 (Dab-2) and sortin nexin 6 (SNX6) that majorly affect TGF-β signaling transduction.(173, 174).

Rab 5 (GTPases) assists the movement of activated receptor complex to early endosomal compartments, where they encounter SARA (phospholipid-pound carrier) that assist to present the major signaling effectors, Smad to the TβRI(175, 176).

The activated TβRI phosphorylates a subclass of Smads called receptor activated Smads (R-Smads) such as Smad2 and Smad3 (177).

In addition, Smads consist of N-terminal MH 1 domain and phospho-serine binding c-terminal domain (Mad-homology 2 domain) (178).

Activated R-Smads bind to the phosphorylated GS domain and the L45 loop of the TβRI via their Madhomology 2 (MH 2) domain and get phosphorylates at both serine residues of their conserved c-terminal sxs motifs (174, 179-181)

This changes the R-Smads conformation and leads to rapid dissociation of R-Smads from the receptor and SARA (182-184)

The c-terminal phosphoserines of R-Smad are recognized by the Mad-homology 2 (MH2) domain of another Smad to lead to homo-oligomerization of R-Smads or heretooligomerization with the unique common partner Smad (Co-Smad) called Smad 4 (174, 182).

Smad 4 is anchored to the cytoplasm by TRAP-1 (scaffolding protein) and is joined to the activated R-Smads (174). TRAP-1 can assist the oligomerization of R-Smad/Co-Smad. The Smad 4 binds high affinity to the R-Smad phosphorylated tails through MH2 domain and form hetero-oligomeric Smads. Phosphorylated Smad 3 binds with importin-β1 and is imported to the nucleus (181).

The Ran GTPases assist the transport and release of the Smad 3 complex in the nucleoplasm (174, 181), but phosphorylated Smad 2 fails to bind to importin due to a structural modification of MH 1 domain, and it is independently imported to the nucleus (181, 182).

The Smad 4 enters the nucleus constitutively and it is exported immediately back to the cytoplasm by the exportin CRM 1 (178, 181, 182). Whether the nuclear R-Smads can also be exported back to the cytoplasm remains unclear. Both Smad3 and Smad4 bind to Smad-binding element (SBE) present in DNA sequences through conserved structural elements in their MH1 domains (174, 182, 184).

Meanwhile, Smad2 fails to bind to Smad-binding element (SBE) because of the structural modification of MH1 domain(178, 182), but Smad 2 interacts with Smad 4 and it participates in

DNA-bound complexes (178, 185). In the nucleus, the R-Smad/ Co-Smad complex interacts in a cell-specific manner with transcription factors via their MH1 or MH2 domains to regulate specifically the transcription of a multiple of TGF-β- responsive genes (182).

Non-DNA-binding transcription factors also interact with nuclear Smads and recruit co-activators (such as p300) through their MH2 domain that leads to acetylation of nucleosomal histones; this is an important step for transcriptional induction (182, 183, 185).

Alternatively, co-repressors bind with MH2 domains of nuclear Smads and recruit histone deacetylase (HDCs), thus leading to transcriptional repression of target genes (182, 186) . Smad6 and Smad7 are inhibitory Smads that block the phosphorylation of Smad2 or Smad3, thus inhibiting TGF-β signaling (174, 187, 188).

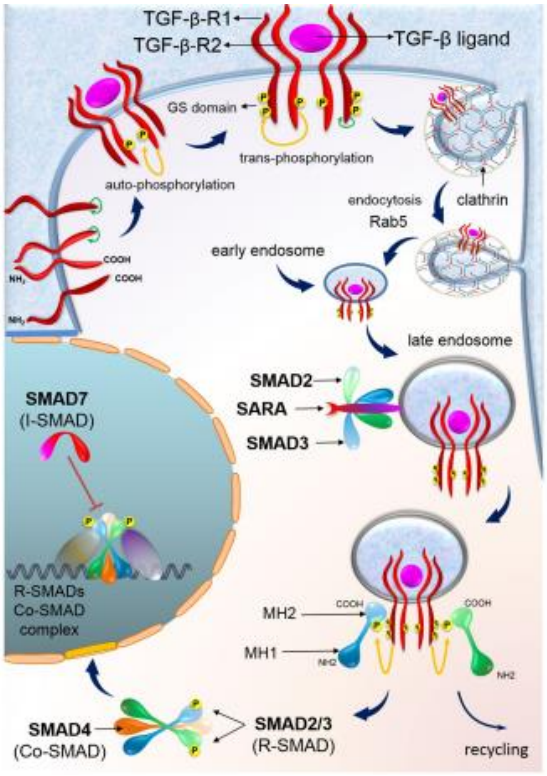

Figure 17 TGF-β Signaling Pathway(189)

I.4.2.3 Role of Curcumin in colorectal carcinogenesis

Many drugs are currently available for treatment of colon cancer but have limited potential because they are very toxic, highly expensive, and highly inefficient in treating colon cancer (190).

Research over the last few decades has shown that curcumin is potent to modulate multiple cellular signaling pathways (including TGF-β signaling pathway) and interacts with numerous molecular targets including transcription factors, growth factors and their receptors, cytokines, enzymes, genes regulating cell proliferation, and apoptosis and have potent anticancer activities like inhibition of cell proliferation, induction of apoptosis, suppression of angiogenesis, and metastasis (190-192).

Curcumin blocks proliferation of cancer cells by arresting them in various phases of the cell cycle by binding directly and indirectly to molecular targets: transcription factors (NF-κB, STAT 3, β-catenin, and AP-1), growth factors (EGF, PDGF, and VEGF), enzymes (COX-2, iNOS, and MMPs), kinases (cyclin D1, CDKs, Akt, PKC, and AMPK), inflammatory cytokines (TNF, MCP, IL-1, and IL-6), upregulation of proapoptotic (Bax, Bad, and Bak), downregulation of antiapoptotic proteins (Bcl 2 and Bcl-xl), induces apoptosis, and blocks invasion of colon cancer in vitro and in vivo (190, 193, 194)

With the anticancer activity of curcumin in colon cancer, curcumin has led to the completion of phase I clinical trials, and there are additional phase II and phase III clinical trials currently being carried out at different research centers around the world. Several studies over the past decades suggested that curcumin is safe and well tolerated even at a very high dose level (such as 12 g/day/adult) in human (195).

Curcumin inhibited TGF-β1-regulated activation of MMP-9 (matrixmetalloproteinase-9), Smad2, ERK1/2,and p38 at dose- and time-dependent manner in MDAMB-231 breast cancer cells (196).

Curcumin treatment in HCT-116 and SW480 colon cancer cell lines decreased tumor growth by suppression of proliferation and induction of apoptosis through the inhibition of proteasome and increased the expression of caspase-3 and caspase-7.

Curcumin has potential to specifically inhibit proteasome activity and increases the expression of p27, and this in turn binds with cyclin E–cdk2 complex and thus controls the cell cycle progression at G1 phase in vivo. This proteasome inhibition role of curcumin in colon cancer can be one of the mechanisms for the chemopreventive effect in human colon cancer treatment (197).

NF-κB is a well-known proinflammatory transcription factor involved in the initiation and progression of cancers. NF-κB induces the expression of growth factors, cytokines, and other factors that are involved in cell proliferation and cell cycle progression. Increased NF-κB expression is associated with cancer cell proliferation, invasion, angiogenesis, metastasis, suppression of apoptosis, and chemoresistance in various cancers. Over expression of NF-κB1and NF-κB2 has an important role in the development of colon cancer (198).

Arecent research study has reported that curcumin blocks the overexpression of NF-κB and inhibits the proliferation of colon cancer (195, 199). Curcumin inhibits NF-κB-targeting genes, including interleukin-(IL)-8, suggesting that curcumin can act as a potential chemopreventive agent against esophageal cancer (199).

TGF-β and Notch signaling pathway have converged to regulate stem cell differentiation. Notch signaling is one of the key pathways constituting the stem cell signaling network. Aberrant activation of this Notch signaling pathway has been reported in colon cancer, breast cancer, and esophageal cancer. Disruption of TGF-β signaling through the loss of β2SP/Smad4 could contribute to the activation of Notch signaling and thus induces the development of esophageal cancer (200).

Curcumin suppresses the Notch signaling pathway through reduction of Notch-1 activation and downregulation of γ-secretase complex proteins such as presenilin1 and nicastrin and induces apoptosis through caspase-3 activation and cancer cell cycle arrest through the down regulation of cyclin D1 expression in esophageal cancer (201).

Curcumin is an effective compound and can be potentially used for treatment of both early stage and advanced stage of colon cancer. Still the role of curcumin on TGF-β signaling in colon cancer cells and the role of TGF-β signaling in curcumin induced anticancer activities have to be elucidated.

There has been an increasing interest concerning the impact of TGF-β signaling pathway on colon cancer progression. It hasbeen recognized that altered function of TGF-β signaling pathway plays a crucial role on initiation, progression, and metastasis of colon carcinogenesis. A molecular mechanism of curcumin in TGF-β-mediated colon cancer progression hasnot yet been investigated. Elucidating the molecular mechanism of curcumin on TGF-β-induced colon carcinogenesis might be helpful for future therapeutic strategies.

Chapter II: Materials and Methods

II.1 Description of the study:

The type of this study is experimental, it was conducted at both Toxicomed Research laboratory and the Galenic Pharmacy Laboratory of the Pharmacy Department, Faculty of Medicine, University of Tlemcen, throughout a period of time started from October 2021 to May 2022.

Some tests and characterizations were carried out by these laboratories:

- Laboratory of Catalysis and Synthesis in Organic Chemistry, Faculty of Science, University of Tlemcen.
- Macromolecules Research Laboratory, Faculty of Science, University of Tlemcen.
- Pharmacognosy Laboratory, Pharmacy Department, Faculty of Medicine, University of Tlemcen.

II.2 Aim and Objectives

The aim of this study is to prepare a novel formulation of an anticancer natural product with in vitro slow extended release.

Main objective of this thesis is to develop a sustained release oral drug delivery system of curcuminoids by preparing a nanocomposite hydrogel formulations through ionotropic gelation.

Secondary goals that could clarify the way to reach the primary goals are:

- To extract curcuminoids from *Curcuma longa*.
- To enhance solubilization of poorly soluble curcuminoids in aqueous media.
- To evaluate the influence of changing concentrations of HPMC excipient by characterizations, in vitro swelling, encapsulation and release behavior profiles.
- To carry out in silico colorectal cancer study of curcumin binding to TGF-β1 receptor by molecular docking.

II.3 Materials

II.3.1 Equipments

Analytical balance type Carat series (Ohaus PAJ1003, USA), Magnetic stirrer (WiseStir MS-MP8, Wisd Laboratory Instruments, Wertheim, Germany), Drying oven (LDO-080N, LabTech, Korea), Centrifuge (Sigma 3-18k, Sartorius, Goettingen, Germany), Ultrasonic cleaner (Branson 200, Branson Ultrasonics Co., USA), Rotary evaporator (IsolabGmbh, Germany), pH meter (Starter3000, Ohaus, USA), UV-visible spectrophotometer (MecasysOptizen 2120 UV, Korea), ATR-FTIR instrument (Cary 640, Agilent Technologies, USA),X-Ray Diffractometer (XRD; Rigaku Miniflex 600, Japan), Zetasizer (ver. 6.30, Malvern Instruments Ltd, Worcestershire, Uk), Laboratory Mill, Laboratory Sieve Chaker (CISA Mod RP.10, Barcelona, Spain), Optical Light Microscope (Leica, Germany), Digital Vernier Caliper (ADA instruments mechanic 150).

II.3.2 Chemicals

Turmeric Rhizomes were purchased from a local store, Acetone (Honeywell, Riedel-de-Haen, Germany), n-Hexane (VWR Chemicals, Karlsruhe, Germany), Sodium Carbonate (Na_2CO_3 Normapur), Methanol (Honeywell, Riedel-de-Haen, Germany), Citric Acid (Sigma-Aldrich, Germany), Tween 80 (Merck, Dermstadt, Germany), Sodium Bicarbonate ($NaHCO_3$, Fluka, Germany), Sodium hydroxide (Fluka, Germany), Sodium Alginate (Low viscosity 4-12 cP, Sigma-Aldrich, Germany), Hydroxypropylmethylcellulose (HPMC, viscosity 7500-14000 mPa.s, Alfa Aesar, Germany), Raw Bentonite (Maghnia- Tlemcen), Calcium chloride $CaCl_2$ (BiochemChemopharma, Montreal, Quebec, Canada), Potassium Dihydrogenphosphate (KH_2PO_4, Sigma-Aldrich, Germany), Sodium chloride (NaCl, Scharlau), Disodium hydrogenphosphate (Na_2HPO_4, Merck, Germany), HCl (37%, AnalaR NORMAPUR).

II.3.3 Laboratory glassware

Burette, Beaker, Filter funnel, Filter paper, Petri dish, Syringe filter, Glass cuvettes, Water bath, Porcelain mortar and pestle, Graduated cylinder, Lab crystallizing dishes, Amber bottle, Conical centrifuge tubes, Round bottom flask.

II.3.4 Computational softwares

Autodock Tools 1.5.7, Audock 4.2.6, Discovery Studio 2021, OriginPro 8.5 software.

Figure 18 Analytical balance Ohaus

Figure 19 Drying oven LabTech

Figure 20 Ultrasonic cleaner Branson 200

Figure 21 Centrifuge Sigma 3-18k

Figure 22 Rotary evaporator Isolab Gmbh

Figure 23 pH meter Starter 3000 Ohau

Figure 24 UV-visible spectrophotometer Mecasys Optizen 2120 UV

Figure 25 Digital Vernier Caliper ADA mechanic 150

II.4 Methods

II.4.1 Preformulation

Preformulation is a group of studies that focus on the physicochemical properties of a drug candidate that could affect the drug performance and the development of a dosage form. This could provide important information for formulation design or support the need for molecular modification. Every drug has intrinsic chemical and physical properties which has been consider before development of pharmaceutical formulation. This property provides the framework for drugs combination with pharmaceutical ingredients in the fabrication of dosage form (202).

The physicochemical properties of the three curcuminoids isolated from *Curcuma longa* L. are summarized below:

II.4.1.1 Curcuminoids

- **IUPAC chemical name**

CUR: (1E,6E)-1,7-bis(4-hydroxy-3-methoxyphenyl)hepta-1,6-diene-3,5-dione(203)

DMC:(1*E*,6*E*)-1-(4-hydroxy-3-methoxyphenyl)-7-(4-hydroxyphenyl)hepta-1,6-diene-3,5-dione (204).

BDMC: (1E,6E)-1,7-bis(4-hydroxyphenyl)hepta-1,6-diene-3,5-dione(205).

- **Synonym**

CUR: Diferuloylmethane(206).

DMC: Monodemethoxycurcumin (204).

BDMC: Didemethoxycurcumin(205).

- **Molecular formula and molecular weight**

The molecular formula of curcumin is $C_{21}H_{20}O_6$, and its molecular weight is 368.38 Daltons (207).

For demethoxycurcumin, the molecular formula is $C_{20}H_{18}O_5$, and its molecular weight is 338.4 Daltons (204).

The molecular formula for bisdemethoxycurcumin is $C_{19}H_{16}O_4$, and the molecular weight is308.3 Daltons (205).

- **Solubility**

Curcumin is Insoluble in water at acidic and neutral pH, and soluble in alkali, polar, non-polar and extremely acidic solvents such as glacial acidic acid (208-210).

- **Pka**

Curcumin is reported to have three different pKa values. The first and second values are from the two phenolic OH groups, and the third value is from the enolic proton.

pK_{a1} =7.75–7.80, pK_{a2} = 8.55, pK_{a3} = 9.05 by the HPLC fluorescence method(211).

- **Melting point**

The melting point of curcumin is 183 °C (212).

- **Physical state and Polymorphism**

Curcumin reported to have 3 crystallin forms:

- Tonnesen et al. (213) reported the crystal structure of curcumin which was obtained via a crystallization process from ethanol at 70 °C (Form-1).
- Sanphui et al. (214) proved that curcumin obtained from other recrystallization processes was reported to have two other polymorphic forms, termed Form-2 and Form-3. Form-2 is metastable and was obtained from the crystallization of curcumin from dimethyl sulfoxide. Form-3 was obtained from a crystallization process with 4,6-dihydroxy-5-nitropyrimidine.
- In addition, the amorphous form of curcumin was also reported.

- **Color**

- At pH<1, curcumin solutions are red in color due to the presence of the protonated form.
- At pH 1–7, curcumin solutions are yellow with the majority of the molecules being in the neutral form.
- At pH values higher than 7.5, curcumin solutions exhibit a color change to orange red (211).

- **Aqueous stability**

Kinetic degradation of curcumin was investigated in various buffer systems at pH 1–11 at 31.5 °C and in fixed ionic systems. Results showed that the degradation of curcumin followed second-order kinetics. In addition, at pH 7.0–7.8, different concentrations of phosphate buffer did not show significant change in the rate of the degradation process.

In another study (215), degradation of curcumin in 0.1 M buffer solutions of pH 3–10 (using citrate, phosphate, and carbonate buffers) at 37 °C followed apparent first-order reaction kinetics at constant ion strength. In these studies, three degradation products were found: vanillin, ferulic acid (FA), and feruloyl methane. Vanillin was found to be the major degradation product and the amount increased as the incubation time was extended. It should also be noted that at pH 7–10 and a temperature of 31.5 °C, the primary degradation products of curcumin were FA and feruloylmethane.

- **Photostability**

Tonnesen et al.(216) have reported an intensive study seeking the identification of photodegradation products of curcumin as these were formed in an isopropanol medium. Curcumin was dissolved in isopropanol and exposed to light (wavelengths of 400–510 nm) for 4 h. Degradation products were extracted through preparative TLC and determined using higher solution mass spectrometry (MS) and nuclear magnetic resonance. The main identified degradation product had the chemical composition of $C_{12}H_{18}O_6$, with a mass spectrum exhibiting a molecular ion at m/e=366 (indicating that two hydrogen atoms were removed from its structure). This main product is postulated as being the result of a cyclization process initiated by light irradiation and can be detected after less than 15 min of irradiation.

In addition, six minor degradation products were also found and identified as vanillin, vanillic acid (VA), ferulic aldehyde, FA, and 4-vinylguaiacol. The sixth degradation product could not be identified with available references, but had the empirical formula of $C_{13}H_8O_4$ (211).

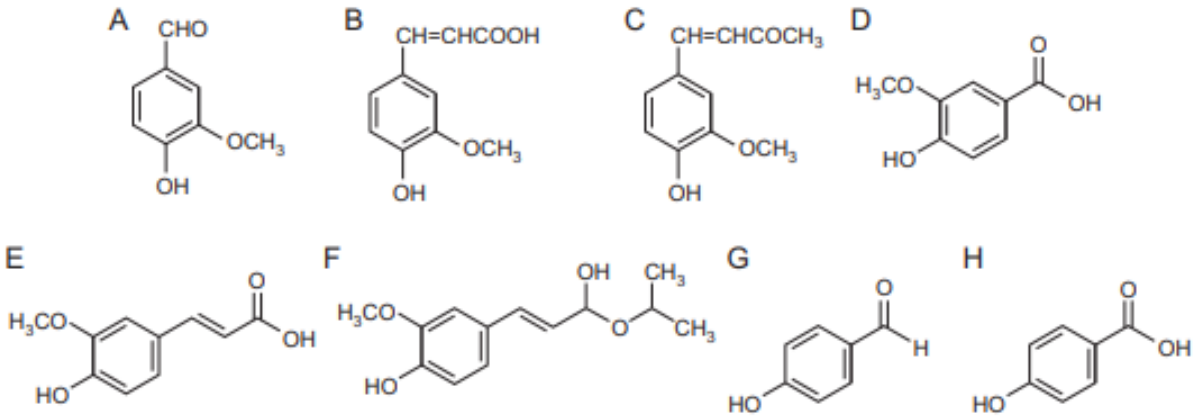

Figure 26 Degradation products of curcumin: (A) vanillin, (B) ferulic acid, (C)feruloylmethane, (D) vanillic acid, (E) ferulic aldehyde, (F) 4-vinylguaiacol, (G) p-hydroxybenzaldehyde, (H) p-hydroxybenzoic acid (216)

- **UV-vis spectroscopy**

On the average, the maximum wavelength was found at 418 nm. The absorption maximum of curcumin in methanol and ethanol was around 420 nm, and the solution exhibited a bright yellow color owing to its p–p* excitation; the n–p* transition was observed at 426 nm in methanol (217).

- **Infrared spectroscopy**

IR analysis of curcumin is summarized in Table II below:

Table II IR spectroscopy peaks of curcumin (216)

FTIR (wave number cm^{-1}) 57	Functional Group
3510	OH
2950–3000	α, β unsaturated, aryl C-H
1627	α, β unsaturated C=O
1602	Conjugated C=C
1429	Phenol C-O
1281	Enol C-O
1268, 1050	=C-O-CH3
1140	C-OH
1150	σ C-CH
1023	σ C-O-C
713	σ CH (aromatic)

- **X-ray diffraction**

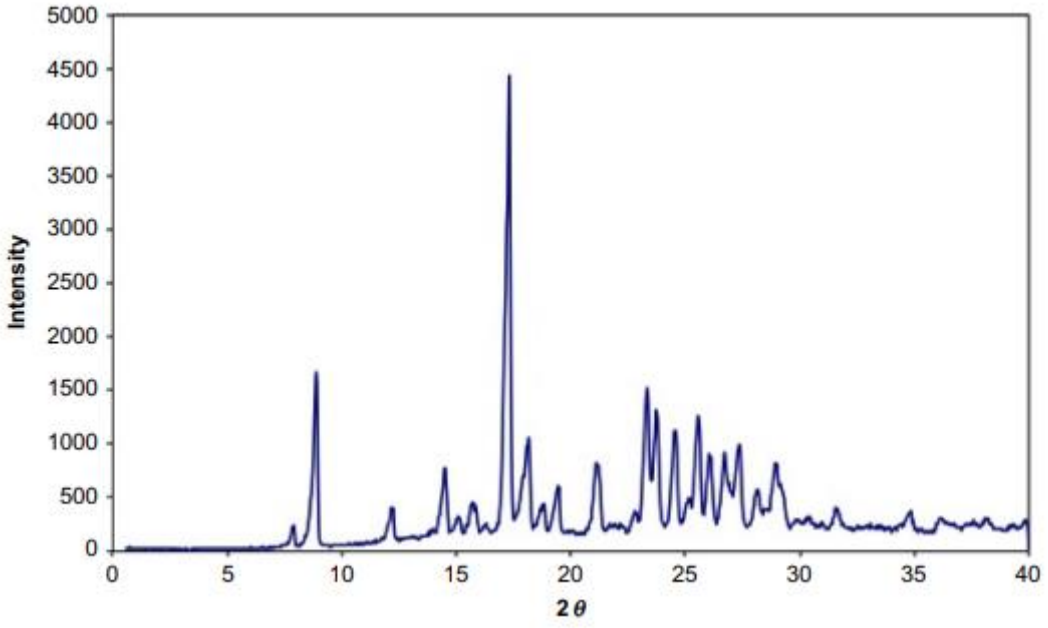

Figure 27 X-ray powder diffraction pattern of the crystal structure of commercially curcumin obtained from *Curcuma longa* (turmeric) containing at least 70% of curcumin (Sigma-Aldrich Chemie GmbH, Germany) (216)

- **Incompatibility**

High performance thin-layer chromatography (HPTLC) showed interaction with four excipients ascorbic acid, ethyl cellulose EC, sodium sodium carboxymethylcellulose Na-CMC and Mg-stearate was also confirmed by both FTIR and DSC. Since interaction of curcumin with ascorbic acid, ethyl cellulose EC, sodium carboxymethylcellulose Na-CMC and Mg-stearate confirmed by all three techniques, it can be concluded that these four excipients should be avoided during formulation development of curcumin (218).

- **Pharmacokinetics**

Pharmacokinetic and bioavailability studies of curcumin have indicated its low intestinal absorption and rapid clearance from the body (219). Metabolism, absorption, biodistribution and excretion of curcumin in rodents have been reported in several studies (220-222).

The overall findings imply that curcumin has a low absorption and rapid clearance following oral use. In a primary research, a dose of 1 g/kg curcumin was administered to rats and resulted in about 75% excretion of curcumin in feces, whereas poor amounts were found in urine (220, 223).

Gutierres and colleagues investigated curcumin levels in rat plasma. In addition, they assessed alterations of insulin sensitivity and glucose tolerance in streptozotocin-diabetic rats treated with curcumin-enriched yoghurt (224). Their results indicated that the elimination half-life of curcumin was 8.64 2.31 (IV) and 32.70 12.92 (oral) minutes. The oral bioavailability was about 0.47%. They showed that the time to reach C_{max} (t_{max}) of curcumin in plasma were 5 min (C_{max}: 3.14 0.9mg/mL; 10 mg/kg IV) and 14 min (C_{max}: 0.06 0.01mg/mL; 500 mg/kg oral) (224, 225) .

II.4.2 Formulation

II.4.2.1 Drug Administration Route

The oral route for drug delivery is regarded as the optimal route for achieving therapeutic benefits. It's the most convenient and extensively used route of drug administration. Because it provides the benefit of effortless administration (226). Despite phenomenal advances in injectable, transdermal, nasal and other routes of administration, the reality is that oral drug delivery remains well ahead of the pack as the preferred delivery route.

Nanotechnology can overcome the major challenges associated with this route of administration: mainly poor solubility, stability and biocompatibility of drugs (227). Specifically, this route is more suitable to achieve drug prolonged release in intestinal tract.

II.4.2.2 Pharmaceutical Dosage Form

The poor oral bioavailability of curcumin and short half-life necessitate frequent administration of large doses to achieve effective plasma and tissue concentrations. A pH sensitive and sustained drug release nanocomposite hydrogel beads of curcumin offers the advantages of enhanced and sustained tissue availability, and reduced dosing frequency.

II.4.2.3 Choice of Excipients

- **Sodium alginate**

➢ Empirical Formula and Molecular Weight

Alginic acid is a linear glycuronan polymer consisting of a mixture of β-(1-4)-D-mannosyluronic acid and α-(1-4)-L-gulosyluronic acid residues, of general formula $(C_6H_8O)n$. The molecular weight is typically 20 000–240 000 (57).

➢ Acidity/alkalinity:

pH = 7.2 (1% w/v aqueous solution) (57)

➢ Solubility:

Practically insoluble in ethanol (95%), ether, chloroform, and ethanol/water mixtures in which the ethanol content is greater than 30%. Also, practically insoluble in other organic solvents and aqueous acidic solutions in which the pH is less than 3. Slowly soluble in water, forming a viscous colloidal solution (57).

➢ Viscosity (dynamic) :

Various grades of sodium alginate are commercially available that yield aqueous solutions of varying viscosity. Typically, a 1% w/v aqueous solution, at 20°C, will have a viscosity of 20–400 mPa s (20–400 cP). Viscosity may vary depending upon concentration, pH, temperature, or the presence of metal ions. Above pH 10, viscosity decreases (57).

➢ Density (true) of Alginic Acid : 1.601 g/cm (57)

➢ Crosslinking

Addition of a calcium salt, such as calcium citrate or calcium chloride, causes crosslinking of the alginic acid polymer resulting in an apparent increase in molecular weight. Films crosslinked with triphosphate (tripolyphosphate) and calcium chloride were found to be insoluble but permeable to water vapor. Drug permeability varies with pH and the extent of crosslinking (57).

- Stability and Storage Conditions :

Sodium alginate is a hygroscopic material, although it is stable if stored at low relative humidities and a cool temperature. Aqueous solutions of sodium alginate are most stable at pH 4–10. Below pH 3, alginic acid is precipitated. A 1% w/v aqueous solution of sodium alginate exposed to differing temperatures had a viscosity 60–80% of its original value after storage for 2 years. Solutions should not be stored in metal containers. Sodium alginate solutions are susceptible on storage to microbial spoilage, which may affect solution viscosity (57).

- Incompatibilities :

Sodium alginate is incompatible with acridine derivatives, crystal violet, phenylmercuric acetate and nitrate, calcium salts, heavy metals, and ethanol in concentrations greater than 5%. Low concentrations of electrolytes cause an increase in viscosity but high electrolyte concentrations cause salting-out of sodium alginate, salting-out occurs if more than 4% of sodium chloride is present (57).

- **Hypromellose HPMC**

Type **:** 2910 Hydroxypropoxy content 7.0–12.0%, Methoxy content 28.0–30.0%

- Structural formula:

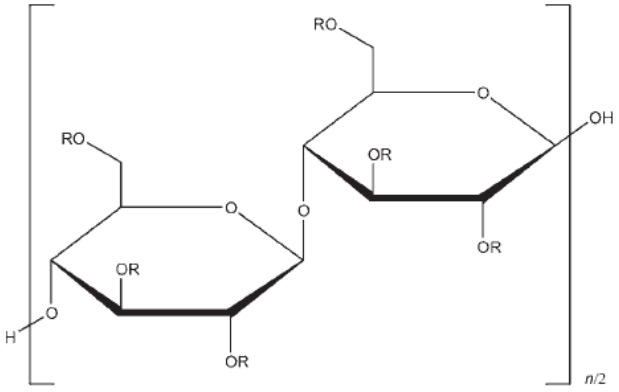

where R is H, CH_3, or $CH_3CH(OH)CH_2$

Figure 28 Chemical structure of HPMC(57)

- pH: Acidity/alkalinity pH = 5.0–8.0 for a 2% w/w aqueous solution (57).
- Melting point

Browns at 190–200°C; chars at 225–230°C. Glass transition temperature is 170–180°C(57).

- Solubility

Soluble in cold water, forming a viscous colloidal solution; practically insoluble in hot water, chloroform, ethanol (95%), and ether, but soluble in mixtures of ethanol and dichloromethane, mixtures of methanol and dichloromethane, and mixtures of water and alcohol (57).

- Incompatibilities

Hypromellose is incompatible with some oxidizing agents. Since it is nonionic, hypromellose will not complex with metallic salts or ionic organics to form insoluble precipitates (57).

- **Bentonite**

Table III Chemical composition of Maghnia Raw Bentonite obtained X-ray Fluorescence analyses (228)

Element	SiO_2	Al_2O_3	Fe_2O_3	MgO	CaO	Na_2O	K_2O	TiO_2	SO_3	LOI
%	51.47	18.5	2.66	6.16	2.86	1.72	1.14	0.25	0.34	17.19

- Physico-Chemical Properties (228) :

- Swelling capacity (2 g / 100 mL): 5mL

- Apparent viscosity:11 cP (centipoises)

- pH: 9.12

- CEC (cation exchange capacity): 61.76 meq/100g

- Specific surface area: 474.64 m^2/g

Table IV Mineral content of Maghnia Raw Bentonite determined by XRD (228)

Sample	Montmorillonite	Illite	Feldpars	Calcite	Quartz
Quantity %	59	5	20	5	11

II.4.2.4 Method of preparation

- **Ionic Gelation**

Ionotropic gelation is based on the ability of polymers to cross link in the presence of counter ions to form hydrogels. Since, the use of alginates, gellan gum, chitosan, and carboxymethyl cellulose for the encapsulation of drug and even cells, ionotropic gelation technique has been widely used for this purpose. Inspite, having a property of encapsulating the drug and acts as release rate retardants (229).

The hydrogel beads are produced by dropping a drug-loaded polymeric solution into the aqueous solution of polyvalent cations. The cations diffuses into the drug-loaded polymeric drops, forming a three dimensional lattice of ionically crossed linked moiety (229).

The alginate based hydrogels containing ionizable groups can take advantage of their ability to undergo volume changes depending upon the pH of the gastrointestinal fluid. When the pH of the medium is altered, hydrogels undergo phase transition, resulting in a change in swelling behavior.

The swelling pattern and drug-release behavior of the beads prepared by ionic gelation using co-polymer contains –COOH functional groups, which may remain unionized at gastric pH, leading to minimum swelling and drug release, but may undergo ionization at intestinal pH, leading to maximum swelling and drug release in the intestine. This could minimize the amount of curcuminoids released into the gastric tract and maximize the release in the intestinal tract (230).

- **Effect of HPMC in hydrogel nanocomposite beads**

The use of Hydroxypropyl-methylcellulose (HPMC) in oral drug delivery systems has been for its several characteristics such as high swellability and surface activity (120, 231).

The swellability characteristic has an important effect on the drug release kinetics since the contact with water or biological fluid results in drug diffusion into the medium leading to polymer chain relaxation with volume expansion (232).

The alginate/HPMC mixture was used previously as an in situ gelling vehicle to enhance ocular bioavailability and patient compliance (233).

- **Effect of sodium bentonite in hydrogel nanocomposite beads**

Addition of clays in gel-forming alginate polymers produces an excellent matrix to control the release of compounds (234), Bentonite is a kind of sedimentary rock that is rich in smectite, which has some excellent properties such as good water absorption, swelling, and drug-carrying capability because of their unique crystal structure (235, 236).

Adding low-cost bentonite to sodium alginates increases the solid content and solves the drawbacks (e.g., low porosity) of single alginate beads. It also improves the mechanical strength because the clay increases viscosity and improves stability.

Furthermore, adding bentonite as a modifying agent in alginates increases the efficiency of encapsulation and controls the release profiles of active ingredients (237).

Alginates and bentonite have been widely utilized to synthesize controlled-release drugs, for example the use of bentonite as a filler agent in sodium alginate regulated the release rate of atrazine and diuron. Bentonite helped in controlling the release of thiram from bentonite–starch–alginate-based formulation in supplying nutrients to plants. The slower release with increasing clay contents is due to the slower swelling behavior of bentonite (238).

II.4.3 Preparation

II.4.3.1 Curcuminoids Extraction

The *Curcuma longa* turmeric roots were washed 3 times with distilled water, cleaned, broken with mortar into small fragments, ground into fine powder, air dried at room temperature for 24 hours and then in the oven at 50 °C until constant weight has been reached, Afterwards the dried rhizomes were powdered by high-speed grinder. The powder obtained was conserved for further use in extraction of curcuminoids (239).

8 g of powder was taken into an opaque bottle containing 80 mL of acetone, after that, the bottle was immersed in Ultrasound bath, this extraction was maintained for 30 mn at room temperature. The extract solution acquired was centrifuged. The acetone in supernatant was evaporated from the mixture of curcuminoids and oleoresin by rotary evaporator at 56°C (240). The crude curcuminoids extract was obtained by adding 10 mL of hexane to the oleoresin-curcuminoids extract, the solution was stirred at 600 rpm for 3 h and then centrifuged, the residue collected was dried in oven at 50 °C (241).

Figure 29 *Curcuma longa* rhizomes

Figure 30 Ultrasound assisted extraction of curcuminoids by acetone

Figure 31 Supernatant of the acetone extract centrifugation

Figure 32 Solvent separation by rotary evaporator

II.4.3.2 Sodium activation of bentonite clay

Raw bentonite powder was grinded and sieved to get a size of 100 µm, 70 g was added to 1 L of (5% w/v) sodium carbonate (soda ash) aqueous solution under continuous stirring of 250 rpm for 6 hours at 60 °C with respect of sodium carbonate/bentonite weight ratio of 1:20. The Na activated Bentonite was obtained by 10000 rpm/mn centrifugation for 10mn, oven dried at 60 °C and subsequently crushed mechanically and grinded into a powder (242).

Figure 33 Sieving of Raw Bentonite

Figure 34 Bentonite suspension in aqueous sodium carbonate solution

II.4.3.3 Formulation of curcuminoids nanosuspension

The method used to prepare nanosuspensions is called CO_2-assisted in situ nanoamorphization method described by Xiangfei Han et al (145), 10mg of curcuminoids was weighted and mixed with 25 mg of citric acid and 30 mg of Tween 80 in a round bottom flask containing 5ml of methanol, methanol was then evaporated by rotary evaporator, following this, 20 ml of aqueous basic solution prepared by dissolving 30 mg of sodium bicarbonate in distilled water was added and then sonicated for 5mn to obtain curcuminoids nanosuspension by acid-base CO_2 assisted effervescence method (243).

The pH of nanosuspension was then adjusted from slight acidic (pH = 4.8) to neutral pH by adding few droplets of NaOH concentrated aqueous solution.

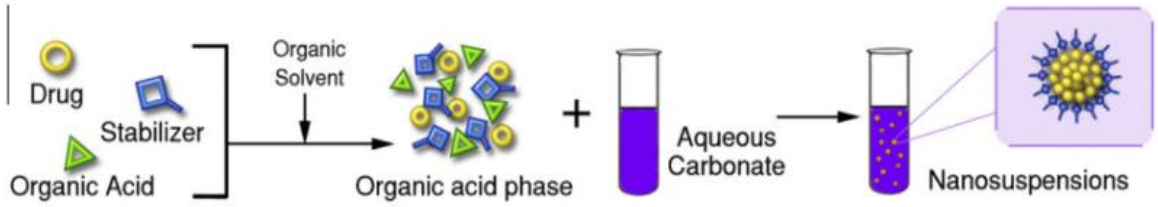

Figure 35 Steps of preparation of nanosuspension by acid-base CO_2 assisted effervescence method (243)

II.4.3.4 Preparation of hydrogel beads by ionotropic gelation

The nanocomposite beads containing curcuminoids nanosuspension were prepared by ionic gelation method using calcium chloride as a crosslinked agent. Na-bentonite was added to 5 mL of Curcuminoids nanosuspension and stirred overnight. After that, 1.5% (w/v) of sodium alginate was added under magnetic stirring for 1 hour followed by the addition of 0.25% (w/v) HPMC with continuous 1h magnetic stirring for the F2 formulation while F1 was formulated without adding HPMC. The resulting NaB-SA-HPMC mixture containing Cur-nanosuspension was added dropwise by the use of burette to 20 mL of 2% (w/v) $CaCl_2$ with a height of 2 cm, the forming beads were left for 10mn in calcium chloride solution to produce rigid beads and then collected to be washed three times by distilled water and dried at 37 °C for 24h (244).

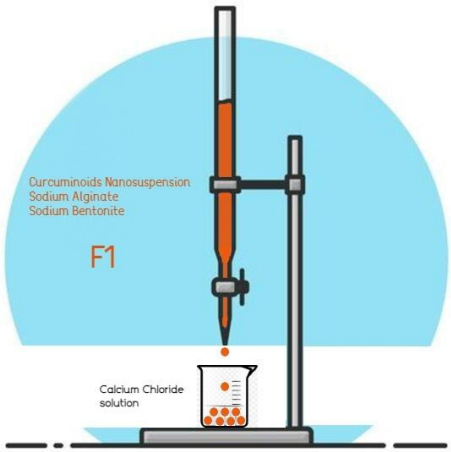

Figure 36 Dripping of drug-polymers-clay mixtures of the F1 formulation on the cross linking solution by ionic gelation method

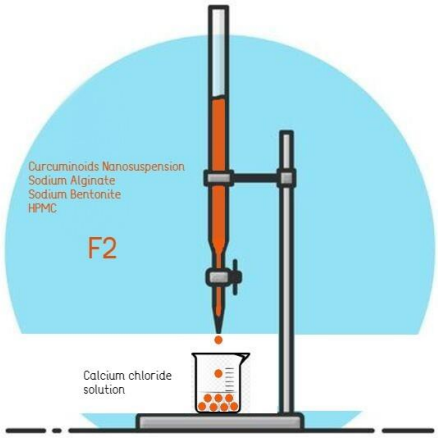

Figure 37 Dripping of drug-polymers-clay mixtures of the F2 formulation on the cross linking solution by ionic gelation method

Table V Final product formulas of F1 and F2 hydrogel beads

F1 beads	F2 beads
Curcuminoids ……..…...….2.5 mg	Curcuminoids ……..…..…...….2.5 mg
Sodium Alginate ……....….. 75 mg	Sodium Alginate ……....…..….. 75 mg
Sodium Bentonite ……...…… 150 mg	Sodium Bentonite …….…… 150 mg
	HPMC …….……..…..…….. 12.5 mg

II.4.4 Controls and Characterizations

Controls and characterization tests were carried out on the cucuminoids, bentonite material, the intermediate product (nanosuspension formulation) and the final product (hydrogel beads).

II.4.4.1 Microscopy identification of *Curcuma longa* powder

Drops of distilled water were added to a few amounts of powder dispersed on microscope slide. Identification of the dried powder was made by light microscopy at 100x magnification to observe the main diagnostic characters with the help of Atlas of Microscopy of medicinal plants, culinary herbs and spices (245).

II.4.4.2 Curcuminoids Yield

The curcuminoids yield obtained by ultrasound-assisted extraction was calculated by the formula (240):

$$\% \text{ of curcuminoids} = \frac{\text{Dry weight of extracted curcuminoids}}{\text{Total weight of turmeric}} \text{ x } 100$$

II.4.4.3 Thin layer chromatography

Sample was prepared by mixing 5mg curcuminoids in 1ml of methanol, the initial point was placed on the spotting base line which was 1cm above the edge of chromatoplate of 9cm.The TLC plate was placed on a beaker filled with a mobile phase that consisted of 10 mL of (99:1) (dichloromethane/methanol) (246), the detection of curcuminoids was revealed by the presence of yellow spots after elution in TLC chamber.

The retention factor was calculated using the formula :

$$Rf = \frac{\text{Distance traveled by individual component of curcuminoids}}{\text{Distance traveled by the solvent}}$$

II.4.4.4 Particle size and polydispersity index of curcuminoids nanosuspension

The mean particle size (PS) and polydispersity index (PDI) of curcuminoids nanosuspensions was measured directly using dynamic light scattering technique (Zetasizer Nano-ZS, Malvern Instru-ments, Worceshtire, UK).

Figure 38 Malvern Zetasizer ver. 6.30 instrument

II.4.4.5 Morphology and Size of Beads

Samples of the beads at different states from different formulations were selected, and their sizes were measured by using a digital vernier caliper.

Photographs of curcuminoids loaded beads before drying, after drying, after swelling in HCl (pH = 1.2), and in PBS (pH = 6.8) were captured to study their morphology.

II.4.4.6 Fourier transform infra red analysis

FTIR spectra of curcuminoids extracted from rhizomes of *Curcuma longa*, curcuminoids nanosuspensions, Alginate-HPMC-bentonite placebo beads, and drug loaded beads were measured by means of an ATR-FTIR spectrophotometer (model Cary 640, Agilent technologies) equipped with diamond over the range 4000-600 cm^{-1} and peak resolution of 4 cm^{-1}.

Figure 39 ATR-FTIR instrument Cary 640 Agilent Technologies

II.4.4.7 X-ray diffraction study

Mineralogical data of natural raw bentonite, bentonite after treatment by Na_2CO_3, curcuminoids and F2 beads were analyzed by Rigaku MiniFlex 600 X–ray diffractometer at 23–25 °C collected from 2.0000 to 60.0000 deg and operated at 15 mA and 40 kV.

Figure 40 Rigaku Miniflex 600X-Ray Diffractometer

II.4.4.8 Drug entrapment efficiency

The drug entrapment efficiency was determined by analyzing indirectly the free drug amount remained in $CaCl_2$ solution. 3mL of $CaCl_2$ solution that contained the beads was used as the sample to measure the absorbance of curcuminoids at 420 nm, 2% (w/v) $CaCl_2$ solution was used as a blank (247). All samples were analyzed in triplicates. The entrapment efficiency was calculated using the equation:

$$\text{DEE (\%)} = \frac{\text{Total Curcuminoids Added-Amount of free Curcuminoids}}{\text{Total Curcuminoids Added}} \text{ x } 100$$

II.4.4.9 Drug Loading

The drug loading in beads was determined by putting 10 mg of beads in 5 mL of methanol (248) and crushing them with lab glass rod and then stirred overnight for 500 rpm. The resultant dispersion was analyzed by spectrophotometer at 420 nm for the drug concentration using methanol as a blank. Drug content was computed using a calibration curve prepared using solutions with concentrations of 2-10 µg/mL of curcuminoids .

All samples were analyzed in triplicates. The drug loading of the beads sample was calculated using the equation:

$$\text{DL (\%)} = \frac{\text{Amount of Curcuminoids loaded in beads sample}}{\text{Weight of the beads sample}} \text{ x } 100$$

II.4.4.10 Swelling index

Swelling index evaluation of curcuminoids loaded nanocomposite beads were carried out in two different aqueous solutions: HCl (pH=1.2), and phosphate buffer (pH=6.8) (249). 10 mg of beads were placed in a small beakerof 20 mL buffer solutions .

The dissolution media were phosphate buffer PBS (pH=6.8) and HCl (pH=1.2) solutions prepared according to the European and American Pharmacopoeia respectively (250, 251).

The experiment was carried out at room temperature. The swelled beads were removed at predetermined time to measure the weight until it reaches the 24^{th} hour for PBS and the 2^{nd} hour for HCl. All samples were analyzed in duplicates.

Swelling index was determined by following formula:

$$SI\ (\%) = \frac{\text{Weight of Swelling Beads} - \text{Weight of Dried Beads}}{\text{Weight of Dried Beads}} \times 100$$

II.4.4.11 Cumulative Drug Release

The in-vitro cumulative release properties of curcuminoids from the nanocomposites hydrogel beads were determined asfollows: The curcuminoids loaded hydrogel beads were added to 20 mL dissolution medium which was agitated at 100 rpm at room temperature. The dissolution media were phosphate buffer PBS (pH =6.8) and HCl (pH = 1.2) solutions prepared according to the European and American Pharmacopoeia respectively. 3mL was withdrawn at predetermined time and was analyzed spectrophotometrically at 420 nm. The dissolution medium was supplied with 3 mL fresh buffer solution to maintain the total volume (252). All samples were analyzed in triplicate. The drug release percent was deter-mined using Equation:

$$\text{Cumulative Drug Release}\ (\%) = \frac{\text{Cumulative amount of curcuminoids released}}{\text{Initial amount of loaded curcuminoids}} \times 100$$

II.4.4.12 Study of Drug Release Kinetics

To explain the curcuminoids release mechanism from F1 and F2 nanocomposite beads, the in vitro drug release data were evaluated kinetically. In this regard, the achieved data of the curcuminoids release were fitted to four common kinetic mathematical models; Zero-order, First-order, Higuchi and Korsmeyer Peppas models.

The first 6 h of the release curve was fitted to the studied kinetic models (253, 254). The correlation coefficient (R^2) in each case was obtained after fitting the pure data to each equation. The obtained value of 'n' diffusional exponent display the mechanism of drug release kinetics.

$n \leq 0.45$, $0.45 < n < 1$, $n = 1$, $n > 1$ respectively suggest that the drug release from the fabricated carrier via Fickian diffusion, non-Fickian transport, case-II transport and a super case II transport.

- Zero Order : $Q = K_0 t$ (255)
- First Order : $LnQ = LnQ_0 - K_1 t$ (256)
- Higuchi : $Q = K_H t^{1/2}$ (257)
- Korsmeyer-Peppas : $LnQ = nLnt + Lnk_p$ (258)

Where the Q, k_0, k_1, k_H, and k_p are the cumulative curcuminoids releases percentage, rate constants of curcuminoids release for Zero-order, First-order, Higuchi, and Korsmeyer-Peppas models, respectively (259).

II.4.4.13 Statistical analysis

All measured data are expressed as mean ± standard deviation (S.D.) by OriginPro 8.5 software. Each measurement was done at least in duplicate (n = 2).

II.4.5 In Silico Molecular Docking

II.4.5.1 Ligand and Protein Download

Curcuminoids were considered for their potential anti-cancer effect, for this reason molecular docking study was predicted, the 3D structure of curcumin, demethoxycurcumin, bisdemethoxycurcumin were downloaded from PubChem in SDF format (203). The three dimensional X-ray crystal structure of TGF- β receptor I kinase (1rw8) was retrieved for molecular docking study from the RCSB protein databank in PDB format (260).

Figure 41 3D structure of TGF-beta receptor I kinase (1rw8) in Discovery Studio 2021

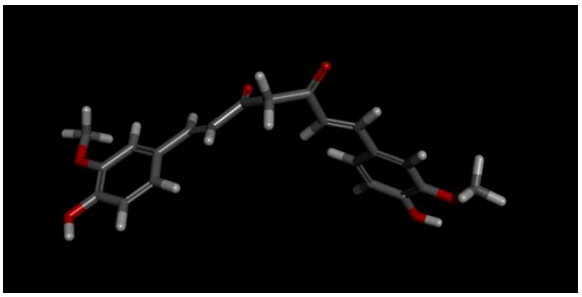

Figure 42 3D structure of curcumin in Discovery Studio 2021

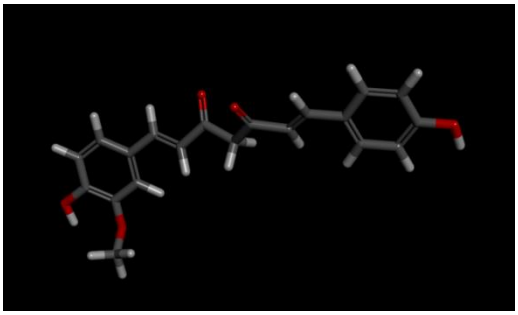

Figure 43 3D structure of demethoxycurcumin in Discovery Studio 2021

Figure 44 3D structure of bisdemethoxycurcumin in Discovery Studio 2021

II.4.5.2 Ligand and Receptor Preparation

Discovery Studio Visualizer 2021 was used to convert the CUR, DMC, BDMC from the SDF to PDB format and removing water molecules from the 1rw8 protein.,

AutoDock Tools 1.5.7 was used to assign polar hydrogens, Kollman charges to 1rw8 protein, then the structures were saved as Pdbqt file format for further analysis. On the other hand, the investigation ligands were loaded, Gasteiger charges and the torsions along with rotatable bonds were assigned and the file is saved as pdbqt format.

II.4.5.3 Molecular Docking by Autodock

The grid and docking parameter file were created using AutoDock Tools 1.5.7 by covering all the components with the grid box to set up the map files. Followed by, performing the molecular docking studies by AutoDock 4.2.6setting up of docking parameter files with search parameter as genetic algorithm and docking parameter utilizing Lamarckian genetic algorithm.

Each of the curcuminoids made a complex with TGF- β receptor I kinase, the run with the lowest free energy of binding was selected to visualize the 3D graphical visualization, Hydrogen bond binding pocket, 3D graphical illustration, 2D Schematic interaction by Discovery Studio Visualizer 2021.

Chapter III: Results and Discussion

III.1 Powder identification

The qualitative microscopic analysis of the crude powder revealed that turmeric observed contains the diagnostic elements such as numerous parenchymatous cells that appeared yellowish due to their interior gelatinized starch, the powder appeared to contain fragments of reticulately thickened vessel, in addition, some trichomes although not frequent to find but occasionally it were attached to a little fragment of epidermis. Because of the majority of starch granules are gelatinized, it's not common to find them, an isolated starch granule was observed. The histo-anatomical observation of the turmeric powder provided a valuable identification of the plant *Curcuma longa* (245).

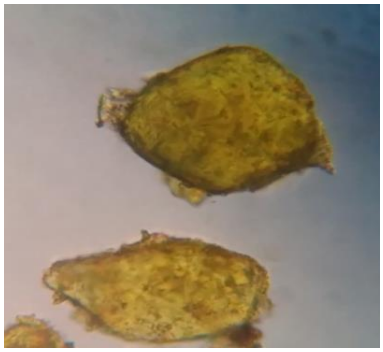

Figure 45 Bright yellow coloring parenchymatous cells filled with gelatinized starch seen as rounded to oval cells with irregular walls

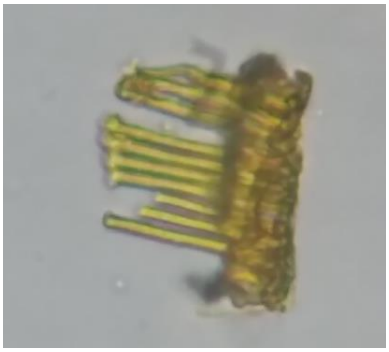

Figure 46 Large reticulately thickened vessel with regularly arranged rectangular pits.

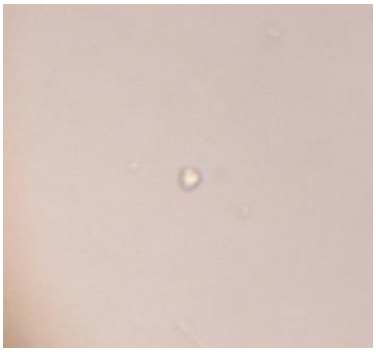

Figure 47 Starch granule

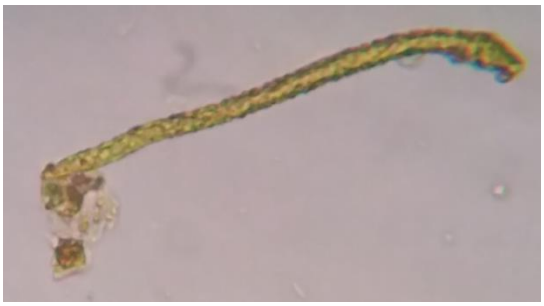

Figure 48 Unicellular, elongated and bluntly pointed trichome attached to fragments of epidermis

III.2 Curcuminoids Yield

Figure 49 *Curcuma longa* powder

Figure 50 Amount of curcuminoids extracted

For an amount of 249 mg of curcuminoids extracted by acetone, the yield obtained was 3.1% comparable to the reference yield of 3.4% extracted by another high frequency ultrasound bath (240).

The slight difference between the two results could be attributed to natural product per solvent ratio during the extraction, the temperature, and also the time of extraction (240).

III.3 Thin Layer Chromatography

The retention factor reached by each component of curcuminoids is summarized in the table VI below, the results of the TLC plate is shown in Fig. 51.

Table VI Retention factors of the different components of curcuminoids separated on silica TLC plate (246)

Yellow colored spots	Rf	Litterature
CUR	0.42	0.47
DMC	0.22	0.28
BDMC	0.11	0.16

Figure 51 TLC of separated curcuminoids

The Rf values of three spots of curcuminoids obtained by ultrasound assisted acetone extraction were close to the Rf values of curcuminoids found in the reference study for the same mobile phase conditions that provided better separation of pigments (246).

III.4 Particule Size Distribution of Nanosuspension

Table VII Z-average and Polydispersity index of Curuminoids Nanosuspension

	Size (r.nm)	% Intensity	Width (r.nm)
Peak 1	120.9	93.9	53.26
Peak 2	7.738	6.1	1.748
	Z-average (r.nm)		
	80.45		
	Pdl		
	0.439		

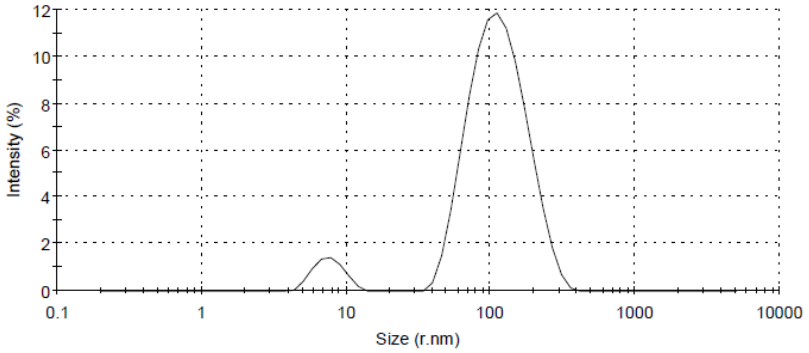

Figure 52 Particle size distribution by Intensity of Curcuminoids Nanosuspension

Figure 53 Yellow colored curcuminoids nanosuspension at pH of 4.8

Figure 54 Orange-red colored curcuminoids nanosuspension at neutral pH

The aim of this part of the study was to produce a low particle size nanosuspension prior to its use for the formulation of nanocomposite hydrogel beads. The Z-average, Polydispersity index (PDI) and size distribution are given in Table VII and Figure 52 respectively.

Particle size is an important parameter related to the capacity of nanoparticulate systems to interact with, in particular, mucosal surfaces. fine particles have an increased bioavailability with prolonged residence time, which shows more adhesive properties than larger particles, The tendency of the particles to stick to mucosal surfaces at the absorption site over an extended period of time achieves an enhanced absorption rate, one example of proven bioavailability, Danazol as a nanosuspension leads to an absolute bioavailability of 82.3% while the conventional dispersion only had 5.2% (261).

The Malvern Zetasizer displayed two distinct peaks at 7.7 nm and 120.9 nm with the highest intensity and a narrowest width for the second peak making an overall mean particule size of 80.45 nm.

A PDI of 1 indicates large variations in particle size; a value of 0 means that there is no variation in size, a value higher than 0.5 tends to be an indicator of aggregation of particles because of the polydisperse system. The nanosuspensions of curcuminoids based on Tween 80 as a stabilizer showed a PDI of 0.439 indicating that the size distribution is monodisperse.

In a previous study with the same method of formulation but with different stabilizers, it has shown that controlling the percentage of stabilizers can decrease the PdI from 0.3-0.4 to 0.1 to reduce the ability of the nanosuspension to aggregate (243).

These data collected from the DLS instrument indicated that the nanosuspension is uniform-sized and homogeneous, however further analysis such as zeta potential is crucial to test the stability of the nanosuspension.

.

III.5 Morphology and Size of Beads

Curcuminoids loaded Na-B/SA and Na-B/SA/HPMC nanocomposite beads were prepared by ionotropic gelation technique using $CaCl_2$ solution as cross-linking solution. When dispersion mixture of sodium alginate, sodium bentonite, and curcuminoids was dropped into the solutions containing calcium ions, gelled spherical Na-B/SA composite beads for the F1 formulation and Na-B/SA/HPMC composite beads for the F2 formulation containing curcuminoids were formed instantaneously due to electrostatic interaction between negatively charged sodium alginate and positively charged calcium ion. Drying the beads resulted a noticeable reduced size after 24h for both F1 and F2 formulation.

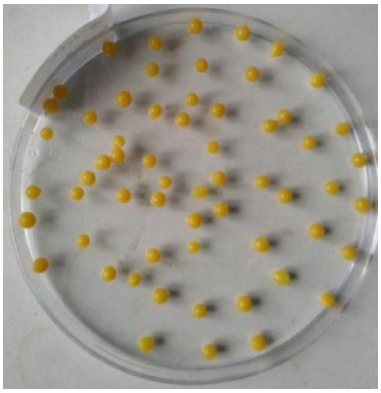

Figure 55 Morphology of F1 Beads before Drying

Figure 56 Morphology of F1 Beads after Drying

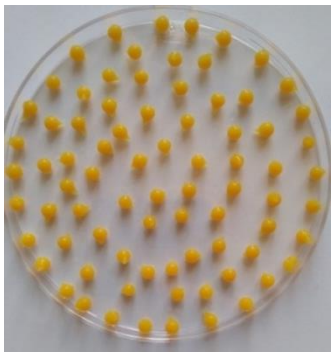

Figure 57 Morphology of F2 Beads before Drying

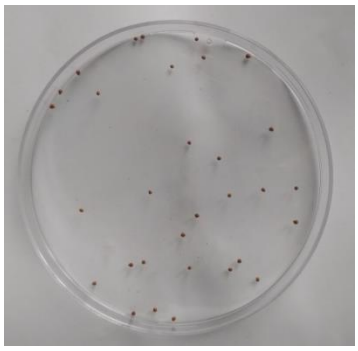

Figure 58 Morphology of F2 Beads after Drying

Particle size of various curcuminoids loaded beads for each formulation was measured by Digital Vernier Caliper.

The F2 beads size during addition of a small amount HPMC polymer (0.25 % w/v) didn't change significantly before or after drying compared to the F1 formulation because the difference in viscosity of the mixture solution did not affect the droplet size during addition of the polymer-clay mixture solution to the cross-linking solution. Argyrios Nochos et al proved already that it can be seen when adding HPMC into alginate beads, not significant effect on the mean particle size appeared (262).

The particle size of F1 and F2 beads after swelling in PBS (pH = 6.8) was within the range of 4.085 ± 0.04 mm (F1) – 4.315 ± 0.06 mm (F2). Increasing the particle size of beads in F2 formulation was found with the increasing incorporation of HPMC as a polymer with sodium alginate. This could be attributed due to the swelling effect of the HPMC polymer (263).

The particle size of F1 and F2 beads after swelling in HCl (pH = 1.2) ranged from 1.515 ± 0.035 mm (F1) – 1.635 ± 0.007 mm (F2). The particle size of beads in F2 was found to be slightly greater than the size of F1 beads.

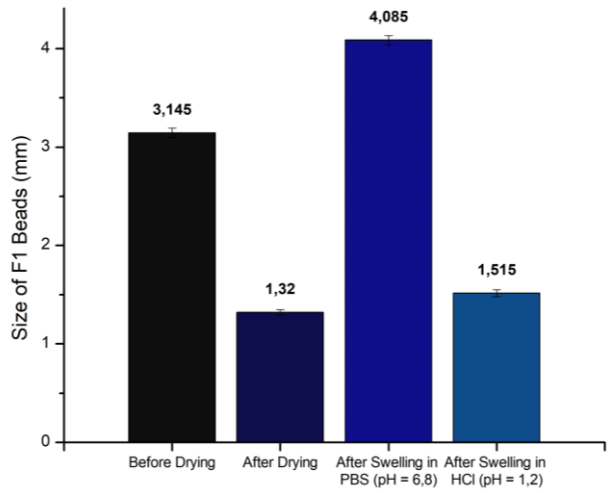

Figure 59 Size of F1 Beads

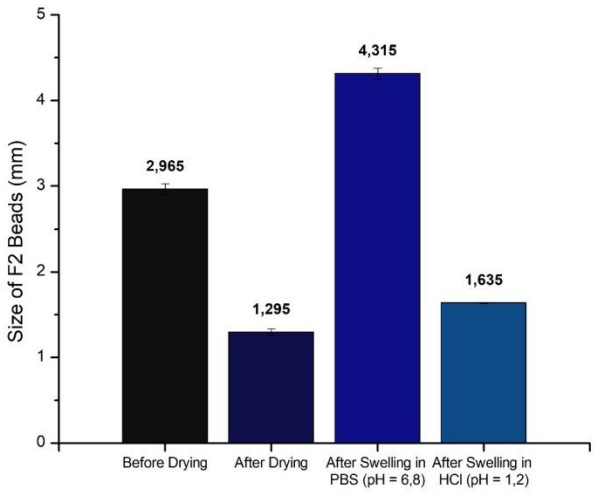

Figure 60 Size of F2 Beads

III.6 Fourier transform infra red analysis

The FTIR spectra of raw bentonite and bentonite treated by Na_2CO_3 are presented in Fig. 61 to explore the effect of sodium activation.

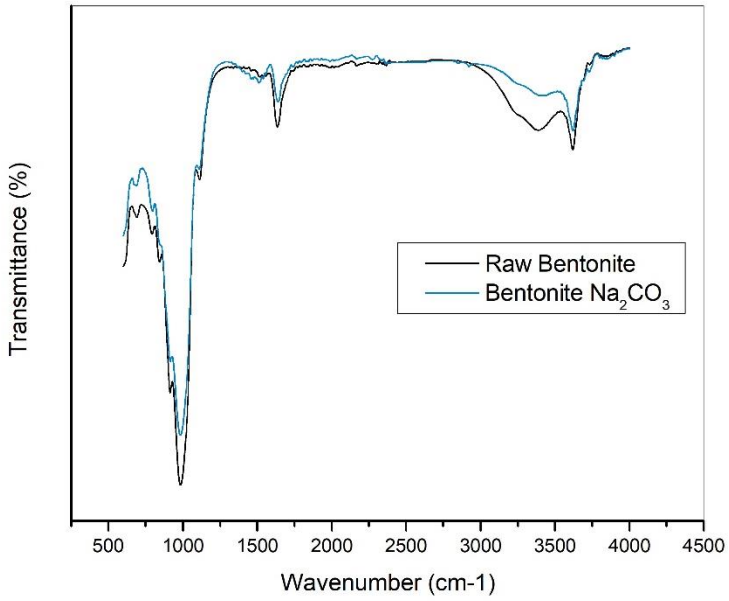

Figure 61 Comparison of FTIR spectra of raw and sodium activated bentonite

The intense peak at 983 cm^{-1} is related to stretching vibrations of Si-O groups (264). Moreover, the peak at 1635 cm^{-1} is for H-O-H bending. The stretching OH vibration appears at 3400 cm^{-1}. The adsorption band at 3619 cm^{-1} in the spectrum is assigned to stretching vibrations of the structural OH groups of dioctahedral bentonite.

After sodium activation, the most significant change was a decrease in the intensity of the band of the Si–O stretching region at 983 cm^{-1} This means that upon the activation process, there is a possibility of the formation of three–dimensional networks of amorphous silica, which may expose more adsorption sites. The increased amount of amorphous silica, as sodium activation progress, resulted in deterioration of the tetrahedral layer.

The intensity of bending and stretching bands at 1635 cm^{-1} characterized the octahedral sheet for Al-OH decreases, which indicates destruction of the octahedral layer.

In addition, a sharp decrease in the absorption band attributed to the OH vibration at 3619 cm^{-1} is due to the removal of the octahedral cations, thus causing the loss of water and hydroxyl groups coordinated to them (265).

The decrease in the characteristic band of bentonite appears at 3400 cm^{-1} which represents the fundamental stretching vibrations of different –OH groups present in Mg–OH–Al, Al–OH–Al, and Fe–OH–Al units in the octahedral layerand this refers to deterioration of this layer(266).

Finally, following the activation process, most band positions did not change, thus suggesting that the basic bentonite structure did not collapse (267).

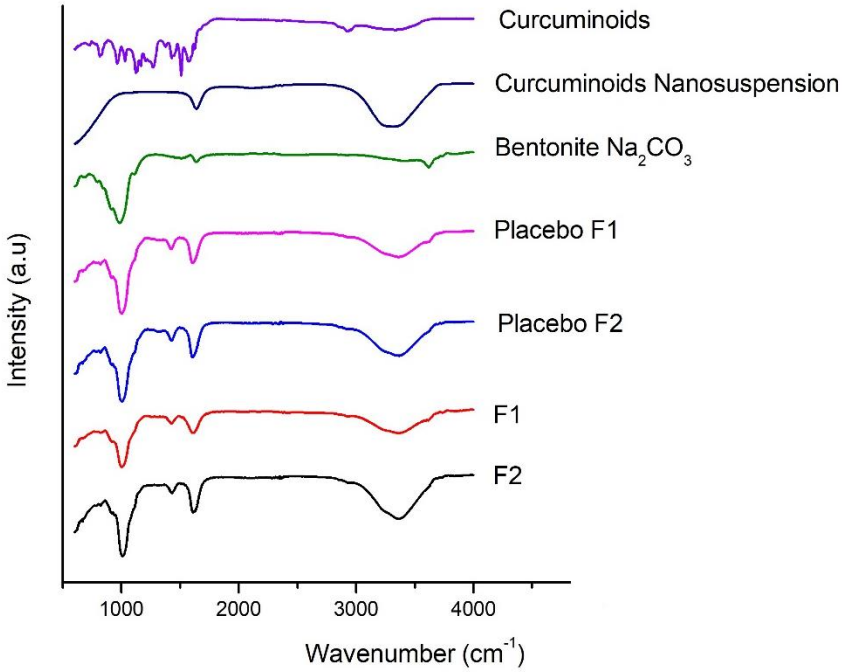

Figure 62 FTIR Spectra of Curcuminoids Hydrogel Beads, F1 without HPMC, F2 with HPMC

The FTIR spectra of curcuminoids, nanosuspension of curcuminoids, curcuminoids loaded F1 and F2 beads and their placebo beads are shown in Fig. 62.

The FTIR spectrum of curcuminoids showed that the IR peaks at 3342.03 cm^{-1}, 2925.48 cm^{-1}, 1623.76 cm^{-1}, 1577.48 cm^{-1} and 1428.99 cm^{-1} resulted from stretching of O-H, C-H, C=O, C=C, Phenol C=O respectively whereas peaks at 1267.10 cm^{-1} and 1124.29 cm^{-1} resulted from C-OCH_3 stretching and C-OH stretching respectively binding to the aromatic ring.

The FTIR spectrum of curcuminoids nanosuspension displayed two characteristic peaks at 1637.26 cm^{-1} and 3318.89 cm^{-1} of the C=O and O-H groups, attributed to the Tween 80 polar head groups located on the outer layer to minimize the surface free energy of the particles by confering a steric repulsion.

In the FTIR spectrum of placebo beads, the characteristic peaks of sodium alginate appeared at 1425 cm^{-1}, 1604 cm^{-1} and 3367 cm^{-1}, for symmetric –COO− stretching vibration, asymmetric –COO− stretching vibration and for the –OH groups, respectively.

In the FTIR spectrum of curcuminoids loaded Na-B/Alginate F1 beads, various characteristic peaks of sodium alginate, HPMC, and curcuminoids nanosuspension appeared without any significant shifting of these peaks, however the peak at 3365 cm^{-1} increased in intensity, which may be due to some physical interactions between the functional groups of the curcuminoids nanosuspension and excipients.

The FTIR analysis confirmed the compatibility of the curcuminoids nanosuspension with the excipients sodium bentonite, sodium alginate, HPMC used to prepare the curcuminoids loaded nanocomposite beads. Since there is no extra peaks appeared in the spectra of the final formulations F1 and F2, This suggests that there were no chemical reactions between the curcuminoids nanosuspension and the polymers, clay excipients (268).

.

III.7 X-ray diffraction study

The qualitative analysis of the main components of raw bentonite are shown in table VIII.

Table VIII qualitative analysis of the main components of raw bentonite

Phase name	Montmorillonite	Si	Alite	Diaspore	Portlandite
Formula	$(Ca)_{0.5}\ (Al)_2\ Si_4O_{12}$	Si	$(Ca)_3\ Si\ O_5$	AlO(OH)	$Ca(OH)_2$

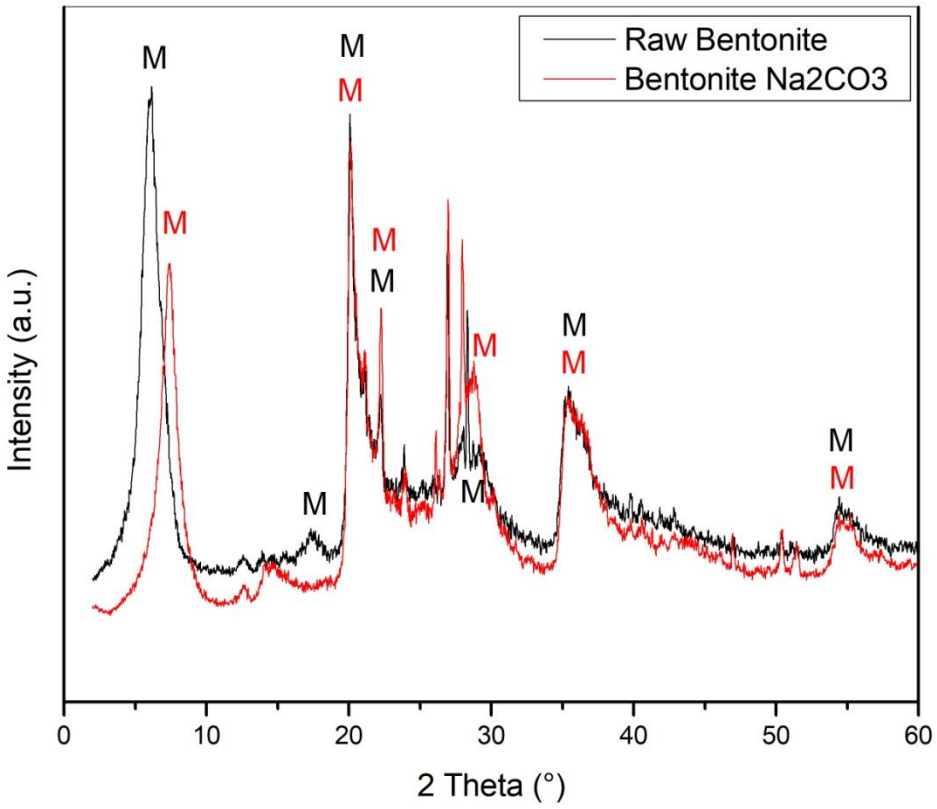

Figure 63 XRD patterns of raw bentonite and sodium bentonite

The XRD patterns of raw bentonite and activated bentonite are shown in Fig. 63. Both patterns exhibits similar diffraction peaks attributed to Montmorillonite (M), the main component of the sample. Another components like Si, Alite (A), Diaspore (D) and Portlandite (P) were also detected in both raw and sodium activated samples (269-271)

The first peak of diffraction at 2θ equals to 6.12 corresponding of spacing of 14.66 Å has slightly shifted to 7.38 with a lower spacing 11.97Å, the resulting spacing has been reported previously for sodium intercalation inside bentonite layers where the spacing were found 11.98 Å after sodium treatment (272-274).

The explanation of the decrease in spacing between layers of bentonite indicates the loss of large volume calcium cations and water molecules, those ions are replaced by small volume sodium cations to confirm the decrease in spacing inside sodium bentonite layers (275).

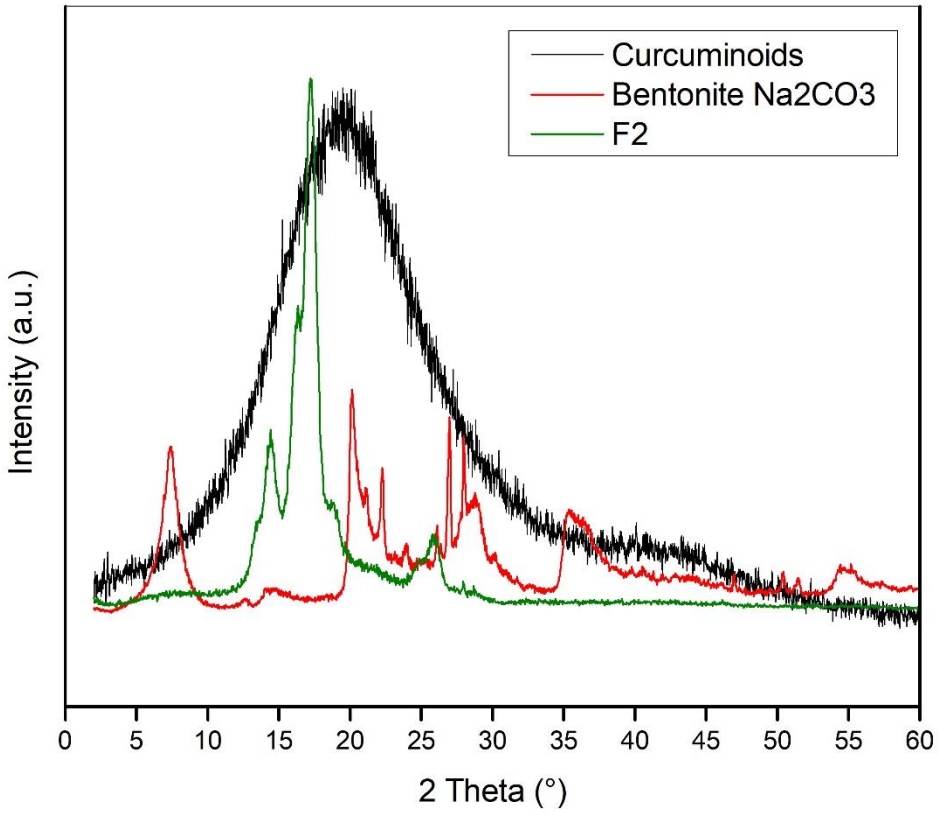

Figure 64 XRD patterns of curcuminoids, sodium bentonite and F2 hydrogel beads

To investigate the molecular dispersion of curcuminoids in polymer matrix, XRD analysis were performed and the diffractograms of curcuminoids, sodium bentonite activated by Na_2CO_3 and F2 Alginate/HPMC/Na-Bentonite beads are represented in Fig 64.

The XRD of curcuminoids showed a large peak in the region 10-30°, indicating the non-crystalline amorphous structure of the drug (214). In the other hand, XRD of F2 nanocomposite beads showed a diffraction peak at 18.83° which corresponds to the HPMC cellulose crystal planes, The diffraction peaks of HPMC are very broad, which indicated their semi-crystalline nature (276).

Because most of the large peak of curcuminoids didn't appear in the diffractogram of the beads with curcuminoids loaded (F2), this proves that the curcuminoids were successfully encapsulated into the Alginate/HPMC/bentonite nanocomposite beads. These results suggest that

the curcuminoids nanosuspension particles were dispersed in the polymeric network of the nanocomposite hydrogel beads (277). That is to say that the disappearance of the some characteristic XRD peaks of curcuminoids after adsorption onto MMT surface is due to the loss of the amorphous structure of curcuminoids upon adsorption on the bentonite clay layers surface.

Similarly, Anitha et al reported the disappearance of the characteristic XRD peaks of curcumin after its loading into dextran sulfate-chitosan nanoparticles due to the amorphous or disordered –crystalline nature of curcumin inside the nanoparticles (278).

The XRD spectrum of the curcuminoids loaded F2 beads demonstrated a decrease in the MMT peaks intensity relative to the exfoliated sodium bentonite clay which indicated an increase in degree of exfoliation due to the drug adsorption rather than increasing the interlayer spacing (279).

The decrease in intensity and the shift of the first peak of MMT in the diffractogram of F2 beads from 2θ equals 7.38 to a lower 2 theta value of 6.12 indicated an intercalation of alginate molecules into the remaining sodium bentonite clay layered structure leading to almost complete exfoliation (279). This may be attributed to the electrostatic repulsion between the negatively charged alginate and MMT that led to the dispersion of the clay layers into the polymer matrix in disordered manner (279).

Exfoliation of clay by the adsorption of drug molecules was also observed by Datta upon the preparation of propranolol loaded MMT-poly lactic-coglycolic acid nanocomposites (280).

III.8 Drug entrapment efficiency

The EE of the beads with different compositions is reported in Table IX.

Table IX Entrapment efficiency of the 2 formulations: F1 and F2

Formulation	DEE (%)
F1	99.29 +/- 0.08 %
F2	99.13 +/- 0.08 %

Both entrapment efficiencies had a high percentage of encapsulation with an increase of the HPMC concentration at a fixed concentration of sodium alginate (1.5 % w/v) and sodium bentonite (3% w/v).The EE didn't vary considerably with the composition of the HPMC for a constant concentration of sodium alginate and sodium bentonite.

The enhancement of entrapment efficiency is explained by the higher specific surface area, porosity and cationic exchange capacity of the sodium bentonite clay (281).

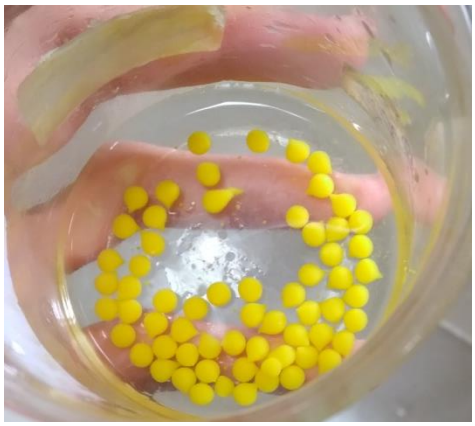

Figure 65 $CaCl_2$ 2% (w/v) cross-linking solution containing the free drug remained and curcuminoids beads

III.9 Drug loading

A calibration curve of curcuminoids was prepared in methanol in the range of 2-10 µg/ml by UV-Visible spectrophotometer. The absorbance of solution was measured at 420 nm. regression coefficient was found 0.99696.

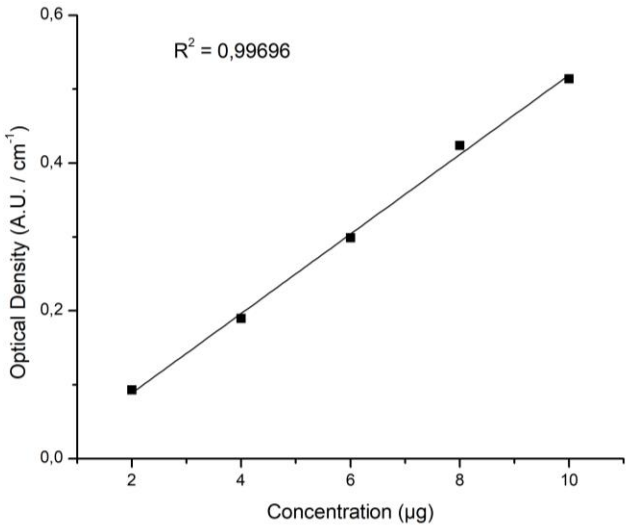

Figure 66 Calibration curve of curcuminoids in methanol

Table X Drug Loading of the formulations F1 and F2

Formulation	DL (%)
F1	0.223 +/- 0.0008 %
F2	0.207 +/- 0.0004 %

Drug loading was found to be in the range of 0.20-0.22 % for beads. It was found that the small concentration of HPMC had no significant change to the drug loading.

The small percentage of the drug loading was due to the small amount of drug added initially compared to the high amount of polymers and bentonite clay. Shi-Bin Wang et Al indicated that the entrapment efficiency of microcapsules increases upon the decrease of the drug load. In the other hand the more amount of drug loaded in the gel beads, the more the percentage of drug will be lost into the liquid medium during encapsulation (282).

III.10 Swelling Test

III.10.1 Swelling Test in HCl (pH = 1.2)

Figure 67 Swelling Test of F1 in HCl (pH = 1.2)

Figure 68 Swelling Test of F2 in HCl (pH = 1.2)

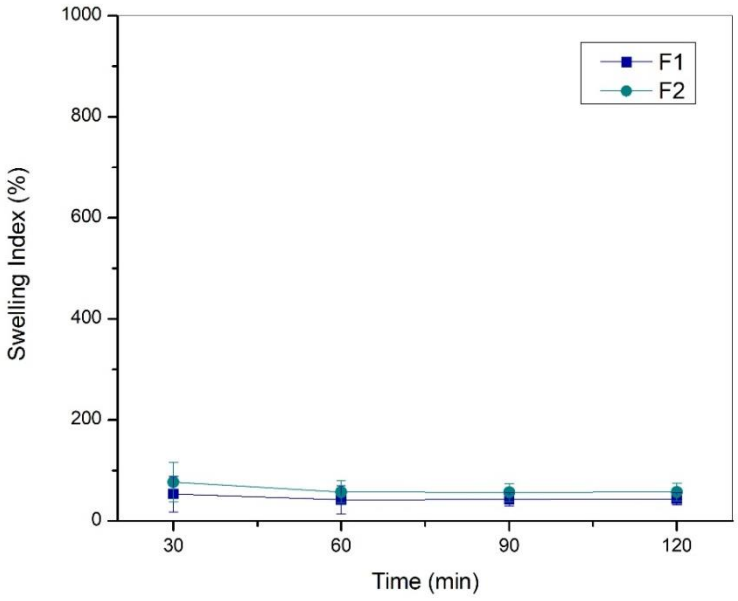

Figure 69 Swelling behavior curves of curcuminoids loaded hydrogel beads in simulated gastric fluid HCl (pH = 1.2)

III.10.2 Swelling Test in PBS (pH = 6.8)

Figure 70 Swelling Test of F1 in PBS (pH = 6.8)

Figure 71 Swelling Test of F2 in PBS (pH = 6.8)

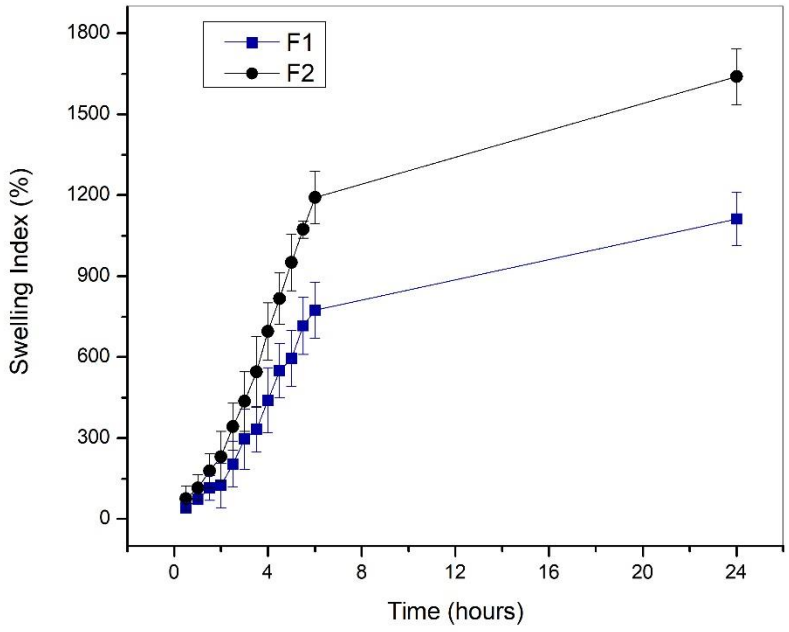

Figure 72 Swelling behavior curves of curcuminoids loaded hydrogel beads in simulated intestinal fluid PBS (pH = 6.8)

The swelling behavior of curcuminoids loaded F1 and F2 nanocomposite beads evaluated in HCl (pH=1.2), and phosphate buffer (pH=6.8) are shown in Figs. 69 and 72, respectively.

The swelling index of both F1 and F2 nanocomposite beads containing curcuminoids sodium remained low in HCl (pH=1.2) during the 2 h in comparison with that in phosphate buffer (pH=6.8), initially. This was occurred due to shrinkage of alginate at acidic pH. Maximum swelling of F1 and F2 was noticed after 24h in phosphate buffer, (pH=6.8) and after which, erosion and dissolution took place. It has been previously reported that the swelling of alginate depends on the progressive displacement of calcium ions within alginate-based beads (283, 284). It has been also reported that the swelling of alginate-based beads can be enhanced by the presence of phosphate ions (in phosphate buffer), which act as calcium sequestrant (284). The increase of volume in wet beads after swelling can be explained due to the absorption of free water that fills the void regions of the polymer network and/or the centre of larger pores and macropores (285).

Therefore, the swelling behavior of curcuminoids loaded nanocomposite beads in phosphate buffer (pH=6.8) could be explained by the ion exchanging between calcium ion of the ionotropically cross-liked beads and the sodium ions present in phosphate buffer, with the influence of calcium sequestrant phosphate ions, which resulted in absorption of water molecules and disaggregation in the polymer-clay matrix structure leading to matrix erosion and dissolution of the swollen beads.

Alginate/Na-B/HPMC based F2 beads exhibited additional swelling in PBS (pH=6.8) solution than F1 beads formulated without HPMC. This behavior can be explained due to the high hydrophilicity and swellability of HPMC. It has been reported that HPMC is a hydrophilic polymer that swells to a significant extent upon contact with water (120).

III.11 Cumulative Drug Release

III.11.1 Calibration Curve

A calibration curve of curcuminoids was prepared in PBS (pH=6.8) in the range of 4-12 µg/ml by UV-Visible spectrophotometer. The absorbance of solution was measured at 420 nm. regression coefficient was found 0.9935.

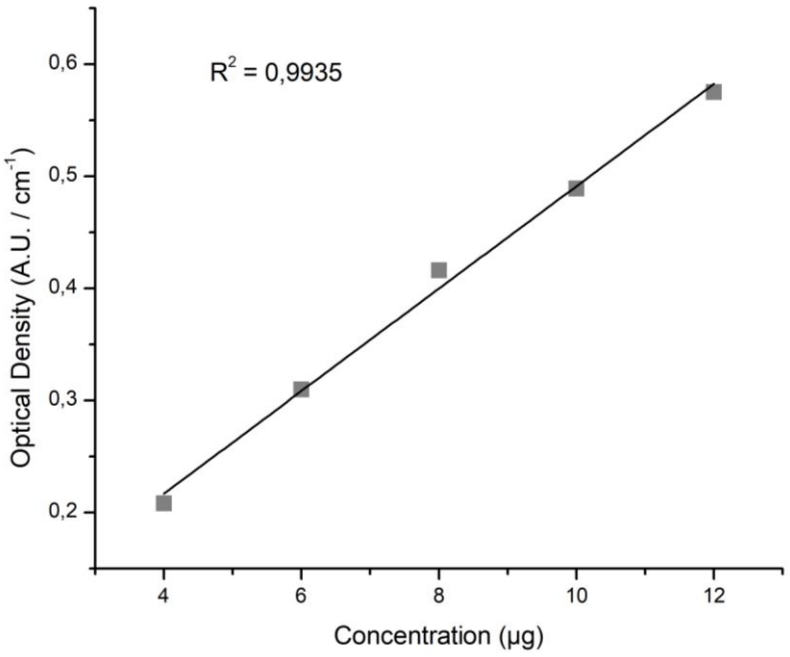

Figure 73 Calibration curve of curcuminoids nanosuspension in PBS (pH=6.8) for the drug release

III.11.2 Cumulative Drug Release in HCl (pH = 1.2)

Figure 74 Cumulative Drug Release of F1 in HCl (pH = 1.2)

Figure 75 Cumulative Drug Release of F2 in HCL (pH = 1.2)

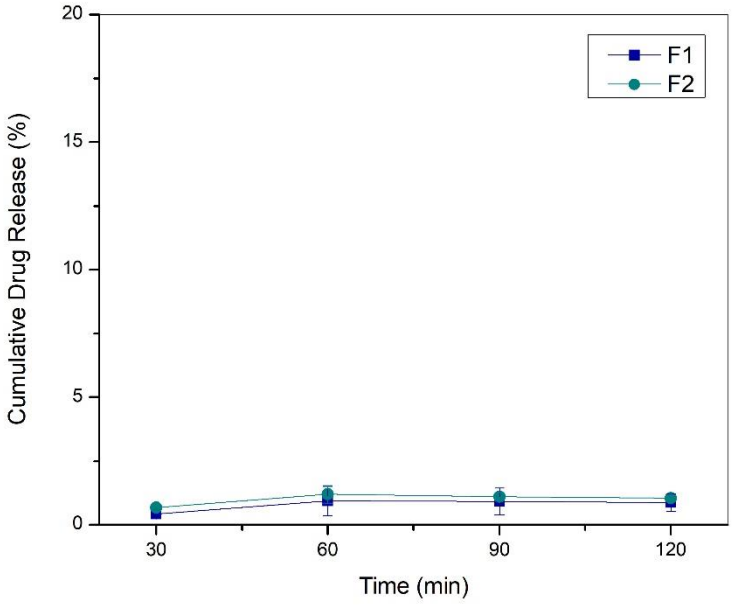

Figure 76 Cumulative drug release curves of curcuminoids loaded hydrogel beads in simulated gastric fluid HCl (pH = 1.2)

III.11.3 Cumulative Drug Release in PBS (pH = 6.8)

Figure 77 Cumulative Drug Release of F1 in PBS (pH = 6.8)

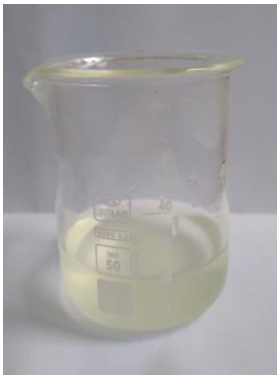

Figure 78 Cumulative Drug Release of F2 in PBS (pH = 6.8)

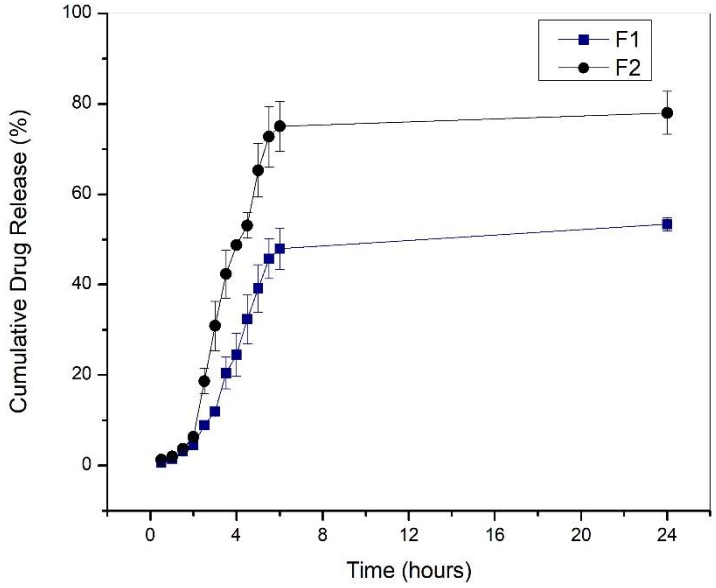

Figure 79 Cumulative drug release curves of curcuminoids from nanocomposite hydrogel beads in simulated intestinal fluid PBS (pH = 6.8)

The in vitro drug release studies were carried out for F1 and F2 curcuminoids loaded nanocomposite beads in simulated gastric fluid HCl medium (pH=1.2) for 2 h and in simulated intestinal fluid phosphate buffer (pH=6.8) for 24 h.

Only less than 1% of curcuminoids release was observed in simulated gastric fluid (pH=1.2) after 2 h, due to the poor solubility of alginate in lower pH (Fig. 76). The trace amounts of release could probably be due to the surface adhered drug (286).

The release profile in simulated intestinal fluid showed 47.95 ± 4.6 % and 75 ± 5.48 % released from F1 and F2 curcuminoids loaded nanocomposite in 6 h, respectively, thereafter the release of curcuminoids remained constant up to 24 h. The reason of the higher drug release in phosphate buffer (pH=6.8) was due to the higher swelling rate of these beads. F1 and F2 curcuminoids loaded nanocomposite beads showed prolonged release of drug over 6 h. It was found to be higher with the F2 formulation where HPMC was used as additional polymer, indicating that the presence of HPMC substantially increases the release rate.

The release tests showed that the incorporation of HPMC in F2 beads, even at small amount (0.25 % w/v), in the alginate increased the release of curcuminoids. This can be attributed to the high swellability of HPMC. In terms of the structure of the polymeric network this is associated with the interactions between alginate, sodium bentonite, HPMC and the curcuminoids. The polymeric network is dominated by physical entanglements between the curcuminoids nanosuspension and alginate/HPMC chains (262).

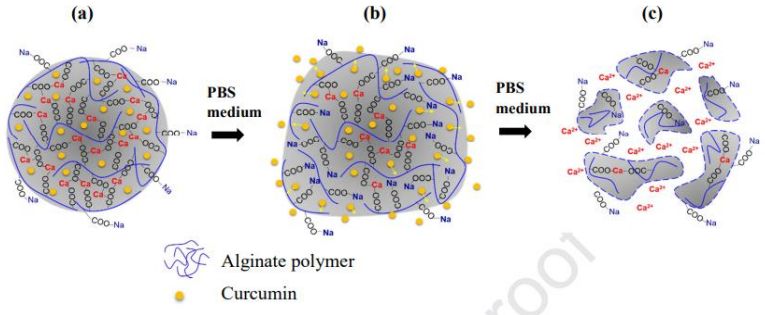

Figure 80 Schematic mechanism of curcumin release and degradation of microspheres. (a) Egg-box model in calcium alginate microspheres loaded curcumin, (b) Na^+ ions replace Ca^{2+} ions, microspheres swells up, curcumin diffuses out; and (c) disruption of 'egg-box' model, alginate matrix is disintegrated and dissolves (287).

The sustained release could be explained due to better adsorption of curcuminoids on the bentonite clay mineral particles (238)

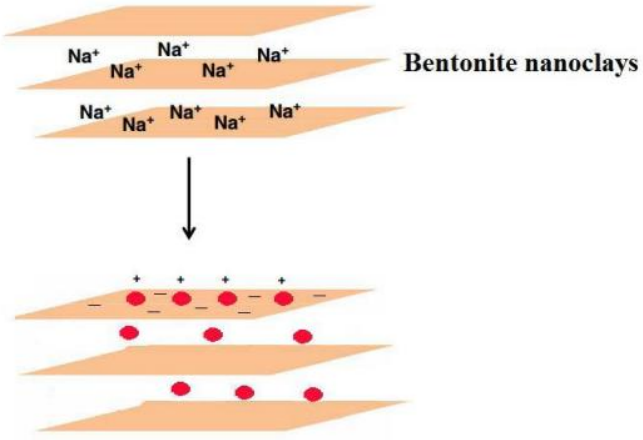

Figure 81 Adsorption of drugs on the negatively charged bentonite layers (288)

.

Finally, these results clearly suggest that the developed nanocomposite beads may not swell in stomach. As they subsequently move to intestine, these beads begin to swell more and behave as matrices for sustained release of loaded curcuminoids. F2 beads had the best cumulative drug release compared to F1 beads. Further, the slowed swelling and erosion of nanocomposite beads in phosphate buffer can be confirmed by the results of release mechanism of swelling and relaxation of matrix (286).

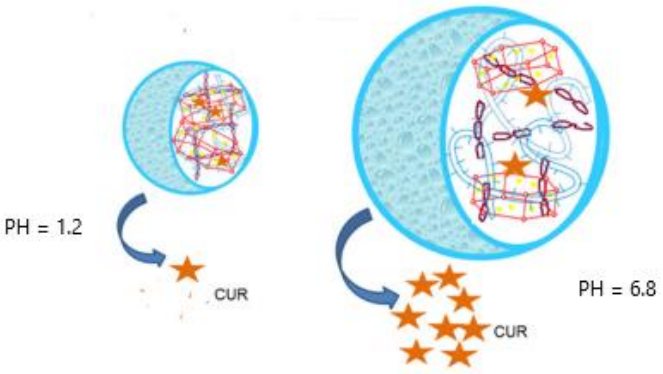

Figure 82 Release behavior of curcuminoids from nanocomposite hydrogel beads at pH=1.2 and pH=6.8 (259)

III.12 Study of Drug Release Kinetics

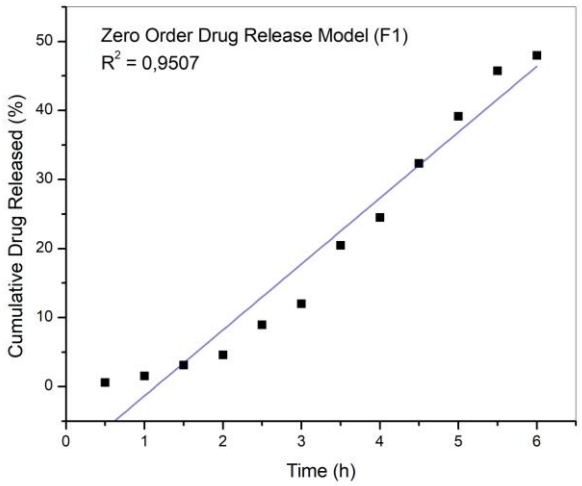

Figure 83 Zero order drug release plot of F1 beads

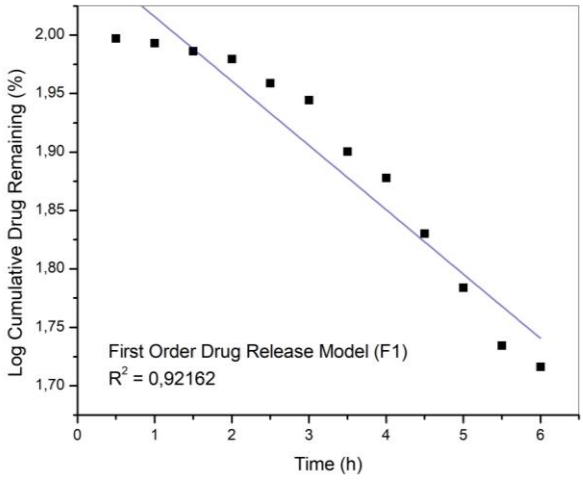

Figure 84 First order drug release plot of F1 beads

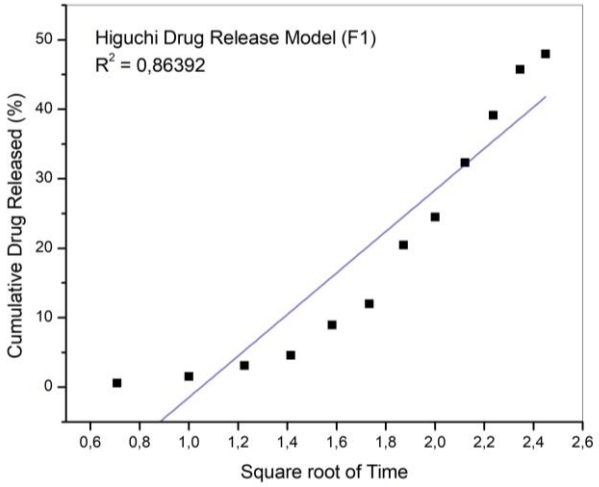

Figure 85 Higuchi drug release model plot of F1 beads

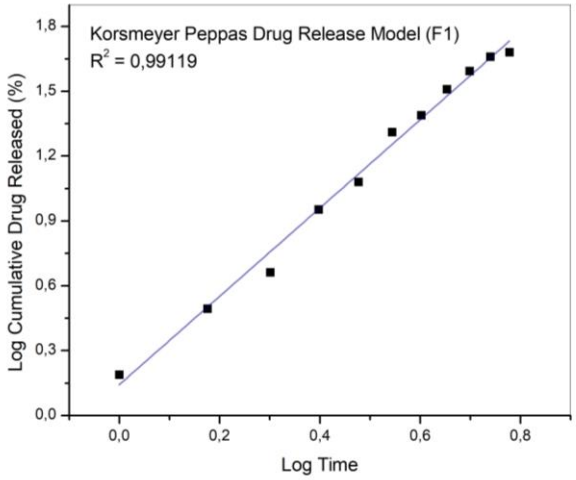

Figure 86 Korsmeyer-Peppas drug release model plot of F1 beads

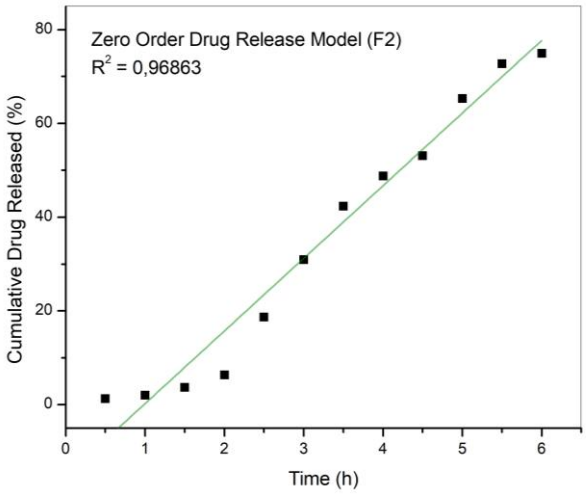

Figure 87 Zero order drug release plot of F2 beads

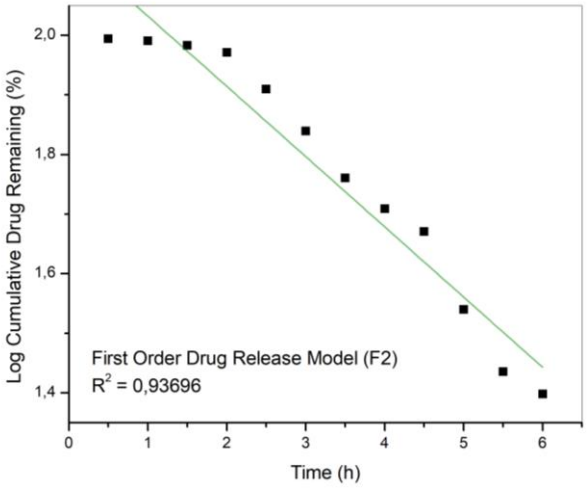

Figure 88 First order drug release plot of F2 beads

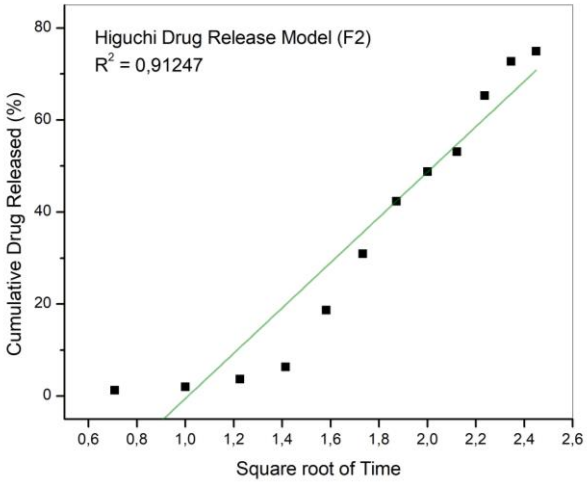

Figure 89 Higuchi drug release model plot of F2 beads

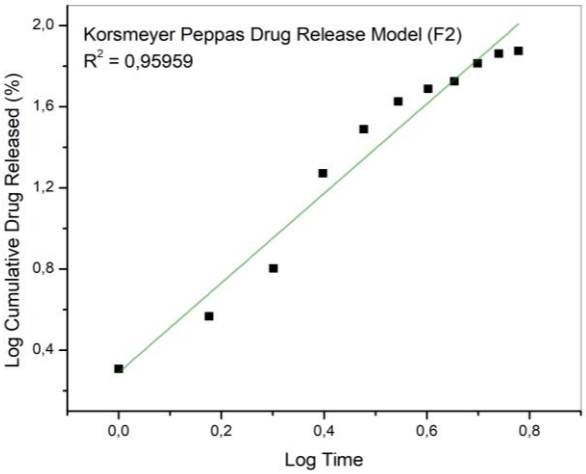

Figure 90 Korsmeyer-Peppas drug release model plot of F2 beads

Curve fitting analysis was done for F1 and F2 formulations to determine the type of drug release kinetic mechanism.

The R^2 correlation coefficient values for various models are listed in Table XI.

Table XI Summary of the various kinetic models followed by F1 and F2 formulations

	R^2					Best model
	Zero order	First order	Higuchi	Korsmeyer-Peppas		
				R^2	n (Slope)	
F1	0.9507	0.92162	0.86392	0.99119	2.04318	Korsmeyer-Peppas
F2	0.96863	0.93696	0.91247	0.95959	2.20761	Zero order

Based on the cumulative drug release results of curcuminoids, the drug release kinetics and the release mechanism were evaluated by fitting the release results into different mathematical models including zero-order, first-order, Higuchi and Korsmeyer-Peppas models. The correlation coefficients (R^2) were used to determine the accuracy and prediction ability of these models. The plots shows the curcuminoids release kinetic models. The best linear line of the F1 (1.5% w/v SA, 3% w/v Na-B) formulation was found on Korsmeyer-Peppas model with the correlation coefficient R^2 = 0.99119, The F2 (1.5% w/v SA, 3% w/v Na-B, 0.25% w/v HPMC) formulation followed the zero order release model with the correlation coefficient R^2 = 0.96863. The zero-order model in F2 beads indicated that the release of curcuminoids from the HPMC based nanocomposite hydrogel is independent of curcuminoids concentration. The correlation coefficient for the F1 formulation indicated the sustained release kinetics of drug carrier is consistent with Korsmeyer–Peppas model (289).

Additionally, the exponent n was used to characterize the release mechanism of curcuminoids, which is determined by the slope in the spot of the Korsmeyer-Peppas model, It can be seen that the n value were 2.04318 and 2.20761 for the F1 and F2 formulations respectively, showing the mechanism followed the super case II transport (case II relaxation) mechanism controlled by swelling/relaxation of polymeric-blend matrix (swelling-controlled release) and erosion of polymeric chains (290).

III.13 In Silico prediction

Figure 91 3d graphical visualization of the binding mode of curcumin against TGF- β receptor I kinase

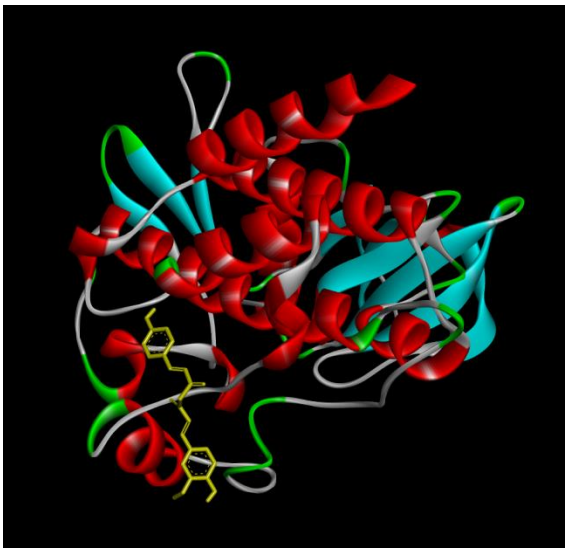

Figure 92 3d graphical visualization of the binding mode of demethoxycurcumin against TGF- β receptor I kinase

Figure 93 3d graphical visualization of the binding mode of bisdemethoxycurcumin against TGF- β receptor I kinase

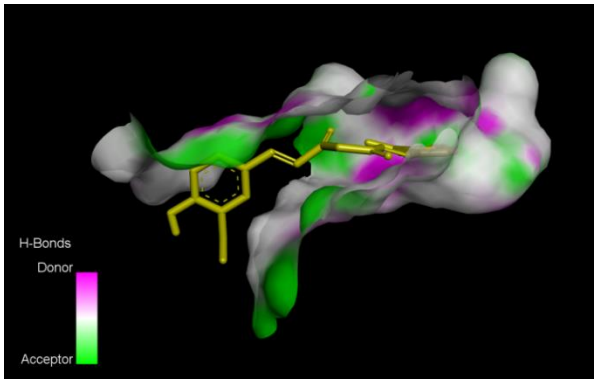

Figure 94 Hydrogen bond binding pocket of curcumin againstTGF- β receptor I kinase

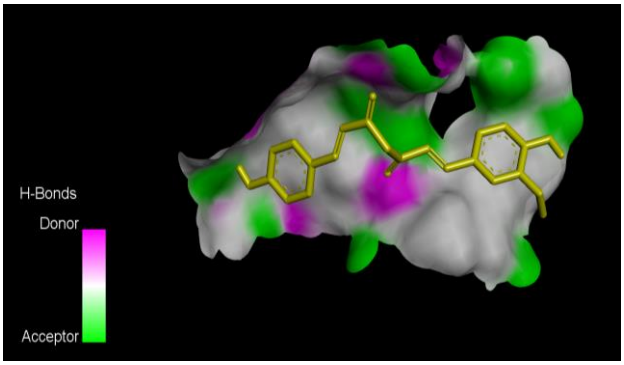

Figure 95 Hydrogen bond binding pocket of demethoxycurcumin against TGF- β receptor I kinase

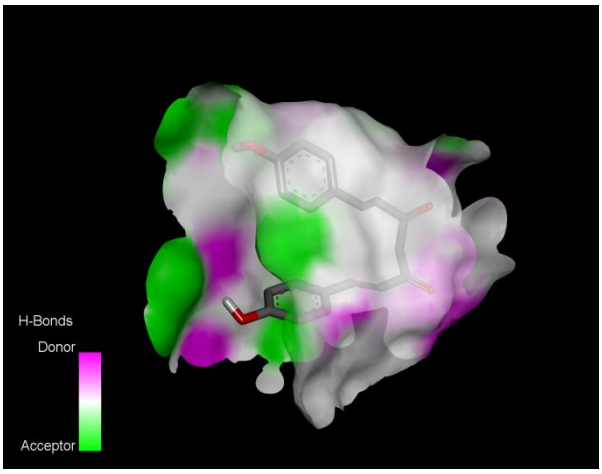

Figure 96 Hydrogen bond binding pocket of demethoxycurcumin against TGF- β receptor I kinase

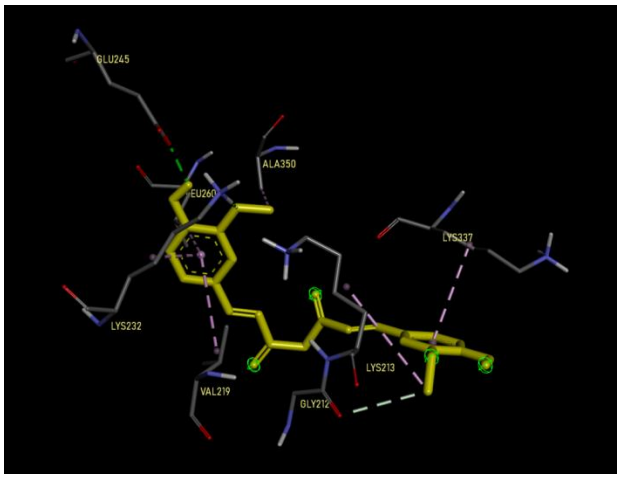

Figure 97 3d graphical illustration of the interaction between curcumin and TGF- β receptor I kinase

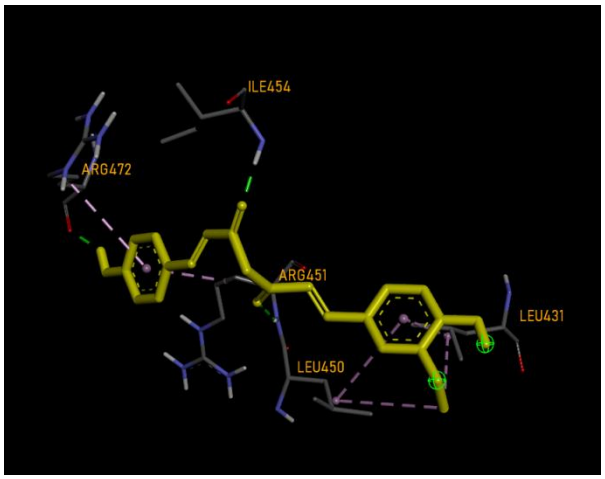

Figure 98 3d graphical illustration of the interaction between demethoxycurcumin and TGF- β receptor I kinase

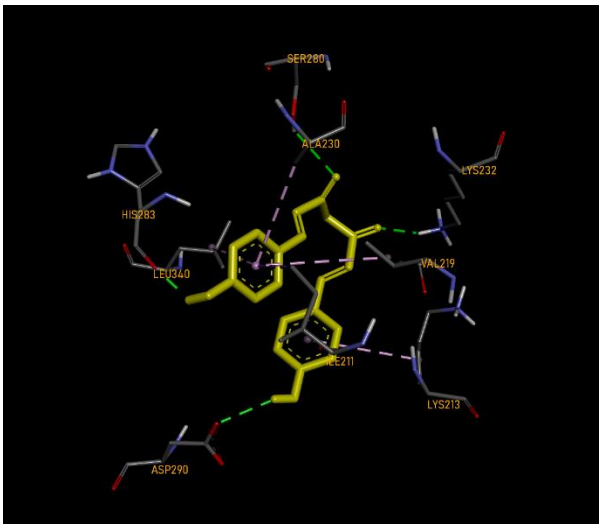

Figure 99 3d graphical illustration of the interaction between bisdemethoxycurcumin and TGF- β receptor I kinase

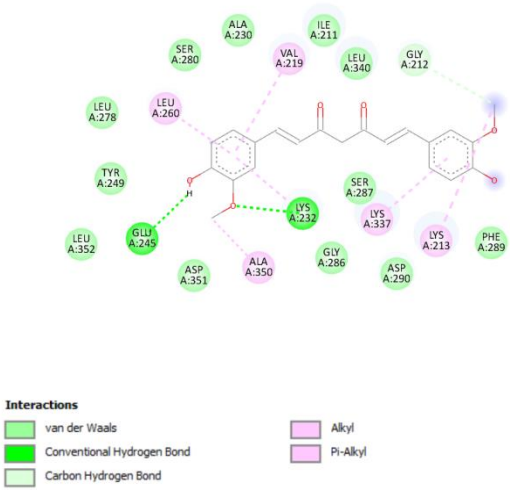

Figure 100 Schematic interaction between curcumin and TGF- β receptor I kinase, green dashed lines indicate hydrogen bonds

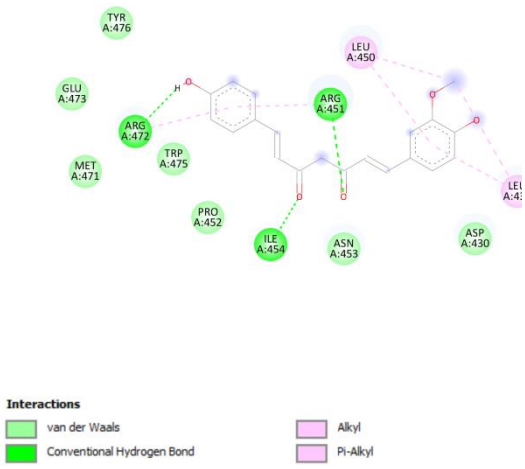

Figure 101 Schematic interaction between demethoxycurcumin and TGF- β receptor I kinase, green dashed lines indicate hydrogen bonds

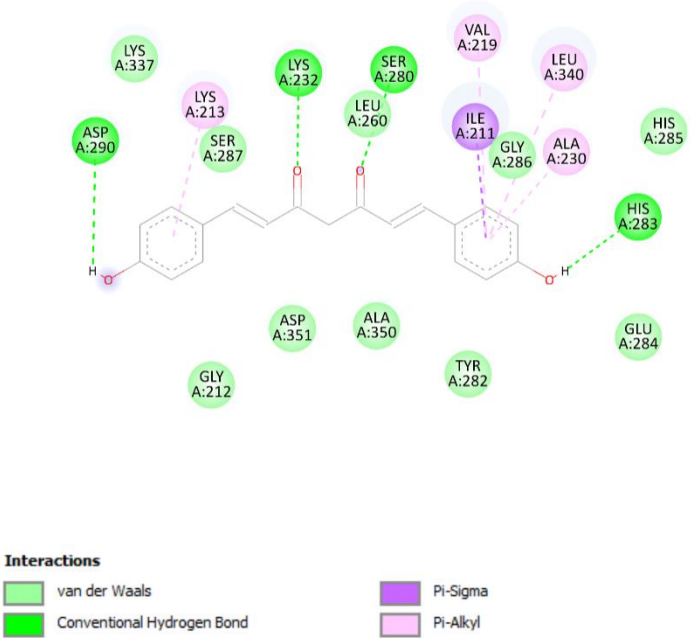

Figure 102 Schematic interaction between bisdemethoxycurcumin and TGF- β receptor I kinase, green dashed lines indicate hydrogen bonds

Table XII Molecular docking results of curcumin, demethoxycurcumin and bisdemethoxycurcumin against TGF β I

Ligand	Binding energy (kcal/mol)	Number of Hydrogen bonds	Aminoacid residues	Distance (Å)
Curcumin	-5.32	2	LYS232	2.36
			GLU245	2.14
Demethoxycurcumin	-5.23	3	ARG451	2.32
			ILE454	1.70
			ARG472	1.98
Bisdemethoxycurcumin	-6.2	4	LYS232	2.19
			SER280	2.78
			HIS283	1.99
			ASP290	2.70

Table XII shows the binding energies obtained with curcuminoids phytochemicals along with interacting residues and bond length of molecular interaction. Amongst all studied phytochemicals, promising strong inhibitions could be observed with Bisdemethoxycurcumin, curcumin.

Curcumin, demethoxycurcumin, bisdemethoxycurcumin docked to TGF- β receptor I kinase with ΔG of -5.32, -5.23 and -6.2 kcal/mol respectively The interactions of curcumin, demethoxycurcumin, bisdemethoxycurcumin to TGF- β receptor I kinase were strongly favored by hydrogen bonds.

Bisdemethoxycurcumin and curcumin exhibited interactions to the same potential active site.Residues like Lys232, Ser280, His283 and Asp290 when docked to TGF- β receptor I kinase seems to play important role in the binding of Bisdemethoxycurcumin.

These data indicate that the TGF- β receptor I kinase will be more stable in binding to bisdemethoxycurcumin and curcumin compared to demethoxycurcumin.

The results suggested that bisdemethoxycurcumin and curcumin have potential to be lead molecules for the development of inhibitor targeting TGF- β receptor I kinase.

Conclusion

In this research, curcuminoids were extracted from turmeric in a simple and easy way by ultrasound assisted extraction using acetone as solvent and the yield of extraction was finely soft clear yellow powder, the components curcumin, demethoxycurcumin and bisdemethoxycurcumin were identified by TLC.

Furthemore, nanosuspension of curcuminoids was prepared by acid-base CO_2 assisted effervescence technique using Tween 80 as stabilizer to improve the solubility of curcuminoids in aqueous solution. In this process, the particle size of the nanosuspension was obtained in the nano-size ranges. Moreover, Raw Bentonite clay was successfully activated by sodium carbonate into sodium Bentonite to inhance the swelling property.

After that, Curcuminoids nanosuspension chosen as the model drug intermediate for oral drug delivery system, hence it was entrapped inside spherical nanocomposite hydrogel beads by ionic gelation method using calcium chloride as a crosslinking agent. Alginate/Na-Bentonite/HPMC nanocomposite combination system was able to efficiently enhance the cumulative drug release and swelling due to the additional synergic swellability of HPMC in simulated intestinal fluid compared to Alginate/Na-Bentonite combination.

It was also demonstrated that the entrapment efficiency was higher over 99% and the drug mechanism of both formulations followed a super case II transport joining the swelling and erosion systems of the polymer matrix.

The In silico prediction results obtained from this study will be valuable for the future in vitro and clinical studies of curcuminoids entrapped inside nanocomposite hydrogel beads as potent TGF beta 1 receptor inhibitors for promising anti-colorectal therapeutics.

The present research work leaves the following future prospects:

- Targeting TGF beta 1 receptor of anti colorectal cancerous activity of the curcuminoids nanocomposite hydrogel drug delivery systems
- Interaction between nanosuspension and polymer-clay matrix may be investigated in details.
- Various plants extract containing poorly soluble phytochemicals can be used to synthesize nanosuspensions.
- Enhancing the swelling and drug release of drug delivery systems by using low cost natural clay materials
- Improving the sustained release mechanism for the delivery oral drugs.
- Elucidating the anticolorectal mechanism of curcumin on the TGF beta 1 receptor via in vitro studies

References

1. Siegel R, Ma J, Zou Z, Jemal A. Cancer statistics, 2014. CA: a cancer journal for clinicians. 2014;64(1):9-29.
2. Siegel R, DeSantis C, Jemal A. Colorectal cancer statistics, 2014. CA: a cancer journal for clinicians. 2014;64(2):104-17.
3. Anand P, Kunnumakkara AB, Newman RA, Aggarwal BB. Bioavailability of curcumin: problems and promises. Molecular pharmaceutics. 2007;4(6):807-18.
4. Jagetia GC, Aggarwal BB. "Spicing up" of the immune system by curcumin. Journal of clinical immunology. 2007;27(1):19-35.
5. Egan ME, Pearson M, Weiner SA, Rajendran V, Rubin D, Glockner-Pagel J, et al. Curcumin, a major constituent of turmeric, corrects cystic fibrosis defects. Science. 2004;304(5670):600-2.
6. Carroll RE, Benya RV, Turgeon DK, Vareed S, Neuman M, Rodriguez L, et al. Phase IIa clinical trial of curcumin for the prevention of colorectal neoplasia. Cancer prevention research. 2011;4(3):354-64.
7. He Z-Y, Shi C-B, Wen H, Li F-L, Wang B-L, Wang J. Upregulation of p53 expression in patients with colorectal cancer by administration of curcumin. Cancer investigation. 2011;29(3):208-13.
8. Naksuriya O, Okonogi S, Schiffelers RM, Hennink WE. Curcumin nanoformulations: a review of pharmaceutical properties and preclinical studies and clinical data related to cancer treatment. Biomaterials. 2014;35(10):3365-83.
9. Safavy A, Raisch KP, Mantena S, Sanford LL, Sham SW, Krishna NR, et al. Design and development of water-soluble curcumin conjugates as potential anticancer agents. Journal of medicinal chemistry. 2007;50(24):6284-8.
10. Sun M, Su X, Ding B, He X, Liu X, Yu A, et al. Advances in nanotechnology-based delivery systems for curcumin. Nanomedicine. 2012;7(7):1085-100.
11. Chattopadhyay I, Biswas K, Bandyopadhyay U, Banerjee RK. Turmeric and curcumin: Biological actions and medicinal applications. Current science. 2004:44-53.
12. Nawaz A, Khan GM, Hussain A, Ahmad A, Khan A, Safdar M. Curcumin: a natural product of biological importance. Gomal Univ J Res. 2011;27(1):07-14.
13. Kunta N. Techno-economic analysis of extraction curcumin from turmeric. 2018.
14. Weiss EA. Spice crops: CABI; 2002.
15. Asta. A concise guide to spices, herbs, seeds, and extractives. American Spice Trade Association. 2002:48-50.
16. Govindarajan V, Stahl WH. Turmeric—chemistry, technology, and quality. Critical Reviews in Food Science & Nutrition. 1980;12(3):199-301.
17. Tainter DR, Grenis AT. Spices and seasonings: a food technology handbook: John Wiley & Sons; 2001.
18. Leong-Škorničková J, ŠÍDA O, Wijesundara S, Marhold K. On the identity of turmeric: the typification of Curcuma longa L.(Zingiberaceae). Botanical Journal of the Linnean Society. 2008;157(1):37-46.

19. Kieliszek M, Edris A, Kot AM, Piwowarek K. Biological activity of some aromatic plants and their metabolites, with an emphasis on health-promoting properties. Molecules. 2020;25(11):2478.
20. Mazza G, Lauro G, Francis F. Natural Food Colorants: Science and Technology. Marcel Decker: New York, NY, USA. 2000:289-314.
21. Plotto A. Turmeric: post-production management. Food and Agriculture Organization http://www.fao.org/fileadmin/user_upload/inpho/docs/Post_Harvest_Compendium_-_Turmeric pdf. 2004 [Accessed 14 June 2022].
22. Akram M, Shahab-Uddin AA, Usmanghani K, Hannan A, Mohiuddin E, Asif M. Curcuma longa and curcumin: a review article. Rom J Biol Plant Biol. 2010;55(2):65-70.
23. Kotra VSR, Satyabanta L, Goswami TK. A critical review of analytical methods for determination of curcuminoids in turmeric. Journal of food science and technology. 2019;56(12):5153-66.
24. Beevers CS, Huang S. Pharmacological and clinical properties of curcumin. Botanics: Targets and Therapy. 2011;1:5-18.
25. Fuchs JR, Pandit B, Bhasin D, Etter JP, Regan N, Abdelhamid D, et al. Structure–activity relationship studies of curcumin analogues. Bioorganic & medicinal chemistry letters. 2009;19(7):2065-9.
26. Patumraj S, Yoysungneon P. Curcumin as a therapeutic agent against cancer. Asian Biomedicine Vol. 1 No. 3 October 2007;239-252.
27. Košťálová D, Bezáková L, Račkovác L, Mošovská S, Šturdík E. Therapeutic potential of curcumin in medicinal chemistry. Acta Chimica Slovaca. 2013;6(1):89-99.
28. Menon VP, Sudheer AR. Antioxidant and anti-inflammatory properties of curcumin. The molecular targets and therapeutic uses of curcumin in health and disease. 2007:105-25.
29. Kim YS, Young MR, Bobe G, Colburn NH, Milner JA. Bioactive Food Components, Inflammatory Targets, and Cancer PreventionDiet, Inflammation, and Cancer Prevention. Cancer prevention research. 2009;2(3):200-8.
30. Rathaur P, Raja W, Ramteke P, John SA. Turmeric: The golden spice of life. International Journal of pharmaceutical sciences and research. 2012;3(7):1987.
31. Kumar A, Dora J, Singh A. A review on spice of life Curcuma longa (turmeric). Int J Appl Biol Pharmaceut Tech. 2011;2:371-9.
32. Sa G, Das T, Banerjee S, Chakraborty J. Curcumin: from exotic spice to modern anticancer drug. Al Ameen J Med Sci. 2010;3:21-37.
33. Shishodia S, Sethi G, Aggarwal BB. Curcumin: getting back to the roots. Annals of the New York Academy of sciences. 2005;1056(1):206-17.
34. Rai M, Pandit R, Gaikwad S, Yadav A, Gade A. Potential applications of curcumin and curcumin nanoparticles: From traditional therapeutics to modern nanomedicine. Nanotechnology Reviews. 2015;4(2):161-72.
35. Zhang R, Li S, Zhu Z, He J. Recent advances in valorization of Chaenomeles fruit: A review of botanical profile, phytochemistry, advanced extraction technologies and bioactivities. Trends in Food Science & Technology. 2019;91:467-82.
36. Jiang T, Ghosh R, Charcosset C. Extraction, purification and applications of curcumin from plant materials-A comprehensive review. Trends in Food Science & Technology. 2021;112:419-30.

37. Wakte PS, Sachin B, Patil A, Mohato D, Band T, Shinde D. Optimization of microwave, ultra-sonic and supercritical carbon dioxide assisted extraction techniques for curcumin from Curcuma longa. Separation and purification technology. 2011;79(1):50-5.
38. Verghese J. Isolation of curcumin from Curcuma longa L. rhizome. Flavour and fragrance journal. 1993;8(6):315-9.
39. Kunwar A, Barik A, Pandey R, Priyadarsini KI. Transport of liposomal and albumin loaded curcumin to living cells: an absorption and fluorescence spectroscopic study. Biochimica et Biophysica Acta (BBA)-General Subjects. 2006;1760(10):1513-20.
40. Li L, Braiteh FS, Kurzrock R. Liposome-encapsulated curcumin: in vitro and in vivo effects on proliferation, apoptosis, signaling, and angiogenesis. Cancer: Interdisciplinary International Journal of the American Cancer Society. 2005;104(6):1322-31.
41. Prasad S, Tyagi AK, Aggarwal BB. Recent developments in delivery, bioavailability, absorption and metabolism of curcumin: the golden pigment from golden spice. Cancer research and treatment: official journal of Korean Cancer Association. 2014;46(1):2-18.
42. Priyadarsini KI. The chemistry of curcumin: from extraction to therapeutic agent. Molecules. 2014;19(12):20091-112.
43. Rajmohan D, Bellmer D. Characterization of Spirulina-alginate beads formed using ionic gelation. International journal of food science. 2019;2019.
44. George M, Abraham TE. Polyionic hydrocolloids for the intestinal delivery of protein drugs: alginate and chitosan—a review. Journal of controlled release. 2006;114(1):1-14.
45. Lee KY, Mooney DJ. Alginate: properties and biomedical applications. Progress in polymer science. 2012;37(1):106-26.
46. Draget KI, Skjåk-Bræk G, Smidsrød O. Alginate based new materials. International journal of biological macromolecules. 1997;21(1-2):47-55.
47. Paques JP, van der Linden E, van Rijn CJ, Sagis LM. Preparation methods of alginate nanoparticles. Advances in colloid and interface science. 2014;209:163-71.
48. De S, Robinson D. Polymer relationships during preparation of chitosan–alginate and poly-l-lysine–alginate nanospheres. Journal of Controlled Release. 2003;89(1):101-12.
49. Braccini I, Pérez S. Molecular basis of Ca2+-induced gelation in alginates and pectins: the egg-box model revisited. Biomacromolecules. 2001;2(4):1089-96.
50. Xu Y, Yang N, Yang J, Hu J, Zhang K, Nishinari K, et al. Protein/polysaccharide intramolecular electrostatic complex as superior food-grade foaming agent. Food Hydrocolloids. 2020;101:105474.
51. Okolie CL, Mason B, Mohan A, Pitts N, Udenigwe CC. Extraction technology impacts on the structure-function relationship between sodium alginate extracts and their in vitro prebiotic activity. Food Bioscience. 2020;37:100672.
52. Liu J, Yang S, Li X, Yan Q, Reaney MJ, Jiang Z. Alginate oligosaccharides: production, biological activities, and potential applications. Comprehensive Reviews in Food Science and Food Safety. 2019;18(6):1859-81.
53. Cao L, Lu W, Mata A, Nishinari K, Fang Y. Egg-box model-based gelation of alginate and pectin: A review. Carbohydrate polymers. 2020;242:116389.
54. Farrés IF, Norton I. Formation kinetics and rheology of alginate fluid gels produced by in-situ calcium release. Food Hydrocolloids. 2014;40:76-84.
55. Gombotz WR, Wee S. Protein release from alginate matrices. Advanced drug delivery reviews. 1998;31(3):267-85.

56. Becker TA, Kipke DR, Brandon T. Calcium alginate gel: a biocompatible and mechanically stable polymer for endovascular embolization. Journal of Biomedical Materials Research: An Official Journal of The Society for Biomaterials and The Japanese Society for Biomaterials. 2001;54(1):76-86.
57. Raymond C Rowe PJSaMEQ. Handbook of Pharmaceutical excipients 6th edition ed.
58. Kumar BP, Chandiran IS, Bhavya B, Sindhuri M. Microparticulate drug delivery system: a review. Indian journal of pharmaceutical science & research. 2011;1(1):19-37.
59. Venkatesan J, Alam MS, Hong EJ, Kim S-K, Shim MS. Preparation of piperlongumine-loaded chitosan nanoparticles for safe and efficient cancer therapy. RSC advances. 2016;6(83):79307-16.
60. Poncelet D, Lencki R, Beaulieu C, Halle J, Neufeld R, Fournier A. Production of alginate beads by emulsification/internal gelation. I. Methodology. Applied Microbiology and Biotechnology. 1992;38(1):39-45.
61. Mathiowitz E. Encyclopedia of controlled drug delivery: Wiley; 1999.
62. Merakchi A, Bettayeb S, Drouiche N, Adour L, Lounici H. Cross-linking and modification of sodium alginate biopolymer for dye removal in aqueous solution. Polymer Bulletin. 2019;76(7):3535-54.
63. Tønnesen HH, Karlsen J. Alginate in drug delivery systems. Drug development and industrial pharmacy. 2002;28(6):621-30.
64. Kim C-K, Lee E-J. The controlled release of blue dextran from alginate beads. International Journal of pharmaceutics. 1992;79(1-3):11-9.
65. Yotsuyanagi T, Ohkubo T, Ohhashi T, Ikeda K. Calcium-induced gelation of alginic acid and pH-sensitive reswelling of dried gels. Chemical and Pharmaceutical Bulletin. 1987;35(4):1555-63.
66. Sugawara S, Imai T, Otagiri M. The controlled release of prednisolone using alginate gel. Pharmaceutical research. 1994;11(2):272-7.
67. Chen S-C, Wu Y-C, Mi F-L, Lin Y-H, Yu L-C, Sung H-W. A novel pH-sensitive hydrogel composed of N, O-carboxymethyl chitosan and alginate cross-linked by genipin for protein drug delivery. Journal of controlled release. 2004;96(2):285-300.
68. Bajpai S, Sharma S. Investigation of swelling/degradation behaviour of alginate beads crosslinked with Ca2+ and Ba2+ ions. Reactive and Functional Polymers. 2004;59(2):129-40.
69. Pillay V, Dangor C, Govender T, Moopanar K, Hurbans N. Drug release modulation from cross-linked calcium alginate microdiscs, 1: Evaluation of the concentration dependency of sodium alginate on drug entrapment capacity, morphology, and dissolution rate. Drug Delivery. 1998;5(1):25-34.
70. Aslani P, Kennedy RA. Studies on diffusion in alginate gels. I. Effect of cross-linking with calcium or zinc ions on diffusion of acetaminophen. Journal of controlled release. 1996;42(1):75-82.
71. Al-Musa S, Fara DA, Badwan A. Evaluation of parameters involved in preparation and release of drug loaded in crosslinked matrices of alginate. Journal of controlled release. 1999;57(3):223-32.
72. Remuñán-López C, Bodmeier R. Mechanical, water uptake and permeability properties of crosslinked chitosan glutamate and alginate films. Journal of controlled release. 1997;44(2-3):215-25.

73. Takka S, Acarturk F. Calcium alginate microparticles for oral administration: III. The effect of crosslink agents and various additive polymers on drug release and drug entrapment efficiency. Pharmazie. 1999;54(2).
74. Takagi I, Nakashima H, Takagi M, YOTSUYANAGI T, IKEDA K. Application of alginate gel as a vehicle for liposomes. II. Erosion of alginate gel beads and the release of loaded liposomes. Chemical and pharmaceutical bulletin. 1997;45(2):389-93.
75. Monshipouri M, Rudolph A. Liposome-encapsulated alginate: controlled hydrogel particle formation and release. Journal of microencapsulation. 1995;12(2):117-27.
76. Xue C, Yu G, Hirata T, Terao J, Lin H. Antioxidative activities of several marine polysaccharides evaluated in a phosphatidylcholine-liposomal suspension and organic solvents. Bioscience, biotechnology, and biochemistry. 1998;62(2):206-9.
77. Ribeiro AJ, Neufeld RJ, Arnaud P, Chaumeil JC. Microencapsulation of lipophilic drugs in chitosan-coated alginate microspheres. International journal of pharmaceutics. 1999;187(1):115-23.
78. Sachan NK, Pushkar S, Jha A, Bhattcharya A. Sodium alginate: the wonder polymer for controlled drug delivery. J Pharm Res. 2009;2(8):1191-9.
79. Gomez d'Ayala G, Malinconico M, Laurienzo P. Marine derived polysaccharides for biomedical applications: chemical modification approaches. Molecules. 2008;13(9):2069-106.
80. Goh CH, Heng PWS, Chan LW. Alginates as a useful natural polymer for microencapsulation and therapeutic applications. Carbohydrate polymers. 2012;88(1):1-12.
81. Liberski AR. Three-dimensional printing of alginate: From seaweeds to heart valve scaffolds. QScience Connect. 2016;2016(2):3.
82. Sosnik A. Alginate particles as platform for drug delivery by the oral route: state-of-the-art. International Scholarly Research Notices. 2014;2014.
83. Augst AD, Kong HJ, Mooney DJ. Alginate hydrogels as biomaterials. Macromolecular bioscience. 2006;6(8):623-33.
84. Abdellatif A, El Hamd M, Saleh K. A formulation, optimization and evaluation of controlled released alginate beads loaded-flurbiprofen. J Nanomed Nanotechnol. 2016;7(357):2.
85. Al-Otoum R, Abulateefeh S, Taha M. Preparation of novel ionotropically crosslinked beads based on alginate-terephthalic acid composites as potential controlled release matrices. Die Pharmazie-An International Journal of Pharmaceutical Sciences. 2014;69(1):10-8.
86. Liakos I, Rizzello L, Bayer IS, Pompa PP, Cingolani R, Athanassiou A. Controlled antiseptic release by alginate polymer films and beads. Carbohydrate polymers. 2013;92(1):176-83.
87. Eisenhour DD, Brown RK. Bentonite and Its Impact on Modern Life. Elements. 2009;5(2):83-8.
88. Park J-H, Shin H-J, Kim MH, Kim J-S, Kang N, Lee J-Y, et al. Application of montmorillonite in bentonite as a pharmaceutical excipient in drug delivery systems. Journal of Pharmaceutical Investigation. 2016;46(4):363-75.
89. Önal M. Physicochemical properties of bentonites: an overview. Communications Faculty of Sciences University of Ankara Series B Chemistry and Chemical Engineering. 2006;52(02).
90. Mahesh K, Murthy HN, Kumaraswamy B, Raghavendra N, Sridhar R, Krishna M, et al. Synthesis and characterization of organomodified Na-MMT using cation and anion surfactants. Frontiers of Chemistry in China. 2011;6(2):153-8.

91. Rolfe BN, McQueen IS, Miller RF, Miller RF. Dispersion characteristics of montmorillonite, kaolinite, and illite clays in waters of varying quality, and their control with phosphate dispersants: US Government Printing Office; 1960.
92. Chen J, Gong G, Zhao L, Sun X. Determination of cation exchange capacity of expansive soils. Rock and mineral analysis. 2000;19(2):152-4.
93. Clem AG, Doehler RW. Industrial applications of bentonite. Clays and Clay minerals. 1961;10(1):272-83.
94. Gleason MH, Daniel DE, Eykholt GR. Calcium and sodium bentonite for hydraulic containment applications. Journal of geotechnical and geoenvironmental engineering. 1997;123(5):438-45.
95. Jiang S, Yang Z, Yang W, Wang S, Liu F, Johnston L, et al. Effect of purified zearalenone with or without modified montmorillonite on nutrient availability, genital organs and serum hormones in post-weaning piglets. Livestock Science. 2012;144(1-2):110-8.
96. Song S, Peng C, Gonzalez-Olivares M, Lopez-Valdivieso A, Fort T. Study on hydration layers near nanoscale silica dispersed in aqueous solutions through viscosity measurement. Journal of Colloid and Interface Science. 2005;287(1):114-20.
97. Norrish K. The swelling of montmorillonite. Discussions of the Faraday society. 1954;18:120-34.
98. Low PF. The swelling of clay: II. Montmorillonites. Soil science society of america journal. 1980;44(4):667-76.
99. Low PF. Nature and properties of water in montmorillonite-water systems. Soil Science Society of America Journal. 1979;43(4):651-8.
100. Malfoy C, Pantet A, Monnet P, Righi D. Effects of the nature of the exchangeable cation and clay concentration on the rheological properties of smectite suspensions. Clays and Clay Minerals. 2003;51(6):656-63.
101. Baker J, Grabowska-Olszewska B, Uwins P. ESEM study of osmotic swelling of bentonite from Radzionkow (Poland). Applied Clay Science. 1995;9(6):465-9.
102. Xu Y, Matsuoka H, Sun D. Swelling characteristics of fractal-textured bentonite and its mixtures. Applied Clay Science. 2003;22(4):197-209.
103. Savjani KT, Gajjar AK, Savjani JK. Drug solubility: importance and enhancement techniques. International Scholarly Research Notices. 2012;2012.
104. Grant GJ, Vermeulen K, Zakowski MI, Stenner M, Turndorf H, Langerman L. Prolonged analgesia and decreased toxicity with liposomal morphine in a mouse model. Anesthesia and analgesia. 1994;79(4):706-9.
105. Kim T, Murdande S, Gruber A, Kim S. Sustained-release morphine for epidural analgesia in rats. The Journal of the American Society of Anesthesiologists. 1996;85(2):331-8.
106. Oh S-T, Kwon O-J, Chun B-C, Cho J-W, Park J-S. The effect of bentonite concentration on the drug delivery efficacy of a pH-sensitive alginate/bentonite hydrogel. Fibers and Polymers. 2009;10(1):21-6.
107. Kevadiya BD, Joshi GV, Patel HA, Ingole PG, Mody HM, Bajaj HC. Montmorillonite-alginate nanocomposites as a drug delivery system: intercalation and in vitro release of vitamin B1 and vitamin B6. Journal of biomaterials applications. 2010;25(2):161-77.
108. Iliescu RI, Andronescu E, Ghitulica CD, Berger D, Ficai A. Montmorillonite-alginate nanocomposite beads as drug carrier for oral administration of carboplatin-preparation and characterization. UPB Sci Bull, Series B: Chem Mat Sci. 2011;73:3-16.

109. Iliescu RI, Andronescu E, Ghitulica CD, Voicu G, Ficai A, Hoteteu M. Montmorillonite–alginate nanocomposite as a drug delivery system–incorporation and in vitro release of irinotecan. International journal of pharmaceutics. 2014;463(2):184-92.

110. 정경희, 강세미, 이재호, 황대연, 정영진. Preparation and characterization of pH-sensitive sodium alginate/poly (vinyl alcohol)/bentonite blend beads for controlled release of diclofenac sodium. 한국고분자학회 학술대회 연구논문 초록집. 2013:121-.

111. Liu B, Luo J, Wang X, Lu J, Deng H, Sun R. Alginate/quaternized carboxymethyl chitosan/clay nanocomposite microspheres: preparation and drug-controlled release behavior. Journal of Biomaterials Science, Polymer Edition. 2013;24(5):589-605.

112. Yan H, Feng Y, Hu W, Cheng C, Liu R, Wang C, et al. Preparation and evaluation of alginate-chitosan-bentonite based beads for the delivery of pesticides in controlled-release formulation. Asian Journal of Chemistry. 2013;25(17):9936-40.

113. Kevadiya B, Patel H, Joshi G, Abdi S, Bajaj H. Montmorillonite-alginate composites as a drug delivery system: Intercalation and In vitro release of diclofenac sodium. Indian journal of pharmaceutical sciences. 2010;72(6):732.

114. Mahkam M, Latifpour A, Rafi AA, Gheshlaghi LM, Takfallah A. Preparation of montmorillonite-pH-sensitive positive charges nanocomposites as a drug delivery system. International Journal of Polymeric Materials and Polymeric Biomaterials. 2015;64(1):32-7.

115. Wertz J-L, Bédué O, Bédué O, Mercier JP. Cellulose science and technology: EPFL press; 2010.

116. Rowe RC, Sheskey P, Quinn M. Handbook of pharmaceutical excipients: Libros Digitales-Pharmaceutical Press; 2009.

117. Embuscado ME. Functionalizing carbohydrates for food applications: texturizing and bioactive/flavor delivery systems: DEStech Publications, Inc; 2014.

118. Sarkar N, Walker L. Hydration—dehydration properties of methylcellulose and hydroxypropylmethylcellulose. Carbohydrate polymers. 1995;27(3):177-85.

119. Ghori MU. Release kinetics, compaction and electrostatic properties of hydrophilic matrices: University of Huddersfield; 2014.

120. Siepmann J, Peppas NA. Modeling of drug release from delivery systems based on hydroxypropyl methylcellulose (HPMC). Advanced drug delivery reviews. 2012;64:163-74.

121. Maderuelo C, Zarzuelo A, Lanao JM. Critical factors in the release of drugs from sustained release hydrophilic matrices. Journal of controlled release. 2011;154(1):2-19.

122. Wen X, Nokhodchi A, Rajabi-Siahboomi A. Oral extended release hydrophilic matrices: formulation and design. Oral controlled release formulation design and drug delivery: Theory to practice", H Wen, K Park (eds), John Wiley & Sons, Inc, Hoboken, New Jersey. 2010:89-100.

123. Li CL, Martini LG, Ford JL, Roberts M. The use of hypromellose in oral drug delivery. Journal of pharmacy and pharmacology. 2005;57(5):533-46.

124. Ghori MU, Ginting G, Smith AM, Conway BR. Simultaneous quantification of drug release and erosion from hypromellose hydrophilic matrices. International journal of pharmaceutics. 2014;465(1-2):405-12.

125. Smith ND. Fourier Transform Infrared Spectroscopy. Analyst. 1996;121:83N.

126. Bracewell RN. The Fourier Transform and Its applications (McGraw-Hill Series in Electrical and Computer Engineering. Circuits and Systems. McGraw-Hill (Boston, Mass.[ua]); 2000.

127. Gerwert K. Molecular reaction mechanisms of proteins as monitored by time-resolved FTIR spectroscopy. Current Opinion in Structural Biology. 1993;3(5):769-73.
128. Chan K, Kazarian SG, Vassou D, Gionis V, Chryssikos GD. In situ high-throughput study of drug polymorphism under controlled temperature and humidity using FT-IR spectroscopic imaging. Vibrational Spectroscopy. 2007;43(1):221-6.
129. Chan KA, Kazarian SG. FTIR spectroscopic imaging of dissolution of a solid dispersion of nifedipine in poly (ethylene glycol). Molecular Pharmaceutics. 2004;1(4):331-5.
130. Chen J-F, Zhang J-Y, Shen Z-G, Zhong J, Yun J. Preparation and characterization of amorphous cefuroxime axetil drug nanoparticles with novel technology: high-gravity antisolvent precipitation. Industrial & engineering chemistry research. 2006;45(25):8723-7.
131. Selva TMG, Selva JSG, Prata RB. Sensing Materials: Diamond-Based Materials. 2021.
132. Wunderlich B. A classification of molecules, phases, and transitions as recognized by thermal analysis. Thermochimica Acta. 1999;340:37-52.
133. Morgan D. DL Bish & JE Post (Editors) Modern Powder Diffraction.(Reviews in Mineralogy, Volume 20). Mineralogical Society of America, Washington, DC, 1989. xi+ 369 pp. Price US70). ISBN: 0.939950. 24.3. Clay Minerals. 1990;25(4):544-5.
134. Ivanisevic I, McClurg RB, Schields PJ. Uses of X-ray powder diffraction in the pharmaceutical industry. Pharmaceutical sciences encyclopedia: drug discovery, development, and manufacturing. 2010:1-42.
135. Cowley J. Diffraction Physics 2nd edn, 4th print. Amsterdam: North-Holland; 1990.
136. Hecq J, Deleers M, Fanara D, Vranckx H, Boulanger P, Le Lamer S, et al. Preparation and in vitro/in vivo evaluation of nano-sized crystals for dissolution rate enhancement of ucb-35440-3, a highly dosed poorly water-soluble weak base. European journal of pharmaceutics and biopharmaceutics. 2006;64(3):360-8.
137. Van Eerdenbrugh B, Van den Mooter G, Augustijns P. Top-down production of drug nanocrystals: nanosuspension stabilization, miniaturization and transformation into solid products. International journal of pharmaceutics. 2008;364(1):64-75.
138. Jacobs C, Müller RH. Production and characterization of a budesonide nanosuspension for pulmonary administration. Pharmaceutical research. 2002;19(2):189-94.
139. Rabinow BE. Nanosuspensions in drug delivery. Nature reviews Drug discovery. 2004;3(9):785-96.
140. Wang Y, Liu Z, Zhang D, Gao X, Zhang X, Duan C, et al. Development and in vitro evaluation of deacety mycoepoxydiene nanosuspension. Colloids and surfaces B: biointerfaces. 2011;83(2):189-97.
141. Wang Y, Zhang D, Liu Z, Liu G, Duan C, Jia L, et al. In vitro and in vivo evaluation of silybin nanosuspensions for oral and intravenous delivery. Nanotechnology. 2010;21(15):155104.
142. Kipp JE, Wong JCT, Doty MJ, Rebbeck CL. Microprecipitation method for preparing submicron suspensions. Google Patents; 2003.
143. Wang Y, Zheng Y, Zhang L, Wang Q, Zhang D. Stability of nanosuspensions in drug delivery. Journal of controlled release. 2013;172(3):1126-41.
144. Jacobs C, Kayser O, Müller R. Production and characterisation of mucoadhesive nanosuspensions for the formulation of bupravaquone. International journal of pharmaceutics. 2001;214(1-2):3-7.

145. Han X, Wang M, Ma Z, Xue P, Wang Y. A new approach to produce drug nanosuspensions CO2-assisted effervescence to produce drug nanosuspensions. Colloids and Surfaces B: Biointerfaces. 2016;143:107-10.
146. Lakshmi P, Kumar GA. Nanosuspension technology: A review.
147. Merkus HG. Particle size measurements: fundamentals, practice, quality: Springer Science & Business Media; 2009.
148. Agarwal V. Emerging analytical techniques used for nanocrystal and nanosuspension. 2019.
149. Christoph H. Particle measurement by dynamic scattered light. LaborPraxis. 1995;19:34-5.
150. Mandal B. Preparation and physicochemical characterization of Eudragit® RL100 Nanosuspension with potential for Ocular Delivery of Sulfacetamide: University of Toledo; 2010.
151. Morris GM, Lim-Wilby M. Molecular docking. Molecular modeling of proteins: Springer; 2008. p. 365-82.
152. Lengauer T, Rarey M. Computational methods for biomolecular docking. Current opinion in structural biology. 1996;6(3):402-6.
153. Kitchen DB, Decornez H, Furr JR, Bajorath J. Docking and scoring in virtual screening for drug discovery: methods and applications. Nature reviews Drug discovery. 2004;3(11):935-49.
154. Chaudhary KK, Mishra N. A review on molecular docking: novel tool for drug discovery. databases. 2016;3(4):1029.
155. Morrison JL, Breitling R, Higham DJ, Gilbert DR. A lock-and-key model for protein–protein interactions. Bioinformatics. 2006;22(16):2012-9.
156. Koshland Jr DE. The key–lock theory and the induced fit theory. Angewandte Chemie International Edition in English. 1995;33(23-24):2375-8.
157. Audie J, Scarlata S. A novel empirical free energy function that explains and predicts protein–protein binding affinities. Biophysical chemistry. 2007;129(2-3):198-211.
158. Fan J, Fu A, Zhang L. Progress in molecular docking. Quantitative Biology. 2019;7(2):83-9.
159. Morris GM, Huey R, Lindstrom W, Sanner MF, Belew RK, Goodsell DS, et al. AutoDock4 and AutoDockTools4: Automated docking with selective receptor flexibility. Journal of computational chemistry. 2009;30(16):2785-91.
160. Mcmartin C, Bohacek RS. QXP: powerful, rapid computer algorithms for structure-based drug design. Journal of computer-aided molecular design. 1997;11(4):333-44.
161. Schnecke V, Kuhn LA. Virtual screening with solvation and ligand-induced complementarity. Virtual Screening: An Alternative or Complement to High Throughput Screening?: Springer; 2000. p. 171-90.
162. Friesner RA, Banks JL, Murphy RB, Halgren TA, Klicic JJ, Mainz DT, et al. Glide: a new approach for rapid, accurate docking and scoring. 1. Method and assessment of docking accuracy. Journal of medicinal chemistry. 2004;47(7):1739-49.
163. Jones G, Willett P, Glen RC, Leach AR, Taylor R. Development and validation of a genetic algorithm for flexible docking. Journal of molecular biology. 1997;267(3):727-48.
164. Venkatachalam CM, Jiang X, Oldfield T, Waldman M. LigandFit: a novel method for the shape-directed rapid docking of ligands to protein active sites. Journal of Molecular Graphics and Modelling. 2003;21(4):289-307.

165. Goodsell DS, Olson AJ. Automated docking of substrates to proteins by simulated annealing. Proteins: Structure, Function, and Bioinformatics. 1990;8(3):195-202.
166. Kuntz ID, Blaney JM, Oatley SJ, Langridge R, Ferrin TE. A geometric approach to macromolecule-ligand interactions. Journal of molecular biology. 1982;161(2):269-88.
167. Wong A, Ma BB. Personalizing therapy for colorectal cancer. Clinical Gastroenterology and Hepatology. 2014;12(1):139-44.
168. Fearon ER. Molecular genetics of colorectal cancer. Annual Review of Pathology: Mechanisms of Disease. 2011;6:479-507.
169. Tabana Y, Dahham S, Shah A, Majid A. Major signaling pathways of colorectal carcinogenesis. Recent Adv Colon Cancer. 2016;1:1-2.
170. Elliott RL, Blobe GC. Role of transforming growth factor Beta in human cancer. Journal of clinical oncology. 2005;23(9):2078-93.
171. Li F, Cao Y, Townsend CM, Ko TC. TGF-β signaling in colon cancer cells. World journal of surgery. 2005;29(3):306-11.
172. Meulmeester E, Ten Dijke P. The dynamic roles of TGF-β in cancer. The Journal of pathology. 2011;223(2):206-19.
173. Hocevar BA, Smine A, Xu X-X, Howe PH. The adaptor molecule Disabled-2 links the transforming growth factor β receptors to the Smad pathway. The EMBO journal. 2001;20(11):2789-801.
174. Moustakas A, Souchelnytskyi S, Heldin C-H. Smad regulation in TGF-β signal transduction. Journal of cell science. 2001;114(24):4359-69.
175. Penheiter SG, Mitchell H, Garamszegi N, Edens M, Doré Jr JJ, Leof EB. Internalization-dependent and-independent requirements for transforming growth factor β receptor signaling via the Smad pathway. Molecular and cellular biology. 2002;22(13):4750-9.
176. Di Guglielmo GM, Le Roy C, Goodfellow AF, Wrana JL. Distinct endocytic pathways regulate TGF-β receptor signalling and turnover. Nature cell biology. 2003;5(5):410-21.
177. Lampropoulos P, Zizi-Sermpetzoglou A, Rizos S, Kostakis A, Nikiteas N, Papavassiliou AG. TGF-beta signalling in colon carcinogenesis. Cancer letters. 2012;314(1):1-7.
178. Wu J-W, Hu M, Chai J, Seoane J, Huse M, Li C, et al. Crystal structure of a phosphorylated Smad2: Recognition of phosphoserine by the MH2 domain and insights on Smad function in TGF-β signaling. Molecular cell. 2001;8(6):1277-89.
179. Itoh S, Itoh F, Goumans MJ, ten Dijke P. Signaling of transforming growth factor-β family members through Smad proteins. European Journal of Biochemistry. 2000;267(24):6954-67.
180. Huse M, Muir TW, Xu L, Chen Y-G, Kuriyan J, Massagué J. The TGFβ receptor activation process: an inhibitor-to substrate-binding switch. Molecular cell. 2001;8(3):671-82.
181. Kurisaki A, Kose S, Yoneda Y, Heldin C-H, Moustakas A. Transforming growth factor-β induces nuclear import of Smad3 in an importin-β1 and Ran-dependent manner. Molecular biology of the cell. 2001;12(4):1079-91.
182. Massagué J. How cells read TGF-β signals. Nature reviews Molecular cell biology. 2000;1(3):169-78.
183. Miyazono K. TGF-β signaling by Smad proteins. Cytokine & growth factor reviews. 2000;11(1-2):15-22.
184. Dong C, Li Z, Alvarez Jr R, Feng X-H, Goldschmidt-Clermont PJ. Microtubule binding to Smads may regulate TGFβ activity. Molecular cell. 2000;5(1):27-34.

185. Gilboa L, Nohe A, Geissendorfer T, Sebald W, Henis YI, Knaus P. Bone morphogenetic protein receptor complexes on the surface of live cells: a new oligomerization mode for serine/threonine kinase receptors. Molecular biology of the cell. 2000;11(3):1023-35.
186. Liberati NT, Moniwa M, Borton AJ, Davie JR, Wang X-F. An essential role for Mad homology domain 1 in the association of Smad3 with histone deacetylase activity. Journal of Biological Chemistry. 2001;276(25):22595-603.
187. Hanyu A, Ishidou Y, Ebisawa T, Shimanuki T, Imamura T, Miyazono K. The N domain of Smad7 is essential for specific inhibition of transforming growth factor-β signaling. The Journal of cell biology. 2001;155(6):1017-28.
188. Datta PK, Moses HL. STRAP and Smad7 synergize in the inhibition of transforming growth factor β signaling. Molecular and cellular biology. 2000;20(9):3157-67.
189. Koveitypour Z, Panahi F, Vakilian M, Peymani M, Seyed Forootan F, Nasr Esfahani MH, et al. Signaling pathways involved in colorectal cancer progression. Cell & bioscience. 2019;9(1):1-14.
190. Shishodia S, Chaturvedi MM, Aggarwal BB. Role of curcumin in cancer therapy. Current problems in cancer. 2007;31(4):243-305.
191. Shehzad A, Lee J, Lee YS. Curcumin in various cancers. Biofactors. 2013;39(1):56-68.
192. Patel BB, Majumdar AP. Synergistic role of curcumin with current therapeutics in colorectal cancer: minireview. Nutrition and cancer. 2009;61(6):842-6.
193. Shehzad A, Lee Y. Curcumin: Multiple molecular targets mediate multiple pharmacological actions: A review. Drugs Fut. 2010;35(2):113.
194. Shehzad A, Wahid F, Lee YS. Curcumin in cancer chemoprevention: molecular targets, pharmacokinetics, bioavailability, and clinical trials. Archiv der Pharmazie. 2010;343(9):489-99.
195. Lao CD, Ruffin MT, Normolle D, Heath DD, Murray SI, Bailey JM, et al. Dose escalation of a curcuminoid formulation. BMC complementary and alternative medicine. 2006;6(1):1-4.
196. Mo N, Li Z-Q, Li J, Cao Y-D. Curcumin inhibits TGF-β1-induced MMP-9 and invasion through ERK and Smad signaling in breast cancer MDA-MB-231 cells. Asian Pacific Journal of Cancer Prevention. 2012;13(11):5709-14.
197. Milacic V, Banerjee S, Landis-Piwowar KR, Sarkar FH, Majumdar AP, Dou QP. Curcumin inhibits the proteasome activity in human colon cancer cells in vitro and in vivo. Cancer research. 2008;68(18):7283-92.
198. Rayet B, Gelinas C. Aberrant rel/nfkb genes and activity in human cancer. Oncogene. 1999;18(49):6938-47.
199. Chung M-Y, Lim TG, Lee KW. Molecular mechanisms of chemopreventive phytochemicals against gastroenterological cancer development. World Journal of Gastroenterology: WJG. 2013;19(7):984.
200. Mendelson J, Song S, Li Y, Maru DM, Mishra B, Davila M, et al. Dysfunctional transforming growth factor-β signaling with constitutively active notch signaling in Barrett's esophageal adenocarcinoma. Cancer. 2011;117(16):3691-702.
201. Subramaniam D, Ponnurangam S, Ramamoorthy P, Standing D, Battafarano RJ, Anant S, et al. Curcumin induces cell death in esophageal cancer cells through modulating Notch signaling. PloS one. 2012;7(2):e30590.
202. Chaurasia G. A review on pharmaceutical preformulation studies in formulation and development of new drug molecules. International journal of Pharmaceutical sciences and research. 2016;7(6):2313.

203. Curcumin PubChem [Available from: https://pubchem.ncbi.nlm.nih.gov/compound/969516.
204. DMC Pubchem [Available from: https://pubchem.ncbi.nlm.nih.gov/compound/5469424.
205. BDMC Pubchem.
206. Aggarwal BB, Kumar A, Bharti AC. Anticancer potential of curcumin: preclinical and clinical studies. Anticancer research. 2003;23(1/A):363-98.
207. Curcumin [Available from: https://pubchem.ncbi.nlm.nih.gov/compound/969516.
208. Bong PH. Spectral and photophysical behaviors of curcumin and curcuminoids. Bulletin of the Korean Chemical Society. 2000;21(1):81-6.
209. Tønnesen HH. Chemistry of curcumin and curcuminoids. ACS Publications; 1992.
210. Tønnesen HH, Másson M, Loftsson T. Studies of curcumin and curcuminoids. XXVII. Cyclodextrin complexation: solubility, chemical and photochemical stability. International journal of pharmaceutics. 2002;244(1-2):127-35.
211. Tønnesen HH, Karlsen J. Studies on curcumin and curcuminoids. Zeitschrift für Lebensmittel-Untersuchung und Forschung. 1985;180(5):402-4.
212. Curcumin Chemspider [Available from: https://www.chemspider.com/Chemical-Structure.839564.html.
213. Tonnesen H, HH T. Structural studies of curcuminoids. I: The crystal structure of curcumin. 1982.
214. Sanphui P, Goud NR, Khandavilli UR, Bhanoth S, Nangia A. New polymorphs of curcumin. Chemical Communications. 2011;47(17):5013-5.
215. Wang Y-J, Pan M-H, Cheng A-L, Lin L-I, Ho Y-S, Hsieh C-Y, et al. Stability of curcumin in buffer solutions and characterization of its degradation products. Journal of pharmaceutical and biomedical analysis. 1997;15(12):1867-76.
216. Lestari ML, Indrayanto G. Curcumin. Profiles of drug substances, excipients and related methodology. 2014;39:113-204.
217. Jasim F, Ali F. Measurements of some spectrophotometric parameters of curcumin in 12 polar and nonpolar organic solvents. Microchemical journal. 1989;39(2):156-9.
218. Shrivastava A, Sharma J, Jain S, Aggrawal KL. Incompatibility studies by high performance thinâ€ layer chromatography: In case of curcumin. Asian Journal of Pharmaceutics (AJP). 2013;7(2).
219. Anand P, Kunnumakkara AB, Newman RA, Aggarwal BBJMp. Bioavailability of curcumin: problems and promises. 2007;4(6):807-18.
220. Wahlström B, Blennow GJApet. A study on the fate of curcumin in the rat. 1978;43(2):86-92.
221. Pan M-H, Huang T-M, Lin J-KJDm, disposition. Biotransformation of curcumin through reduction and glucuronidation in mice. 1999;27(4):486-94.
222. Ireson C, Orr S, Jones DJ, Verschoyle R, Lim C-K, Luo J-L, et al. Characterization of metabolites of the chemopreventive agent curcumin in human and rat hepatocytes and in the rat in vivo, and evaluation of their ability to inhibit phorbol ester-induced prostaglandin E2 production. 2001;61(3):1058-64.
223. Sharma RA, Steward WP, Gescher AJJTmt, health tuoci, disease. Pharmacokinetics and pharmacodynamics of curcumin. 2007:453-70.
224. Gutierres VO, Campos ML, Arcaro CA, Assis RP, Baldan-Cimatti HM, Peccinini RG, et al. Curcumin pharmacokinetic and pharmacodynamic evidences in streptozotocin-diabetic rats support the antidiabetic activity to be via metabolite (s). 2015;2015.

225. Mirzaei H, Shakeri A, Rashidi B, Jalili A, Banikazemi Z, Sahebkar AJB, et al. Phytosomal curcumin: A review of pharmacokinetic, experimental and clinical studies. 2017;85:102-12.
226. Banker GS, Rhodes C. Modern Pharmaceutics marcel Dekker. New York. 1990:387-97.
227. Agrawal U, Sharma R, Gupta M, Vyas SP. Is nanotechnology a boon for oral drug delivery? Drug discovery today. 2014;19(10):1530-46.
228. Babahoum N, Ould Hamou M. Characterization and purification of Algerian natural bentonite for pharmaceutical and cosmetic applications. BMC chemistry. 2021;15(1):1-11.
229. Patil J, Kamalapur M, Marapur S, Kadam D. Ionotropic gelation and polyelectrolyte complexation: the novel techniques to design hydrogel particulate sustained, modulated drug delivery system: a review. Digest Journal of Nanomaterials and Biostructures. 2010;5(1):241-8.
230. Kulkarni RV, Sa B. Polyacrylamide-grafted-alginate-based pH-sensitive hydrogel beads for delivery of ketoprofen to the intestine: in vitro and in vivo evaluation. Journal of Biomaterials Science, Polymer Edition. 2009;20(2):235-51.
231. Chang SA, Gray DG. The surface tension of aqueous hydroxypropyl cellulose solutions. Journal of Colloid and Interface Science. 1978;67(2):255-65.
232. Brannon-Peppas L. Preparation and characterization of crosslinked hydrophilic networks. Studies in polymer science. 8: Elsevier; 1990. p. 45-66.
233. Liu Z, Li J, Nie S, Liu H, Ding P, Pan W. Study of an alginate/HPMC-based in situ gelling ophthalmic delivery system for gatifloxacin. International journal of pharmaceutics. 2006;315(1-2):12-7.
234. Benli B. Effect of borax addition on the structural modification of bentonite in biodegradable alginate-based biocomposites. Journal of applied polymer science. 2013;128(6):4172-80.
235. Günister E, Pestreli D, Ünlü CH, Atıcı O, Güngör N. Synthesis and characterization of chitosan-MMT biocomposite systems. Carbohydrate Polymers. 2007;67(3):358-65.
236. He Y, Wu Z, Tu L, Han Y, Zhang G, Li C. Encapsulation and characterization of slow-release microbial fertilizer from the composites of bentonite and alginate. Applied Clay Science. 2015;109:68-75.
237. Céspedes FF, García SP, Sánchez MV, Pérez MF. Bentonite and anthracite in alginate-based controlled release formulations to reduce leaching of chloridazon and metribuzin in a calcareous soil. Chemosphere. 2013;92(8):918-24.
238. Singh B, Sharma D, Kumar R, Gupta A. Controlled release of the fungicide thiram from starch–alginate–clay based formulation. Applied Clay Science. 2009;45(1-2):76-82.
239. Naresh D Joshi AAK, Makarand N Cherekar. Extraction and Purification of Curcumin from Turmeric. Asian Journal of Plant Science and Research. 2021;11(8):256-9.
240. Sahne F, Mohammadi M, Najafpour GD, Moghadamnia AA. Extraction of bioactive compound curcumin from turmeric (Curcuma longa L.) via different routes: A comparative study. Pakistan Journal of Biotechnology. 2016;13(3):173-80.
241. Pawar H, Gavasane A, Choudhary P. A novel and simple approach for extraction and isolation of curcuminoids from turmeric rhizomes. Nat Prod Chem Res. 2018;6(1):2329-68361000300.
242. Musaab Ibrahim Magzoub. Dhahran (SA); Mustafa Saleh Nasser DSIAH, Dhahran (SA); Mohamed Ahmed Nasr Eldin Mahmoud, Dhahran (SA); Abdullah Saad Sultan, Dhahran (SA), inventor; King Fahd University of Petroleum and Minerals, Dhahran (SA), assignee. METHOD OF PRODUCING SODUM BENTONITE. USJun. 13, 2017.

243. Wang Y, Wang C, Zhao J, Ding Y, Li L. A cost-effective method to prepare curcumin nanosuspensions with enhanced oral bioavailability. Journal of Colloid and Interface Science. 2017;485:91-8.
244. Song P, Wu Y, Zhang X, Yan Z, Wang M, Xu F. Preparation of covalently crosslinked sodium alginate/hydroxypropyl methylcellulose pH-sensitive microspheres for controlled drug release. BioResources. 2018;13(4):8614-28.
245. Jackson BP, Snowdon DW. Atlas of microscopy of medicinal plants, culinary herbs and spices1990.
246. Péret-Almeida L, Cherubino A, Alves R, Dufossé L, Glória M. Separation and determination of the physico-chemical characteristics of curcumin, demethoxycurcumin and bisdemethoxycurcumin. Food Research International. 2005;38(8-9):1039-44.
247. Dai YN, Li P, Zhang JP, Wang AQ, Wei QJB, disposition d. A novel pH sensitive N-succinyl chitosan/alginate hydrogel bead for nifedipine delivery. 2008;29(3):173-84.
248. Song S, Wang Z, Qian Y, Zhang L, Luo EJJoa, chemistry f. The release rate of curcumin from calcium alginate beads regulated by food emulsifiers. 2012;60(17):4388-95.
249. Hazra M, Mandal DD, Mandal T, Bhuniya S, Ghosh MJSPJ. Designing polymeric microparticulate drug delivery system for hydrophobic drug quercetin. 2015;23(4):429-36.
250. Monograph TJEDftQoM, Health Care of the Council of Europe e. European Pharmacopoeia. 2017;9:3104-5.
251. Convention GM, Pharmacopoeia GCftFotA, Convention NM, Pharmacopoeia NCfRt, Convention USP, editors. Pharmacopoeia of the United States of America: The United States Pharmacopoeia1893: United States Pharmacopoeial Convention, Incorporated.
252. Joy R, John F, George JJRoNDDViN. Preparation and Characterisation of Niosomal Emulsions as Novel Drug Delivery Vehicle Derived from Natural Seaweeds. 2019:79.
253. Moydeen A, Padusha A. MS; Aboelfetoh, EF; Al-Deyab, SS; El-Newehy, MH Fabrication of electrospun poly (vinyl alcohol)/dextran nanofibers via emulsion process as drug delivery system: Kinetics and in vitro release study. Int J Biol Macromol. 2018;116:1250-9.
254. Mate CJ, Mishra S, Srivastava P. In vitro release kinetics of graft matrices from Lannea coromandelica (Houtt) gum for treatment of colonic diseases by 5-ASA. International journal of biological macromolecules. 2020;149:908-20.
255. Javanbakht S, Pooresmaeil M, Namazi HJCp. Green one-pot synthesis of carboxymethylcellulose/Zn-based metal-organic framework/graphene oxide bio-nanocomposite as a nanocarrier for drug delivery system. 2019;208:294-301.
256. Javanbakht S, Nazari N, Rakhshaei R, Namazi HJCp. Cu-crosslinked carboxymethylcellulose/naproxen/graphene quantum dot nanocomposite hydrogel beads for naproxen oral delivery. 2018;195:453-9.
257. Rasoulzadeh M, Namazi HJCP. Carboxymethyl cellulose/graphene oxide bio-nanocomposite hydrogel beads as anticancer drug carrier agent. 2017;168:320-6.
258. Pooresmaeil M, Namazi HJC, Biointerfaces SB. Surface modification of graphene oxide with stimuli-responsive polymer brush containing β-cyclodextrin as a pendant group: Preparation, characterization, and evaluation as controlled drug delivery agent. 2018;172:17-25.
259. Pooresmaeil M, Namazi H. Facile preparation of pH-sensitive chitosan microspheres for delivery of curcumin; characterization, drug release kinetics and evaluation of anticancer activity. International journal of biological macromolecules. 2020;162:501-11.
260. 1RW8 RCSB [Available from: https://www.rcsb.org/structure/1RW8.

261. Krishna KB, Prabhakar C. A review on nanosuspensions in drug delivery. Int J Pharma and Bio Sci. 2011;2(1):549-58.
262. Nochos A, Douroumis D, Bouropoulos N. In vitro release of bovine serum albumin from alginate/HPMC hydrogel beads. Carbohydrate Polymers. 2008;74(3):451-7.
263. Wan LSC, Heng PWS, Wong LF. Matrix swelling: A simple model describing extent of swelling of HPMC matrices. International journal of pharmaceutics. 1995;116(2):159-68.
264. Tabak A, Afsin B, Caglar B, Koksal E. Characterization and pillaring of a Turkish bentonite (Resadiye). Journal of Colloid and Interface Science. 2007;313(1):5-11.
265. Ajemba RO. Structural alteration of bentonite from nkaliki by acid treatment: studies of the kinetics and properties of the modified samples. International Journal of Advances in Engineering & Technology. 2014;7(2):379.
266. Manohar D, Noeline B, Anirudhan T. Adsorption performance of Al-pillared bentonite clay for the removal of cobalt (II) from aqueous phase. Applied Clay Science. 2006;31(3-4):194-206.
267. Al-Essa K. NaCl-activated Jordanian bentonite for olive mill waste water treatment: Evaluation of physicochemical properties, adsorption of phenolic compounds: Isotherms and thermodynamic studies. RESEARCH JOURNAL OF PHARMACEUTICAL BIOLOGICAL AND CHEMICAL SCIENCES. 2018;9(3):1362-84.
268. Bharate SS, Bharate SB, Bajaj AN. Interactions and incompatibilities of pharmaceutical excipients with active pharmaceutical ingredients: a comprehensive review. Journal of Excipients and Food Chemicals. 2016;1(3):1131.
269. Zaghouane-Boudiaf H, Boutahala M, Sahnoun S, Tiar C, Gomri F. Adsorption characteristics, isotherm, kinetics, and diffusion of modified natural bentonite for removing the 2, 4, 5-trichlorophenol. Applied clay science. 2014;90:81-7.
270. Arbaoui F, Boucherit MN. Comparison of two Algerian bentonites: physico-chemical and retention capacity study. Applied Clay Science. 2014;91:6-11.
271. El-Kebir A, Harrane A, Belbachir M. Protonated montmorillonite clay used as green non-toxic catalyst for the synthesis of biocompatible polyglycidol. Arabian Journal for Science and Engineering. 2016;41(6):2179-84.
272. Chouli F, Benyoucef A, Yahiaoui A, Quijada C, Morallon E. A conducting nanocomposite via intercalative polymerisation of 2-methylaniline with aniline in montmorillonite cation-exchanged. Journal of Polymer Research. 2012;19(11):1-9.
273. Toumi I, Benyoucef A, Yahiaoui A, Quijada C, Morallon E. Effect of the intercalated cation-exchanged on the properties of nanocomposites prepared by 2-aminobenzene sulfonic acid with aniline and montmorillonite. Journal of alloys and compounds. 2013;551:212-8.
274. Zehhaf A, Morallon E, Benyoucef A. Polyaniline/montmorillonite nanocomposites obtained by in situ intercalation and oxidative polymerization in cationic modified-clay (sodium, copper and iron). Journal of Inorganic and Organometallic Polymers and Materials. 2013;23(6):1485-91.
275. Ourari A, Tennah F, Ruíz-Rosas R, Aggoun D, Morallón E. Bentonite Modified Carbon Paste Electrode as a Selective Electrochemical Sensor for the Detection of Cadmium and Lead in Aqueous Solution. Int J Electrochem Sci. 2018;13:1683-99.
276. Vaezi K, Asadpour G. Effects of HCl Hydrolyzed Cellulose Nanocrystals From Waste Papers on the Hydroxypropyl Methylcellulose/Cationic Starch Biofilms. Waste and Biomass Valorization. 2022;13(4):2035-51.

277. Reddy OS, Subha M, Jithendra T, Madhavi C, Rao KC. Curcumin encapsulated dual cross linked sodium alginate/montmorillonite polymeric composite beads for controlled drug delivery. Journal of pharmaceutical analysis. 2021;11(2):191-9.
278. Anitha A, Deepagan V, Rani VD, Menon D, Nair S, Jayakumar R. Preparation, characterization, in vitro drug release and biological studies of curcumin loaded dextran sulphate–chitosan nanoparticles. Carbohydrate Polymers. 2011;84(3):1158-64.
279. Ahmed MFA. Use of alginate/montmorillonite nanocomposites as a drug delivery system for curcumin. 2015.
280. Datta M. Clay–polymer nanocomposites as a novel drug carrier: Synthesis, characterization and controlled release study of Propranolol Hydrochloride. Applied clay science. 2013;80:85-92.
281. Doulia D, Leodopoulos C, Gimouhopoulos K, Rigas F. Adsorption of humic acid on acid-activated Greek bentonite. Journal of Colloid and Interface Science. 2009;340(2):131-41.
282. Wang SB, Chen AZ, Weng LJ, Chen MY, Xie XL. Effect of Drug-loading Methods on Drug Load, Encapsulation Efficiency and Release Properties of Alginate/Poly-L-Arginine/Chitosan Ternary Complex Microcapsules. Macromolecular bioscience. 2004;4(1):27-30.
283. Del Gaudio P, Colombo P, Colombo G, Russo P, Sonvico F. Mechanisms of formation and disintegration of alginate beads obtained by prilling. International journal of pharmaceutics. 2005;302(1-2):1-9.
284. Al-Kassas RS, Al-Gohary OM, Al-Faadhel MM. Controlling of systemic absorption of gliclazide through incorporation into alginate beads. International journal of pharmaceutics. 2007;341(1-2):230-7.
285. Hoffman AS. Hydrogels for biomedical applications. Advanced drug delivery reviews. 2012;64:18-23.
286. Nayak AK, Pal D. Development of pH-sensitive tamarind seed polysaccharide–alginate composite beads for controlled diclofenac sodium delivery using response surface methodology. International journal of biological macromolecules. 2011;49(4):784-93.
287. Uyen NTT, Hamid ZAA, Ahmad NB. Synthesis and characterization of curcumin loaded alginate microspheres for drug delivery. Journal of Drug Delivery Science and Technology. 2020;58:101796.
288. Hosseini F, Hosseini F, Jafari SM, Taheri A. Bentonite nanoclay-based drug-delivery systems for treating melanomaHosseini et al. Bentonite nanoclay-based drug-delivery system. Clay Minerals. 2018;53(1):53-63.
289. Ge M, Li Y, Zhu C, Liang G, SM JA, Hu G, et al. Preparation of organic-modified magadiite–magnetic nanocomposite particles as an effective nanohybrid drug carrier material for cancer treatment and its properties of sustained release mechanism by Korsmeyer–Peppas kinetic model. 2021;56(25):14270-86.
290. Singh Y. Martin's physical pharmacy and pharmaceutical sciences. New Jersey: Department of Pharmaceutics Ernest Mario School of Pharmacy Rutgers, The State University of New Jersey. 2006.

Abstract

Curcumin is widely used in potent anti-inflammatory herbal drug. But main problem with curcumin when given orally is its poor solubility and bioavailability due to less GI absorption. The purpose of this study was to investigate the release of curcuminoids from alginate/Na-Bentonite/hydroxypropyl-methylcellulose (HPMC) nanocomposite hydrogel beads. First curcuminoids were extracted by Ultrasound-assisted extraction, after that, it was formulated as a nanosuspension, then incorporated with the polymer-clay mixture to form a nanocomposite hydrogel beads by ionic gelation method. in silico anticolorectal prediction of curcuminoids was evaluated by molecular docking software AutoDock targeting the TGF-beta 1 receptor. Drug entrapment efficiency (DEE), drug loading (DL), swelling index (SI), in vitro cumulativee drug release, DLS, FTIR and XRD were all investigated. Average particule size of the nanosuspension was found 80 nm, DEE was found to be higher than 99% over a small percentage of DL. The results of the in vitro cumulative drug release profiles indicated that curcuminoids released from beads at (pH=1.2) were 1%, and at (pH=6.8), the amounts of curcuminoids released increased significantly to 74% over a sustained release of 6 h. An enhanced cumulative drug release of curcuminoids at pH 6.8 for the HPMC based beads. XRD analysis provided an encapsulation of curcuminoids as well as exfoliated sodium bentonite clay for the HPMC formulation. In silico anticolorectal prediction revealed that the three curcuminoids: curcumin, demethoxycurcumin, bisdemethoxycurcumin could potentially bind to TGF-beta 1 receptor. This study provided a novel formulation and demonstrated a sustained release profile and pH sensitivity, which can be considered as good approach for oral drug delivery application.

Keywords: curcuminoids, nanocomposite, beads, hydrogel, anticolorectal, TGF-beta 1 receptor

Résumé

La curcumine est largement utilisée comme médicament anti-inflammatoire puissant à base de plantes, mais le principal problème de la curcumine lorsqu'elle est administrée par voie orale est sa faible solubilité et biodisponibilité en raison d'une absorption gastro-intestinale réduite. L'objectif de cette étude était d'examiner la libération des curcuminoïdes à partir de billes d'hydrogel nanocomposites d'alginate/Na-Bentonite/hydroxypropyl-méthylcellulose (HPMC). Les curcuminoïdes ont d'abord été extraits par ultrasons, puis ils ont été formulés sous forme de nanosuspension, avant d'être incorporés au mélange polymère-argile pour former des billes d'hydrogel nanocomposites par une méthode de gélification ionique. La prédiction anticolorectale in silico des curcuminoïdes a été évaluée par le logiciel de docking moléculaire AutoDock en ciblant le récepteur TGF-beta 1. Le test d'encapsulation (DEE), la charge médicamenteuse (DL), l'indice de gonflement (SI), la libération cumulative du médicament in vitro, la DLS, la FTIR et la XRD ont été étudiés. La taille moyenne des particules de la nanosuspension était de 80 nm, le DEE était supérieur à 99% avec un faible pourcentage de DL. Les résultats des profils de libération cumulative de médicament in vitro ont indiqué que les curcuminoïdes libérés des billes à (pH=1,2) étaient de 1%, et à (pH=6,8), les quantités de curcuminoïdes libérés ont augmenté de manière significative à 74% sur une libération soutenue de 6 h. Une libération cumulative de médicament améliorée de curcuminoïdes à pH 6,8 pour les billes à base de HPMC. L'analyse XRD a montré une encapsulation des curcuminoïdes ainsi que de l'argile de bentonite de sodium exfoliée pour la formulation à base d'HPMC. La prédiction anticolorectale in silico a révélé que les trois curcuminoïdes : curcumine, déméthoxycurcumine, bisdeméthoxycurcumine pourraient potentiellement se lier au récepteur TGF-beta 1. Cette étude a fourni une nouvelle formulation et a démontré un profil de libération soutenue et une sensibilité au pH, ce qui peut être considéré comme une bonne approche pour l'application de l'administration orale de médicaments.

Mots clés : curcuminoïdes, nanocomposite, billes, hydrogel, anticolorectal, récepteur TGF-beta 1

الملخص

يستخدم الكركمين على نطاق واسع في الأدوية العشبية القوية المضادة للالتهابات. لكن المشكلة الرئيسية مع الكركمين عند تناوله عن طريق الفم هي ضعف قابلية الذوبان والتوافر البيولوجي بسبب انخفاض امتصاص الجهاز الهضمي. كان الغرض من هذه الدراسة هو التحقيق في إطلاق الكوركومينويد من كرات هيدروجيل المركبات النانوية hydroxypropyl-methylcellulose / Na-Bentonite / (HPMC).تم استخلاص الكوركومينويد الأول عن طريق الاستخلاص بمساعدة الموجات فوق الصوتية ، وبعد ذلك ، تمت صياغته كمعلق نانوي ، ثم تم دمجه مع خليط البوليمر والطين لتشكيل حبيبات هيدروجيل مركّبة متناهية الصغر بطريقة الهلام الأيوني. تم تقييم التنبؤ بمضادات القولون والمستقيم للسيليكو من خلال برنامج الالتحام الجزيئي AutoDock الذي يستهدف مستقبل TGF-beta 1. تم فحص كفاءة احتباس الدواء (DEE) ، وتحميل الدواء (DL) ، ومؤشر التورم (SI) ، وإطلاق الأدوية التراكمية في المختبر ، و DLS ، و FTIR و XRD. تم العثور على متوسط حجم الجسيمات لتعليق النانو 80 نانومتر ، وجد أن DEE أعلى من 99 ٪ على نسبة صغيرة من DL. أشارت نتائج ملفات تعريف إطلاق الدواء التراكمي في المختبر إلى أن الكوركومينويد المنطلق من الكريات عند (الرقم الهيدروجيني = 1.2) كان 1٪ ، وعند (pH = 6.8) ، زادت كميات الكوركومينويد المنبعثة بشكل ملحوظ إلى 74٪ على مدى الإطلاق المستمر لـ 6 ساعات. إطلاق دواء تراكمي محسّن من curcuminoids عند درجة الحموضة 6.8 للخرز القائم على HPMC . قدم تحليل XRD تغليفًا للكوركومينويد بالإضافة إلى طين بنتونايت الصوديوم المقشر لتركيبة HPMC. أظهر التنبؤ بمضادات القولون والمستقيم السيليكو أن الكركمينات الثلاثة: الكركمين ، ديميثوكسيكوركومين ، ثنائي ميثوكسيكوركومين يمكن أن ترتبط بمستقبل TGF-beta 1. قدمت هذه الدراسة صياغة جديدة وأظهرت ملف تعريف إطلاق مستدام وحساسية الأس الهيدروجيني ، والتي يمكن اعتبارها نهجًا جيدًا لتطبيق توصيل الدواء عن طريق الفم.

الكلمات المفتاحية: الكوركومينويد ، المركب النانوي ، الكريات ، الهيدروجيل ، مضاد القولون والمستقيم ، مستقبلات TGF-beta 1.